DEVELOPMENT OF A NADYLATED RNA CAPTURE METHOD

DISSERTATION ZUR ERLANGUNG DES DOKTORGRADES DER NATURWISSENSCHAFTEN (DR. RER. NAT.) DER FAKULTÄT FÜR BIOLOGIE UND VORKLINISCHE MEDIZIN DER UNIVERSITÄT REGENSBURG

Vorgelegt von Alice Véronique Griselin

Aus Lyon, Frankreich

Im Jahr 2024

Das Promotionsgesuch wurde eingereicht am:

27.03.2024

Die Arbeit wurde angeleitet von:

Prof. Dr. Gunter Meister

Unterschrift:

_____

ABSTRACT

The 7-methylguanosine cap structure protects the 5'-end of most cellular RNAs and plays a crucial role in post-transcriptional gene regulation. Nucleotide-containing coenzymes have been discovered to be covalently linked to the 5'-end of RNA, but the biological roles of these so-called "non-canonical caps" are still unclear. The identification of RNAs modified with nicotinamide adenosine dinucleotide (NAD) has been possible by the development of specific capture methods for NADylated RNAs. However, these protocols rely heavily on the prior modification of the NAD moiety, and thus are associated with several limitations and biases. This thesis explored two new approaches to directly target the 5'-NAD structure. On the one hand, we attempted to generate antibodies recognizing the NAD cap. However, we were unsuccessful in identifying candidates suitable for NADylated RNAs enrichment. On the other hand, we used NAD- and NMN-binding aptamers to enrich NADylated RNAs. This capture approach can be combined to a decapping step in order to increase the specificity of the enrichment. To this end, we expressed and purified the human deNADding enzyme Nudt12. Nudt12-treatment of NADylated RNAs yields monophosphorylated RNAs that can directly be ligated to an adapter and used for library preparation and sequencing. Although our capture-decapping approach still requires further optimization before *in vivo* applications, it expands the toolbox of methods for capturing NADylated RNAs by offering a previously unavailable alternative: directly binding the NAD modification.

A mon père

TABLE OF CONTENTS

LIST OF FIGURES

LIST OF TABLES

LIST OF ABBREVIATIONS

Abbreviation	Full description
ADP	Adenosine diphosphate
ADPRC	Adenosine diphosphate-ribosylcyclase
AMP	Adenosine monophosphate
APB	Acryloylaminophenyl boronic acid
ATP	Adenosine triphosphate
BSA	Bovine serum albumin
CBC	Cap-binding complex
CoA	Coenzyme A
CTD	C-terminal domain
CTP	Cytidine triphosphate
CuAAC	Copper-catalyzed azide–alkyne cycloaddition
DMEM	Dulbecco's modified Eagle's medium
DNA	Deoxyribonucleic acid
dp-Coa	Dephospho-CoA
ELISA	Enzyme-linked immunosorbent assay
EMSA	Electrophoretic mobility assay
FAD	Flavine adenine dinucleotide
FBS	Fetal bovine serum
FH	Flag-HA tag
GST	Glutathione S-transferase
GTP	Guanosine triphosphate
His	Histidine
HPLC	High-performance liquid chromatography
IgG	Immunoglobulin G
Im-NMN	Nicotinamide mononucleotide imidazolate
IP	Immunoprecipitation
K_D	Dissociation constant
LC	Liquid chromatography

miRNA	microRNA
mRNA	Messenger RNA
MS	Mass spectrometry
mtRNA	Mitochondrial RNA
NAD	Nicotinamide adenine dinucleotide
NADH	Reduced nicotinamide adenine dinucleotide
ncRNA	Non-coding RNA
NMN	Nicotinamide mononucleotide
NP1	Nuclease P1
NR	Nicotinamide riboside
NRD	N-terminal regulatory domain
nt	Nucleotide
OVA	Ovalbumin
P/S	Penicillin/streptomycin
PAA	Polyacrylamide
PAGE	Polyacrylamide gel electrophoresis
PBS	Phosphate-buffered saline
Pre-miRNA	Precursor-miRNAs
Pre-mRNA	Pre-messenger RNA
RLU	Relative light unit
RNA	Ribonucleic acid
RNA Pol II	RNA polymerase II
RNAP	*E. coli* RNA polymerase
RNP	Ribonucleic particle
rRNA	Ribosomal RNA
SAM	S-adenosyl-L-methionine
scaRNA	Small Cajal body-specific RNA
SELEX	Systematic evolution of ligands by exponential enrichment
snoRNA	Small nucleolar RNA
snRNA	Small nuclear RNA
SPAAC	Strain-promoted azide-alkyne cycloaddition
TBS	Tris-buffered saline
TMG	Trimetyhlguanosine

UDP-Glc	UDP-glucose
UDP-GlcNAc	Uridine diphosphate N-acetyl glucosamine
UTP	Uridine triphosphate
UTR	Untranslated region
RT	Room temperature

Notes: Unless specified otherwise, units were abbreviated according to the International System of Units (ISU), chemical names were abbreviated according to the International Union of Pure and Applied Chemistry (IUPAC), proteins were abbreviated according to the Universal Protein Resource (UniProt) and gene were abbreviated according to the Gene National Center for Biotechnology Information (NCBI) recommendations.

AUTHOR CONTRIBUTIONS

The coupling reaction of nucleosides and carriers, the validation and estimation of the reaction efficiency, and all HPLC analyses were performed by Robert Hett (AG Meister, Biochemistry I, Faculty of Biology and Preclinical Medicine, University of Regensburg, Germany).

The mass spectrometry measurements were performed by Dr. Astrid Bruckmann and her group (Mass Spectrometry Facility, Faculty of Biology and Preclinical Medicine, University of Regensburg, Germany).

The generation of monoclonal antibodies, the immunization, the fusion of myeloma and splenic B cells of immunized mice, and the detection ELISA were done by Dr. Regina Feederlee and her group (Core Facility Monoclonal Antibodies, Helmholtz Munich, Germany).

1 INTRODUCTION

1.1 EUKARYOTIC GENE EXPRESSION IN A NUTSHELL

Organism responses to environmental and developmental stimuli are mediated by a cascade of coordinated cellular processes. At the heart of this complex regulation lies the central dogma of molecular biology (Crick, 1970), which describes the flow of genetic information through three fundamental processes: the genetic information is encoded within a double-stranded DNA molecule that can be replicated or transcribed into a single-stranded RNA molecule, which in turn can serve as a template for protein synthesis through translation.

Eukaryotes are characterized by a nucleus, in contrast to prokaryotes. This subcellular compartment is delineated by a membrane enclosing the genetic information; thus, eukaryotic DNA replication and RNA transcription are spatially separated from protein synthesis (Carmo-Fonseca, 2002). In the course of evolution, other membrane-bound organelles were acquired by eukaryotes through the endosymbiosis of bacteria: mitochondria, found in all eukaryotic cells, and plastids, present in plants, algae, and protists (Archibald, 2015).

The transcription of specific DNA units, the genes, into RNA transcripts is carried out by dedicated machineries, the RNA polymerases (Girbig *et al.,* 2022). Eukaryotic genes are usually monocistronic: one gene is transcribed in one RNA transcript. Mitochondria and plastids possess their own genome and transcription machineries; the transcription of their RNA generally generates polycistronic transcripts, reminiscent of their prokaryotic origin (Liere *et al.,* 2011; Shokolenko and Alexeyev, 2017). RNA can be divided into two classes: non-coding RNA and messenger RNA (mRNA). In the nucleus, RNA polymerases I and III transcribe non-coding housekeeping RNAs, such as the highly abundant ribosomal RNA (rRNA) and transfer RNA (tRNA) (Khatter *et al.,* 2017), while RNA polymerase II transcribes pre-messenger RNA (pre-mRNA) and numerous species of long and small non-coding RNAs (Osman and Cramer, 2020). RNAs undergo various processing mechanisms. In the case of pre-messenger RNA, the non-coding introns are excised from its body, and

the coding exons are ligated together by the spliceosome, a large ribonucleoparticle (RNP) complex (Will and Lührmann, 2011). After additional modifications, the mature messenger RNA is exported from the nucleus to the cytoplasm, where it can be stored or decoded for translation into protein by the ribosome, another multi-subunit RNP (Klinge and Woolford, 2019). Ultimately, RNAs are degraded by different mechanisms (Tatosyan *et al.,* 2020). Gene expression regulation can therefore occur at the DNA (epigenetic, transcriptional), RNA (post-transcriptional), or protein (translational, post-translational) level.

1.2 RNA METABOLISM: A VIEW FROM THE CAP

The ends of a RNA molecule are determinants for its stability and biological roles. In a cellular environment, RNA can be easily degraded either by endoribonucleases, which cleave within the internal phosphodiester bond between two nucleotides, or by exoribonucleases, which catalyze the removal of nucleotides one by one from the ends of the RNA (reviewed in Tatosyan, Ustyantsev, and Kramerov 2020). Therefore, safeguarding the extremities of a RNA until its function has been fulfilled becomes essential. This protection can be achieved by shielding the RNA ends with protein complexes, with chemical modifications, or by the addition of non-encoded nucleotides (reviewed in Gagliardi and Dziembowski 2018). These terminal modifications and additional structures deposited at the 5'- and 3'-ends of RNAs are commonly described as "cap" and "tail", respectively, and play critical roles in the fate of the RNA.

1.2.1 A variety of canonical cap structures

The diversity of RNA cap structures arises from different factors, such as the identity of the first nucleotide incorporated during transcription, the transcription machinery involved, the capped RNA species, or the organism (Anreiter *et al.,* 2023).

1.2.1.1 The 7-methylguanosine cap and cap-proximal modifications

The most prominent and well-studied 5'-terminal RNA modification is the 7-methylguanosine cap, which consists of a N^7-methylguanosine (m^7G) connected to the first transcribed nucleotide (N) through an inverted 5'-5'-triphosphate bridge (Figure

1A) (Furuichi, 2015). The m^7G cap is added co-transcriptionally to the RNA polymerase II transcripts in eukaryotes. Its absence on bacterial and archaeal transcripts distinguishes it as a typical feature of eukaryotic RNA (Galloway and Cowling, 2019; Pelletier *et al.,* 2021).

In lower eukaryotes, the m^7G cap is present as its minimal structure: the cap 0 (m^7GpppN) (Hsu and Stevens, 1993). In higher eukaryotes, this cap structure undergoes additional cap-proximal methylations to form an extended structure: further methylation of the ribose (2'-*O*-methylation) of the first and second nucleotides form the cap 1 (m^7GpppN_m) and the cap 2 ($m^7GpppN_mN_m$) structure, respectively (Figure 1B) (Adams and Cory, 1975; Wei *et al.,* 1975b). The abundance levels of cap 2 vary between cell types, tissues, and organisms (for example, the cap 2 has been identified on 40% of the mRNA in HEK293T cells) and increase throughout the mRNA lifetime (Despic and Jaffrey 2023). The ribose methylations of the cap 1 and cap 2 structures play an important role in self-recognition and innate immune response (Wang *et al.,* 2010; Züst *et al.,* 2011; Devarkar *et al.,* 2016; Abbas *et al.,* 2017; Drazkowska *et al.,* 2022; Despic and Jaffrey, 2023). A hypermethylated cap 4 structure has even been identified in kinetoplastids, in which the first four encoded nucleotides are 2'-*O*-methylated (Perry *et al.,* 1987).

The double methylation at the N^2 of the m^7G cap 0 structure generates the trimethylated guanosine cap (abbreviated as $m_3^{2,2,7}G$, m^3G, or TMG cap) (Figure 1B). This trimethylated cap is present on certain small nuclear and nucleolar RNAs that help in pre-mRNA splicing (U1, U2, U4, and U5 snRNAs) (Busch *et al.,* 1982; Bochnig *et al.,* 1987), pre-rRNA processing (U3 and U8 snoRNAs) (Reddy *et al.,* 1979; Tyc and Steitz, 1989), and telomere addition (telomerase RNA) (Jády *et al.,* 2004), as well as on some selenoprotein mRNAs (Wurth *et al.,* 2014).

When the first nucleotide of the transcript is an adenosine, it can be further methylated at the N^6 position to produce a m^6A_m cap ($m^7Gpppm^6A_m$) (Figure 1C) (Wei *et al.,* 1975a). Analysis of capped mRNAs from HEK293T cells revealed that 92% of mRNAs starting with an adenosine nucleoside carry the m^6A_m modification (Akichika *et al.,* 2019).

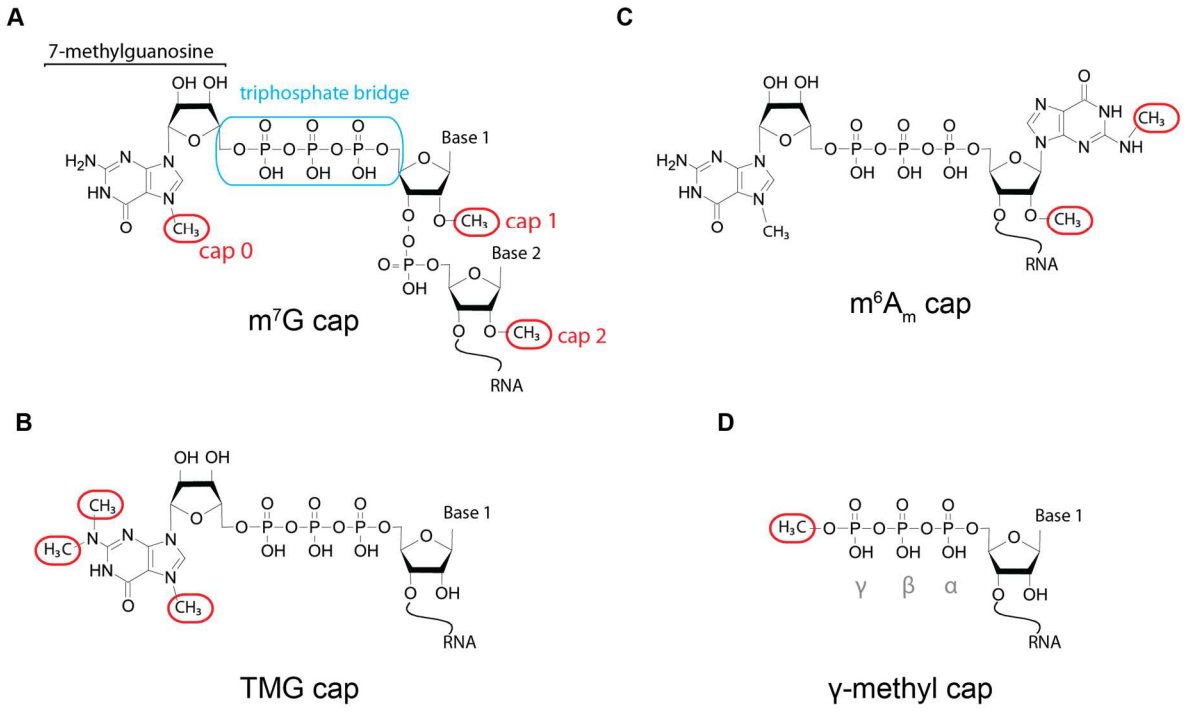

Figure 1. Chemical structure of eukaryotic cap structures. (A) m^{7}G-capped RNA. A *N*^{7}-methylguanosine is connected by an inverted 5'-5' triphosphate bridge to the first transcribed nucleotide and forms the cap 0 structure. Additional methylations on the ribose of the first and second nucleotides form the cap 1 and cap 2 structure, respectively. (B) m^{6}A$_m$-capped RNA. The adenosine is methylated at the *N*^{6} position in addition to the ribose methylation. (C) m$_3^{2,2,7}$G-capped RNA (trimethylated, TMG). The *N*^{7}-methylguanosine is double-methylated at the *N*^{2} position. (D) Gamma-methyl-capped RNA. The gamma-phosphate is methylated. Methylations are circled in red. Adapted from Warminski et al, 2017.

Mono-, di-, and trimethylated guanosine caps have been reported in some yeast precursor molecules of transfer RNA (tRNA) (Ohira and Suzuki, 2016). Of note, a non-methylated guanosine cap (GpppN) has been observed in insect oocyte mRNA (Kastern and Berry, 1976).

1.2.1.2 5'-end phosphate methylations

In addition to the wide-spread m^{7}G cap, other non-nucleotide cap structures have been found on the 5'-end of specific subsets of RNAs.

On the one hand, the γ-methyl cap results from the methylation of the terminal gamma-phosphate of a triphosphorylated transcript (mpppG) (Figure 1D). It has been identified in four RNAs: mammalian U6 spliceosomal RNA (Singh and Reddy, 1989), 7SK small nuclear RNA (Gupta *et al.,* 1990), mouse B2 non-coding RNA (Shumyatsky *et al.,* 1990), and plant U3 small nucleolar RNA (Shimba *et al.,* 1992).

On the other hand, monomethylation of 5'-α-monophosphorylated cytoplasmic histidine-accepting transfer RNA (Martinez *et al.*, 2017a) and dimethylation of 5′-α-monophosphorylated specific precursor microRNA (pre-miR-145 and pre-mi-23b) (Xhemalce *et al.,* 2012) have been reported.

1.2.2 Biosynthesis of the cap(s)

This variety of cap structures results from the action of different capping enzymes. The addition and modifications of the cap can occur co- or post-transcriptionally. For instance, all transcripts generated by the RNA Pol II receive co-transcriptionally a m^7G cap, but while the messenger RNAs keep their m^7G cap, the m^7G cap of most non-coding RNAs undergoes further post-transcriptional methylation, or is even lost by cleavage during maturation (reviewed in Byszewska *et al.,* 2014; Furuichi 2015).

1.2.2.1 The m^7G cap of RNA Pol II transcripts

The transcription of DNA by the RNA polymerase II is a highly regulated process and consists of several phases: the assembly of the pre-initiation complex, initiation of transcription, elongation, and termination (reviewed in Cramer 2019). The carboxyl-terminal domain (CTD) of the largest subunit of the RNA Pol II contains repeats of an amino acid sequence with the consensus sequence tyrosine-serine-proline-threonine-serine-proline-serine. The dynamic phosphorylation of this domain recruits the transcription machinery and numerous processing factors to the pre-mRNA (reviewed in Harlen and Churchman 2017b), including the capping and cap-modifying enzymes. Thus, m^7G capping and RNA Pol II transcription are tightly linked to each other.

After the transcription of 20 to 60 nucleotides, the DRB sensitivity-inducing factor (DSIF) binds to the RNA Pol II and recruits the negative elongation factor (NELF) (Figure 2). RNA Pol II pauses near the promotor region and RNA synthesis is stopped, a step known as "promotor-proximal pausing". The basal transcription factor II H (TFIIH) phosphorylates the CTD at the Serine 5 (Ser5) residue. The phosphorylated Serine 5 (phospho-Ser5) of the CTD and DSIF recruit the RNA guanylyltransferase and 5'-phosphatase capping enzyme (RNGTT in mammals) (McCracken *et al.,* 1997; Ho *et al.,* 1998; Wen and Shatkin, 1999). The C-terminal guanylytransferase domain of RNGTT binds to the phosphorylated CTD, and its N-terminal triphosphatase domain

is positioned close to the RNA exit site of RNA Pol II. RNGTT hydrolyzes the terminal γ-phosphate of the nascent mRNA, generating a diphosphorylated RNA (Chu *et al.,* 2011). When the nascent RNA is long enough (~22 nt) to reach the active site of the C-terminal guanylytransferase domain, RNGTT transfers a GMP moiety to the terminal β-phosphate, forming a basic cap structure (GpppN). The interactions between phospho-Ser5 and DSIF stimulate the guanylytransferase activity (Ho and Shuman, 1999; Wen and Shatkin, 1999). The requirement of the guanylytransferase for a diphosphorylated RNA ensures that capping is restricted to *de novo* synthesized RNA as substrate and excludes monophosphorylated RNA resulting from endonucleolytic cleavage (Tsukamoto *et al.,* 1998a, 1998b).

The catalytic subunit RNA guanine-N^7-methyltransferase 2 (RNMT) is also recruited to the phospho-Ser5 of the CTD (Pillutla *et al.,* 1998). RNMT together with its activating subunit RNMT-activating mini-protein (RAM) catalyzes the methylation of the methyl group at the N^7 position and generates the canonical m^{7}G cap 1 structure (m^{7}GpppN$_m$) (Gonatopoulos-Pournatzis *et al.,* 2011).

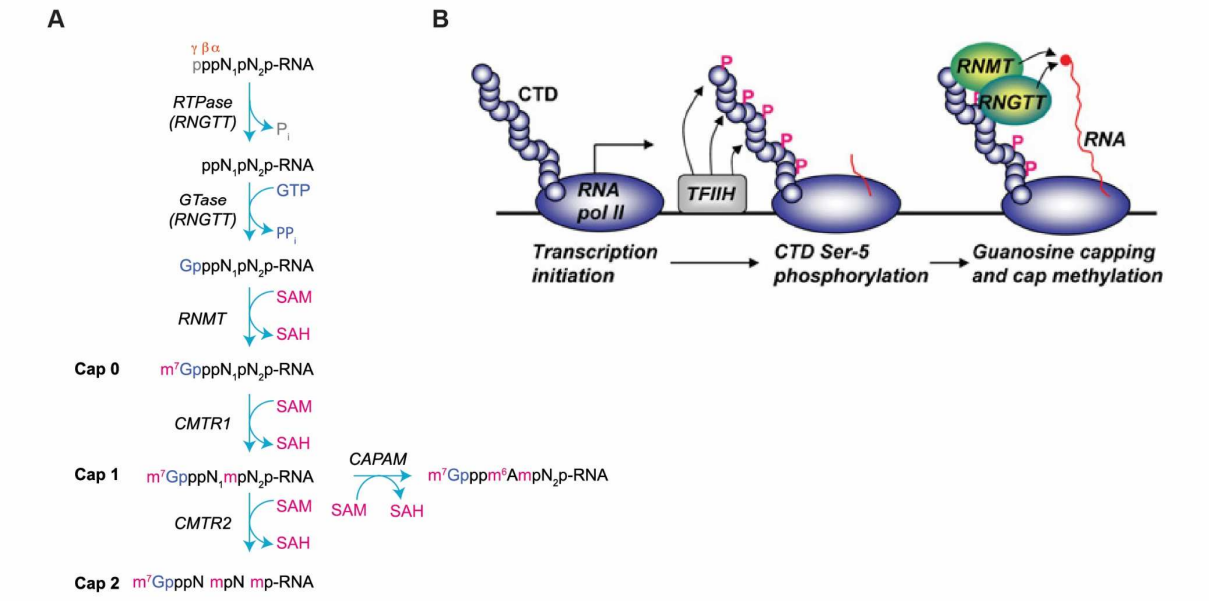

Figure 2. Overview of the canonical capping pathway. (A) In mammals, the RNA triphosphatase (RTPase) domain of the RNA guanylyltransferase and 5'-phosphatase (RNGTT) hydrolyzes the γ-phosphate of the nascent RNA. The guanylytransferase (GTase) domain of RNGTT transfers a GMP molecule to the terminal β-phosphate of the RNA. Finally, the guanine-N^7-methyltransferase (RNMT) transfers a methyl group from S-adenosyl-L-methionine (SAM) to the N^7 position of the terminal guanine, generating the minimal cap 0 structure. Additionnally, the Cap Methyltransferase 1 or 2 (CMTR1 and CMRT2, respectively) catalyze the 2'-O-methylation of the ribose of the first or second transcribed nucleotide, generating the cap 1 and cap 2 structure, respectively. When the first transcribed nucleotide is an adenine, the cap-specific adenosine N^6-methyltransferase (CAPAM) transfers a methyl residue to the N^6 position of adenine. N, nitrogenous bases (adenine, cytosine, guanine, and uracil). (B) Interplay of RNA transcription and capping. Shortly after transcription initation, the core transcription factor II H (TFIIH) phosphorylates the Serin 5 residue of the carboxyl-terminal domain (CTD) of the RNA polymerase II (Pol II). The capping machinery is recruited. The RNA Guanylyltransferase And 5'-Phosphatase

(RNGTT) and the RNA guanine-N^7- methyltransferase 2 (RNMT) cap the nascent RNA. Adapted from Cowling 2009; Pelletier, Schmeing, and Sonenberg 2021.

The ribose of the first transcribed nucleotide is methylated by the Cap Methyltransferase 1 (CMTR1) (Bélanger *et al.,* 2010). This methyltransferase is also recruited to the phospho-Ser5 of the RNA Pol II CTD (Haline-Vaz *et al.,* 2008; Inesta-Vaquera *et al.,* 2018) and methylates the nascent RNA when it reaches ~29 nucleotides, generating the cap 1 structure (m^7GpppN_m).

If the first transcribed nucleotide is an adenosine, its base can be methylated by the cap-specific adenosine N6-methyltransferase (CAPAM) (Akichika *et al.,* 2019), previously identified as the phosphorylated CTD interacting factor 1 (PCIF1). As its former name indicates, CAPAM is also recruited by the phosphor-Ser5 of the RNA Pol II CTD (Fan *et al.,* 2003; Hirose *et al.,* 2008).

Afterwards, RNGTT recruits the positive elongation factor b (P-TEFb), which phosphorylates Ser2 of the CTD, DSIF and NELF. Phosphorylated NELF is released from the RNA Pol II, and this enables the transition of RNA Pol II from arrested to productive elongation (Mandal *et al.,* 2004).

The ribose of the second cap-proximal nucleotide can be methylated by the Cap Methyltransferase 2 (CMTR2). Although CMRT2 is present both in the cytoplasm and in the nucleus (Werner *et al.,* 2011), its activity is found almost exclusively in the cytoplasmic fraction (Langberg and Moss, 1981), suggesting that this methylation step occurs after export of the capped RNA to the cytoplasm. The basis for the selectivity of the enzyme is still unclear.

1.2.2.2 The TMG cap of the snRNAs and snoRNAs

The biogenesis of most spliceosomal snRNAs (i.e. U1, U2, U4, and U5 snRNAs) requires a nucleocytoplasmic shuttling, mediated in part by cap modifications (reviewed in Gruss *et al.,* 2017). These U snRNAs are transcribed in the nucleus by RNA Pol II, acquired the m^7G cap as for the other RNA Pol II transcripts and are exported in the cytoplasm (detailed in 1.2.3.1). There, the U snRNAs assemble with the survival motor neuron (SMN) complex and a ring of Sm proteins. The Sm ring provides a binding site for the trimethylguanosine synthase 1 (Tgs1) (Mattaj, 1986; Plessel *et al.,* 1994). Tgs1 successively transfers two methyl groups from SAM to the N^2 position of guanosine to generate the TMG cap, and the activity of Tgs1 is strictly dependent on the

methylation of guanine N^7, thus only active on RNAs that already have a m^7G cap (Zhu *et al.,* 2001; Mouaikel *et al.,* 2003; Hausmann and Shuman, 2005; Hausmann *et al.,* 2008; Monecke *et al.,* 2009).

Some small nucleolar RNA (snoRNAs) are independently transcribed by RNA Pol II and thus receive a m^7G cap. However, they are not exported in the cytoplasm but remained in the nucleus. During their 5'-end processing, the cap can either be removed or be further post-transcriptionally modified (reviewed in Kufel and Grzechnik 2019). When the cap is retained, snoRNAs are directed to the Cajal bodies of the nucleus where a shorter nuclear isoform of Tgs1 hypermethylated the m^7G cap to a TMG cap (Mouaikel *et al.,* 2002; Girard *et al.,* 2008).

1.2.2.3 The gamma-methyl cap of the 7SK and U6 RNA

The 7SK long non-coding RNA and the U6 spliceosomal RNA are both transcribed by RNA Pol III (reviewed in Zhou and Van Bortle 2023).

The methylphosphate capping enzyme (MePCE) was originally named Bicoid-interacting protein 3 (BCDIN3). MePCE binds to the nascent 7SK RNA and transfers a methyl group from SAM to the gamma-phosphate at the 5'-end of 7SK, generating the γ-methyl cap (Jeronimo *et al.,* 2007; Yang *et al.,* 2019). Subsequently, the RNA-binding protein La binds to its 3'-oligo-uridine tail, the La-related protein 7 (Larp7) displaces La, and together, MePCE, Larp7, and the 7SK RNA form the 7SK core small nuclear ribonucleoprotein complex (reviewed in Hasler, Meister, and Fischer 2021).

Although U6 has not been conclusively shown to be capped by MePCE, the enzyme has been found to be associated with the U6 promotor region (Xue *et al.,* 2010) and the specificity of MePCE for U6 has been confirmed *in vitro* (Yang *et al.,* 2019). In contrast to 7SK, MePCE dissociates from U6 after the capping event. A conserved 5'-triphosphate and a hairpin structure followed by a short single-stranded region with an AUAUAC sequence act as a consensus signal for the capping of U6 (Singh *et al.,* 1990).

1.2.3 Roles of the cap in gene expression regulation

The cap plays a crucial role in the RNA lifecycle: it promotes splicing of proximal exons and the 3'-end processing, mediates its nucleocytoplasmic transport, recruits the

initiating translation factors, and protects it from degradation (Galloway and Cowling, 2019; Rambout and Maquat, 2020; Vidya and Duchaine, 2022).

1.2.3.1 The cap as a protein binding platform

Shortly after capping, the cap structure is recognized by the heterodimeric cap-binding complex (CBC), composed of the nuclear cap-binding proteins NCBP1 and NCBP2 (Visa *et al.,* 1996). Once bound to the cap, the CBC serves as a binding platform and interacts with numerous factors involved in the maturation and the export of the RNA (reviewed in Gonatopoulos-Pournatzis and Cowling 2014; Rambout and Maquat 2020).

During the maturation of the pre-messenger RNA, the non-coding introns are excised from its body, and the coding exons are ligated together by the spliceosome (reviewed in Will and Lührmann 2011). The transcription/complex (TREX) is recruited to the 5'-cap-proximal exon of the pre-mRNA. Capping, splicing and RNA export are coupled (Luo and Reed, 1999): on the one hand, the CBC interacts with the CTD of Pol II and the RNA, on the other hand, the CBC interacts with the export factor binding protein/Aly protein (Aly/Ref), a component of TREX (Figure 3A) (Izaurralde *et al.,* 1994; Lewis *et al.,* 1996; Görnemann *et al.,* 2005; Pabis *et al.,* 2013).

The 3'-end of the RNA transcript is processed near its polyadenylation signal in its 3'-end. A long stretch of adenosines (the so-called poly(A) tail) is added by poly(A) polymerases (reviewed in Passmore and Coller 2022). Furthermore, protein factors that are specifically bound to the 5'- and 3'-ends of the RNA can interact with each other, including the CBC (Flaherty *et al.,* 1997).

Although both messenger RNAs and pre-U snRNAs are m^7G-capped and are bound by the CBC, they are not recognized by the same export factors. In the case of the mRNA, the CBC interacts with the subunit Aly/REF of TREX already present on the RNA following splicing. TREX recruits the major mRNA export receptor: the tip-associating protein (TAP) and the nuclear export factor (NXF1) (Grüter *et al.*, 1998). Additionally, the CBC interacts directly with the heterogeneous ribonucleoprotein C (hnRNP C), which only binds to RNAs longer than 300 nucleotides (McCloskey *et al.*, 2012; Dantsuji *et al.*, 2023) (Figure 3B). Together, these factors target the spliced mRNA for export to the cytoplasm through the nucleopore complex (Cheng *et al.*, 2006).

The m^{7}G-capped U snRNAs are exported differently. For this RNA species, the interaction between the CBC and the nuclear export receptor exportin-1 (XPO1) (also known as Chromosome Region Maintenance 1 (CRM1)) is mediated by the phosphorylated adaptor of RNA export (PHAX) (Ohno *et al.*, 2000; Segref *et al.*, 2001). HnRNP C does not bind to short RNAs and therefore do not prevent the recruitment of PHAX, as it is the case for mRNAs (McCloskey *et al.*, 2012) (Figure 3C). PHAX recruits the Ras-Related Nuclear Protein (Ran)GTP and directs the U snRNAs for export through the nucleopore complex. Once in the cytoplasm, their cap is hypermethylated (see 1.2.2.2). Subsequently, the TMG cap and the Sm protein ring act as a bipartite nuclear import signal: the TMG cap is specifically recognized and bound by snurportin-1, mediating the re-import of the mature snRNP into the nucleus (Huber *et al.*, 1998; Strasser *et al.*, 2005), where they are involved in splicing.

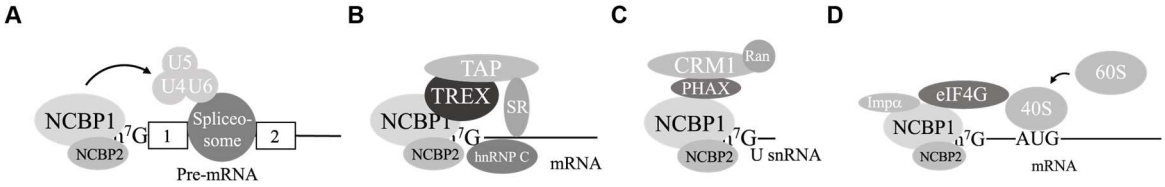

Figure 3. Functions of the cap-binding complex. The cap-binding complex (CBC) consists of the nuclear cap-binding proteins 1 and 2 (NCBP1 and 2) and binds to the m^{7}G cap. The CBC plays a role in: (A) Pre-messenger splicing. CBC interacts with the spliceosome and contributes to the recognition of the 5'-cap-proximal splice site of the first intron. (B) Messenger RNA export by interacting with the transcription export complex (TREX), the tip-associating protein (TAP), and the heterogeneous ribonucleoprotein C (hnRNP C), Serine-Arginine–rich proteins (SR proteins) function as adaptors for mRNA export. (C) Spliceosomal RNA export by interacting with the phosphorylated adaptor of RNA export (PHAX). The export is mediated by the Chromosome Region Maintenance 1 (CRM1) in a Ras-Related Nuclear Protein (Ran)GTP-dependent manner (D) Pioneer round of translation. CBC interacts with eIF4G and recruits the small ribosomal subunit 40S. Adapted from (Kataoka, 2023).

The m^{7}G cap structure is also essential for the translation initiation of most eukaryotic mRNAs (Muthukrishnan *et al.,* 1975). The CBC can mediate the very first round of translation, namely, pioneer round of translation (Figure 3D) (Ishigaki *et al.,* 2001). Afterwards, the CBC is exchanged by the eukaryotic translation initiation factor (eIF4E) that recognizes and binds to the m^{7}G moiety of the cap (Marcotrigiano *et al.,* 1997). The eIF4E subunit is part of the eukaryotic initiation factor 4F complex (eIF4F), which also contains the RNA helicase eIF4A, and the scaffold protein eIF4G. In turn, eIF4F recruits eIF3 that binds to the small subunit of the ribosome. Subsequently, the small ribosomal subunit with some additional initiation factors scan the 5'-untranslated region (5'-UTR) of the mRNA until the recognition of the translation start codon, where the large subunit joins and the synthesis of the polypeptide chain begins (translation elongation) (reviewed in Dever, Dinman, and

Green 2018). Additionally, protein factors associate between the 5'- and the 3'-end of the mRNA, such as the poly(A) binding proteins (PABP). They interacts with eIF4G, leading to circularization of the mRNA in a closed loop, thereby enhancing the translation process (Gallie, 1991; Kahvejian *et al.,* 2005), and protecting the RNA from exoribonucleases attacks.

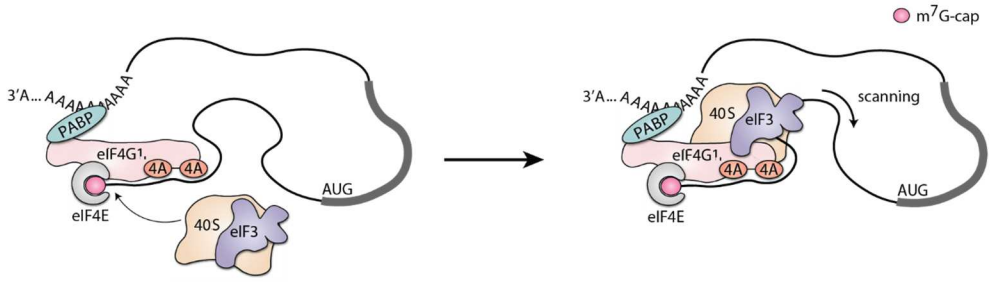

Figure 4. Canonical cap-dependent initiation. The eukaryotic initiation factor eIF4F is made up by three eukaryotic initiation factors (eIF): the cap-binding protein eIF4E, the helicase eIF4A, and the scaffold protein eIF4G1. eIF4G1 interacts with eIF3, which recruits the small ribosomal subunit 40S, which starts to scan the messenger RNA until the AUG start codon. Additionally, eIF4G1 interacts with the poly(A)-binding protein (PABP), thus the messenger RNA forms a closed loop. Adapted from Shestakova et al., 2023.

1.2.3.2 mRNA decay

The first step of RNA degradation for the nearly all mRNAs in eukaryotes is the removal of the poly(A) tail by the deadenylase complexes and in mammals, this deadenylation step occurs in the cytoplasm (reviewed in Passmore and Coller, 2022). Subsequently, the degradation of the deadenylated mRNAs can occur through two main pathways: the 5′-3′ or the 3'-5' decay pathway (Figure 5). Both decay pathways require the digestion of the RNA body and the removal and degradation of the cap structure.

In the 5'-3′ decay pathway, the removal of the cap structure by the Dcp2/Dcp1 decapping complex (1.2.4.1) occurs rapidly after the shortening of the poly(A) tail and leaves a 5'-phosphorylated end. Afterwards, the monophosphorylated RNA is degraded by the 5'-3' exonuclease Xrn1 (Mugridge *et al.,* 2018).

In the 3'-5' decay pathway, the RNA body is first degraded by the cytoplasmic exosome, a multi-subunit complex consisting of 3'-5' exoribonucleases (reviewed in (Łabno *et al.,* 2016a). When reaching the 5'-end of the RNA, the exosome releases free cap dinucleotides or short capped oligonucleotides (Wang and Kiledjian, 2001), which are further decapped by DcpS (1.2.4.2).

A subset of RNAs (some mRNAs, snRNA, pre-miRNA) can undergo an alternative degradation pathway after deadenylation through uridylation (reviewed in Yu and Kim, 2020; Liudkovska and Dziembowski, 2021). The Terminal Uridylyl Transferases (TUT4 and TUT7) add a stretch of 12-14 uridines at the 3'-end of RNAs with shortened poly(A) tails (Lim *et al.,* 2014). In turn, this modification recruits the decapping enzyme Dcp2 or the 3'-5' exoribonuclease Dis3L2 (Chang *et al.,* 2013; Ustianenko *et al.,* 2013; 2016), resulting in the degradation of uridylated RNA substrates.

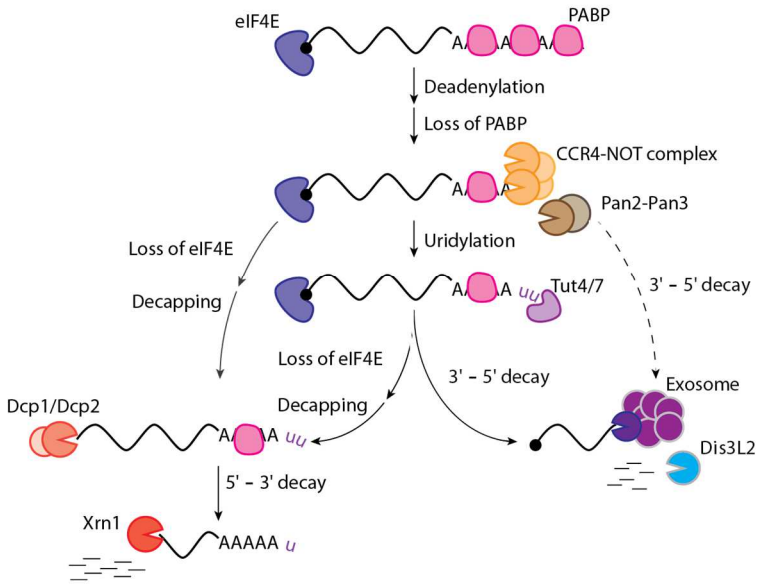

Figure 5. Schematic of the cytoplasmic RNA decay pathways. The RNA is deadenylated by the Pan2-Pan3 complex followed by the CCR4-NOT complex, leading to the shortening of the poly(A) tail and the dissociation of the poly(A)-binding protein (PAPB). In some cases, the deadenylated RNA can be uridylated afterwards. In the 5'-3' decay pathway, the Dcp2/Dcp1 decapping complex is recruited and removes the cap. The cytoplasmic Xrn1 exonuclease degrades the RNA body in the 5'-3' direction. In the 3'-5' decay pathway, the exosome or Dis3L2 degrades the RNA body and generate capped oligonucleotide fragments. Adapted from Rissland 2016.

Degradation of aberrant mRNAs can also be initiated independently of a first deadenylation step or triggered through preliminary quality control mechanisms, such as by endonucleolytic cleavage, nonsense-mediated decay (NMD), or non-stop decay (NSD). *In fine*, all these mechanisms either activate mRNA decapping, 5'-degradation by XRN1, or 3'-RNA degradation by the exosome (reviewed in Schoenberg 2011; Graille and Séraphin 2012; Monaghan *et al.,* 2023).

1.2.4 Degradation of the cap

Due to the inverted 5'-5' triphosphate link between the m^7G moiety and the first transcribed nucleotide, the exonuclease XRN1 and the exosome are unable to degrade the cap structure. Therefore, cap-specific cleavage enzymes are required to initiate the 5'-3' decay pathway and to terminate the 3'-5' decay pathway. They belong to two classes with different structures and catalytic activities: Nudix hydrolases, histidin triad (HIT) proteins, and Rai1/DXO family proteins (reviewed in Grudzien-Nogalska and Kiledjian 2017; Kramer and McLennan 2019).

1.2.4.1 Decapping enzymes

Three enzymes have been validated for their decapping activity in mammals: Dcp2 (also known as Nudt20), Nudt16, and Nudt3 (Figure 6). They all belong to the name-giving nucleoside diphosphate-linked moiety X (Nudix) family of protein, which is characterized by a consensus Nudix catalytic sequence. The members of the Nudix family cleave a wide range of substrates through their pyrophosphohydrolase activity, such as (di)nucleotides, dinucleotide coenzymes, but also some non-nucleotide small molecules (reviewed in Carreras-Puigvert *et al.,* 2017; Srouji *et al.,* 2017).

The decapping protein 2 (Dcp2) is the major decapping enzyme in eukaryotes. It binds to m^7G-capped RNAs and cleaves only the cap structure from RNAs of a minimum of 25 nucleotides, generating m^7GDP and a 5′-monophosphorylated RNA. Dcp2 contains two major protein domains: the catalytic Nudix domain and a N-terminal regulatory domain (NRD). The NRD specifically recognizes the m^7G nucleotide of the mRNA cap. Furthermore, it harbors the two conserved boxes A and B. Box A contributes to the specificity of Dcp2 and box B contributes to RNA binding (Lykke-Andersen, 2002; van Dijk *et al.,* 2002; Wang *et al.,* 2002; Piccirillo *et al.,* 2003). Dcp2 specifically recognizes a stem-loop element that is localized ten nucleotides downstream of the cap (Li *et al.,* 2008, 2009).

Dcp2 interacts through its NRD with its main activating factor Dcp1 (She *et al.,* 2008). This interaction is further stabilized by the scaffolding factor enhancer of mRNA decapping 4 (Edc4). These three interactions are necessary to stimulate Dcp2 decapping activity on the mRNA cap in metazoan (Chang *et al.,* 2014). Dcp2 also

interacts with numerous additional factors that enhance its decapping activity (reviewed in Vidya and Duchaine 2022).

Nudt16 was initially identified as a specific U8 snoRNA decapping enzyme (Tomasevic and Peculis, 1999; Ghosh *et al.,* 2004), but was later shown to be another cytoplasmic mRNA decapping protein (Song *et al.,* 2010). Nudt16 preferentially removes the cap of a subset of transcripts containing adenylate-uridylate-rich elements (ARE) compared to Dcp2 (Song *et al.,* 2010; Li *et al.,* 2011).

Nudt3 is a cytoplasmic protein that specifically targets a small subset of mRNAs transcripts involved in cellular migration (Grudzien-Nogalska *et al.,* 2016; Sahu *et al.,* 2020). The mechanism responsible for the specificity of Nudt16 and Nudt3 is currently unknown.

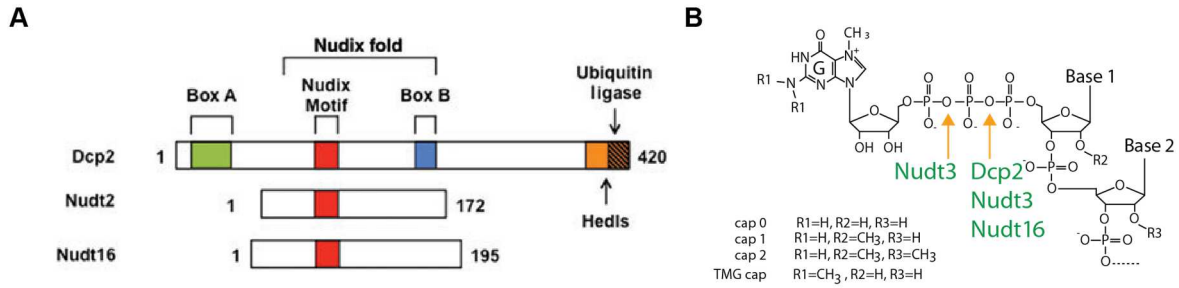

Figure 6. Decapping enzymes of the m^{7}G cap. (A) Schematic representation of the human decapping enzymes mentioned in the text. Proteins with decapping activity are aligned relative to their Nudix motif. (B) The cleavage sites of the decapping enzymes on a m^{7}G-capped RNA substrate are indicated by a yellow arrow. In red, Nudix hydrolase domain; in green, box A; in blue, box B; in orange, regulatory domains encompassing the binding sites for Edc4 (Hedl); in stripped orange, regulatory domains encompassing the binding sites ubiquitin ligases. Adapted from Grudzien-Nogalska and Kiledjian 2017; Kramer and McLennan 2019.

1.2.4.2 Scavengers of the cap

The accumulation of capped oligonucleotide fragments resulting from RNA degradation was suggested to be potentially harmful for the cell since they can interact with cap-binding proteins, and thus need to be eliminated (Bail and Kiledjian, 2008). Mammals possess two decapping scavenger enzymes that process such truncated capped oligonucleotides: the decapping scavenger protein (DcpS) and the fragile histidine triad protein (FHIT). Both belong to the histidine triad protein family, which is characterized by conserved histidine moieties. Their members hydrolyze nucleotide derivatives (reviewed in Brenner *et al.,* 1999).

The decapping scavenger DcpS (reviewed in (Krempl *et al.*, 2023) hydrolyzes the mRNA cap (m^{7}GpppN) into m^{7}GMP and nucleotide diphosphate (Wang and Kiledjian,

2001; Liu *et al.,* 2002; Gu *et al.,* 2004) (Figure 7). DcpS cleaves only cap dinucleotides or small capped oligonucleotides with a body length shorter than three nucleotides (Fuchs *et al.,* 2020). The generated m^7GMP is finally degraded into 7-methylguanosine and inorganic phosphate by the GMP-specific cytosolic nucleotidase III (cNIII) (Buschmann *et al.,* 2013). DcpS is also involved in the degradation of m^7GDP resulting from the 5'-3' degradation pathway or from Fhit cleavage activities, but only after m^7GDP has been phosphorylated to a m^7GTP intermediate by an enzyme yet unknown in mammals (a nucleoside diphosphate kinase in yeast) (Taverniti and Séraphin, 2015).

Fhit is able to hydrolyze the cap structure *in vitro* (Bojarska *et al.,* 1999) and has been identified to be involved in the degradation of the remaining of the m^7GpppG cap structures into m^7GDP and m^7GMP (Taverniti and Séraphin, 2015) (Figure 7).

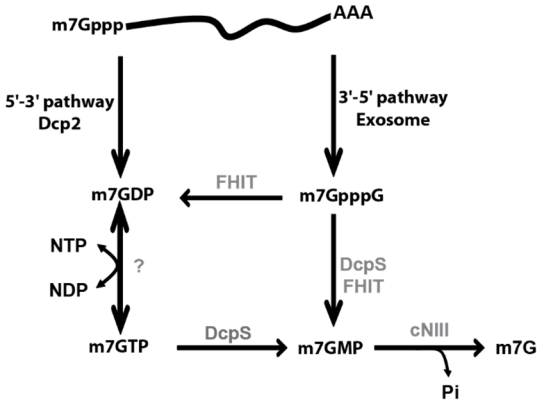

Figure 7. Schematic of RNA decay pathways and cap (di-)nucleotide elimination mechanisms. Enzymes involved in the generation of cap (di-)nucleotides in the 5′-3′ and 3′-5′ mRNA decay pathways are indicated, as well as the resulting decay products. Adapted from Taverniti and Séraphin 2015.

1.2.4.3 5'-end capping quality control

RNA capping is error-prone, as any biological process. Incompletely capped endogenous RNAs could potentially be mistakenly recognized as foreign ("non-self") RNAs by cellular surveillance systems and trigger the innate immune response (Thompson *et al.,* 2021). The capping process generates intermediates that cannot be degraded by exonucleases, since these proteins require a 5'-monophosphate for the recognition of their degradation substrates. To prevent the accumulation of defectively capped RNA, the decapping exonuclease DXO/Rai1 family of enzymes

preferentially functions on incompletely capped RNA and uncapped triphosphorylated RNA (Jiao *et al.,* 2010, 2013; Chang *et al.,* 2012).

Rai1 and Dxo1 in yeast, and DXO in mammals, possess decapping and pyrophosphatase activity towards aberrant 5'-end transcripts (p-RNA, ppp-RNA, and Gppp-RNA) that generates 5'-monophosphorylated RNA (Figure 8). This RNA product is then accessible for degradation either by the intrinsic 5'- to 3'-exoribonuclease activity of DXO or by exoribonucleases. DXO also shows *in vitro* activity against m^7G-capped RNA (Chang *et al.,* 2012; Jiao *et al.,* 2013). However, decapping is inhibited in the presence of the cap-binding proteins NCBP2 and elF4E, indicating that decapping by DXO of m^7G-capped RNAs is most likely prevented by the cap-binding proteins protecting the 5'-end of mature RNAs in a cellular environment (Jiao *et al.,* 2013).

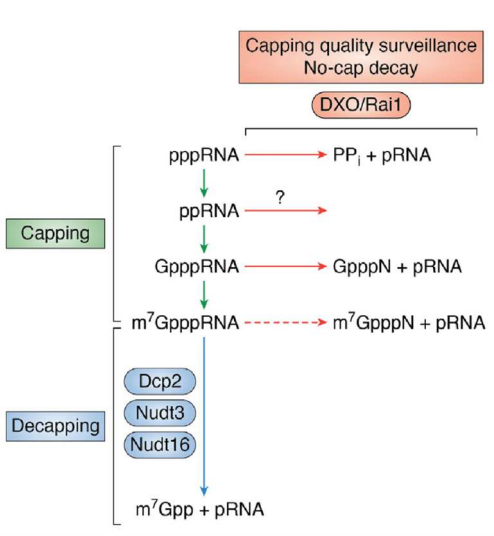

Figure 8. Schematic of eukaryotic m^7G capping, decapping, and capping quality surveillance reactions. The DXO/Rai family enzymes recognize and degrade the intermediates of the capping pathway. It is not known whether DXO/Rai1 enzymes also have activity toward ppRNA. Dcp2, Nudt3 and Nudt16 are the classical decapping enzymes that act on m^7G-capped RNAs. In green, capping reactions; in blue, decapping reactions; in red, cap quality control reactions. Adapted from Doamekpor *et al.,* 2022.

1.3 AN EXPANDING DIVERSITY OF 5'-END RNA MODIFICATIONS

1.3.1 "Cap-like" structures

The development of sensitive and high-throughput methods has allowed the recent uncovering of previously unknown modifications on the 5'-end of RNA in all domains

of life (reviewed in Doamekpor *et al.,* 2022; Mattay, 2022). Their 5'-beginning position and structure led them to be quickly named as "non-canonical caps" or "cap-like" as opposed to the canonical eukaryotic m^7G cap. These cap-like structures can be classified into two groups: coenzyme-derived caps and dinucleotide polyphosphate caps.

1.3.1.1 Coenzymes caps

Coenzymes are organic molecules that, upon binding to a protein, contribute to its enzymatic activity. Many of them derived from nucleotides (White, 1976; Kirschning, 2022). To date, the coenzymes identified at the 5'-end of a RNA are the following: nicotinamide adenine dinucleotide (NAD), flavine adenine dinucleotide (FAD), coenzyme A (CoA), UDP-glucose (UDP-Glc), and uridine diphosphate N-acetyl glucosamine (UDP-GlcNAc)(Figure 9). Among them, 5'-NAD remains the most ubiquitous and best studied coenzyme-derived cap-like structure.

NAD is derived from vitamin B3 (niacin). It plays an important role in energy metabolism and redox reactions, but it can also act as a substrate or cofactor for many other enzymes (Chini *et al.,* 2021; Covarrubias *et al.,* 2021). NAD can exist in an oxidized state (NAD^+) and a reduced state (NADH). Hereafter, NAD^+ is referred as NAD, and NADH is specified. NAD consists of a nicotinamide riboside linked by a pyrophosphate bridge to an adenosine (Figure 9A). 5'-NAD-linked RNAs have first been detected in bacteria (Chen *et al.,* 2009). This came as an unexpected discovery, since only eukaryotic RNAs were thought to be protected at their 5'-end by chemical modification or the addition of a non-encoded residue. Since then, NADylated RNAs have been reported in yeast (Walters *et al.,* 2017), in humans (Jiao *et al.,* 2017), in plants (Wang *et al.*, 2019b; Zhang *et al.*, 2019a), and in archaea (Gomes-Filho *et al.,* 2023).

FAD is derived from vitamin B2 (riboflavin). Like NAD, it is involved in numerous biological processes, mainly encompassing in oxidation and reduction reactions; it can also act as a cofactor for other metabolic enzymes (Walsh and Wencewicz, 2012; Barile *et al.,* 2016). FAD exists in an oxidized state (quinone or FAD), a half-reduced form (semiquinone or FADH) and a fully reduced state (hydroquinone $FADH_2$). FAD consists of a riboflavin linked by a pyrophosphate bridge to an adenosine (Figure 9B).

FADylated RNAs have been detected in bacteria, yeast, and mammals (Wang *et al.,* 2019a).

Coenzyme A is derived from vitamin B5 (pantothenate). It is involved in numerous cellular metabolism pathways such as energy production or biosynthesis of fatty acids and amino acids; coenzyme A can also be covalently attached to protein in response to oxidative stress (Pietrocola *et al.,* 2015; Gout, 2018). Coenzyme A consists of pantethein linked by a pyrophosphate bridge to an adenosine (Figure 9C). Dephospho-CoAlated RNAs in different acylated states (acetyl, succinyl or methylmalonyl) have been detected in bacteria (Kowtoniuk *et al.,* 2009) and in mammals (Shao *et al.,* 2023).

UDP-Glc and UDP-GlcNAC are nucleotide sugars. They are involved in metabolic pathways such as glycolysis in yeast and mammals; they are used as cell wall precursors in bacteria (Mikkola, 2020). They consist of a glucose or a *N*-acetyl glucose linked by a pyrophosphate bridge to an uridine (Figure 9D). They have been identified to be 5'-linked to RNA in bacteria, yeast, and mammals (Wang *et al.,* 2019a).

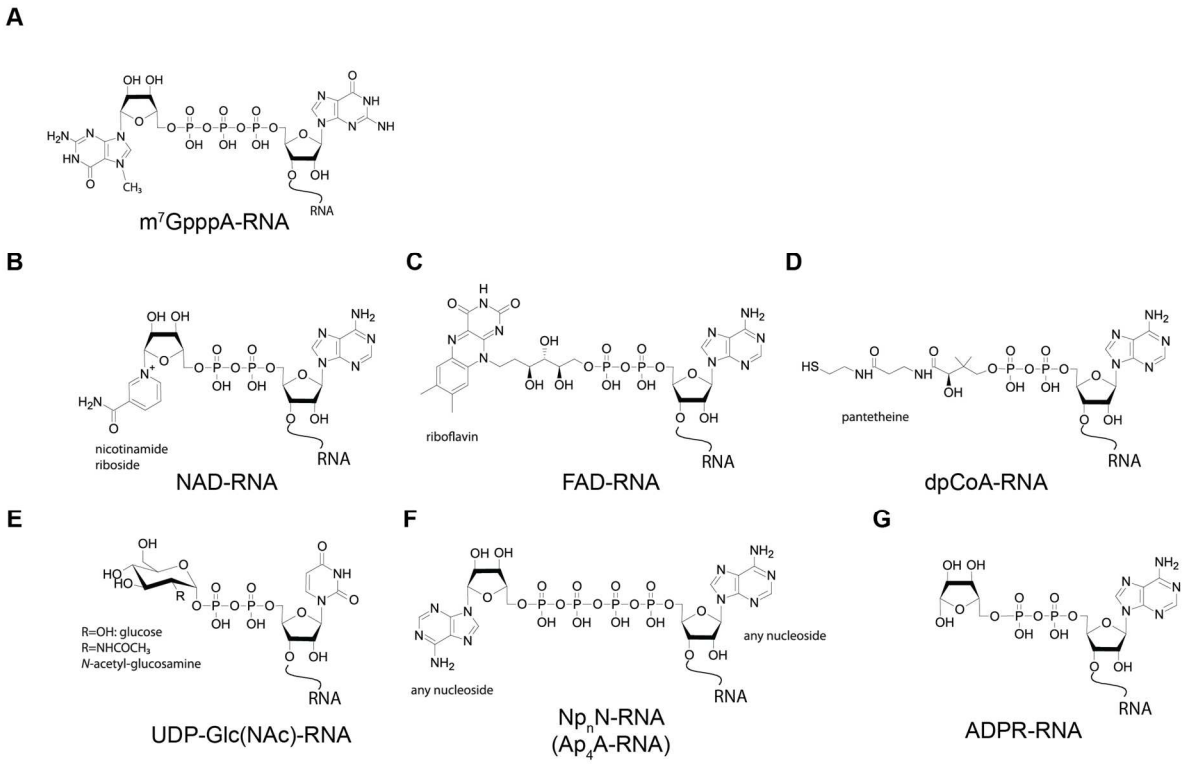

Figure 9. Chemical structures of the various cap-like structures found at the 5'-end of RNA. Structure of the m7G cap 1 structure is shown for comparison. (B) NADylated RNA is similar in size to m7G-capped RNA. NAD can exist in the oxidized form (NAD+) and in the reduced form (NADH). (C) FADylated RNA has a bulky three-ring structure. (D) CoAylated RNA contains a long hydrocarbure chain. Coenzyme A can exist in different acylated states; here, dephospho-CoA is shown. (E) 5'-UDP–glucose-RNA (UDP-N-acetyl-glucosamine-RNA). (F) 5'-NpnN

can have various compositions of nucleotide and phosphate bridge length; here Ap4A is shown as an example. (G) ADP-ribosylated RNA. Adapted from Mattay 2022.

1.3.1.2 Dinucleotide polyphosphate caps

Dinucleotide polyphosphates (Np_nNs) are produced during the loading of amino acids onto tRNAs by certain aminoacyl-tRNA synthetases (Guranowski, 2000). They are also by-products generated during the addition of ubiquitin to proteins, a post-translational modification mark that affect the protein fate, for instance targeting them for degradation (Götz *et al.,* 2019). The intracellular concentrations of dinucleotide polyphosphates are elevated during cellular stress and are thought to act as signaling molecules called alarmones, although their biological functions are still unclear (reviewed in Ferguson *et al.,* 2020; Syal, Rs, and Reddy 2021). They consists of two nucleotides connected by a polyphosphate bridge of several phosphates, whose number varies (Figure 9F).They have been identified at the 5'-end of bacterial RNA with different lengths of the polyphosphate bridge and under different methylated forms as Ap_4N, Ap_3A, m^6Ap_3A, Ap^3G, m^7Gp_4Gm, Ap_5A, and mAp_5G, mAp_4G, mAp_5A, and $^2mAp_5G$ in *E. coli* (Luciano *et al.,* 2019; Hudeček *et al.,* 2020; Luciano and Belasco, 2020). Very recently, Ap_4A has been reported on the 5'-end of RNA in human and rat cell lines (František Potužník *et al.,* 2023).

1.3.1.3 ADP-ribosylation of RNA

ADP-ribosylation is a chemical process in which one or more adenosine diphosphate-ribose (ADP-ribose) groups from NAD are transferred to a substrate. This is a highly conserved post-translational modification of proteins (Palazzo *et al.,* 2017). However, it has recently been discovered that this chemical process can also occur on the terminal phosphate of groups of RNA. Different pools of ADP-ribosylated RNA have been detected in mammalian cells (Weixler *et al.,* 2022), however their exact identity is not yet known (Figure 9G).

1.3.2 An ongoing identification process of NADylated RNAs

1.3.2.1 Detection and quantification of NADylated RNA levels

The first proof of the *in vivo* occurrence of a metabolite linked to cellular RNAs was provided by mass spectrometry analysis of total RNA in *E. coli* and *S. venezuelae* by the Liu lab in 2009 (Chen *et al.,* 2009; Kowtoniuk *et al.,* 2009). They digested total cellular RNA into nucleotides with nuclease P1 (NP1), which hydrolyses RNA by cleaving the phosphodiester link between the nucleotides but does not cleave pyrophosphate and triphosphate linkages. The resulting nucleotide mix (NppN or NpppN) was then analyzed by liquid chromatography–tandem mass spectrometry (LC-MS/MS), allowing the detection of 5'-NAD- and 5'-CoA-linked RNAs.

Building on this approach, CapQuant implemented the addition of cap nucleotide standards and high-performance liquid chromatography (HPLC) enrichment step of the cap nucleotides after NP1 digestion (Wang *et al.,* 2019; 2023). This mass spectrometry-based technique allowed the identification and quantification of cap nucleotides with improved sensitivity and accuracy. When applied to analyze and quantify the cap epitranscriptomic landscape of the polyadenylated RNAs in human lymphoblast cells and mouse tissues, NADylated RNAs were detected with an abundance of 1.9 fmol and 7.1 fmol per µg of RNA in a human lymphoblast cell line and in mouse liver, respectively. NADylated RNAs levels are thus extremely low compared to canonical m^{7}G-capped RNAs levels (Figure 10).

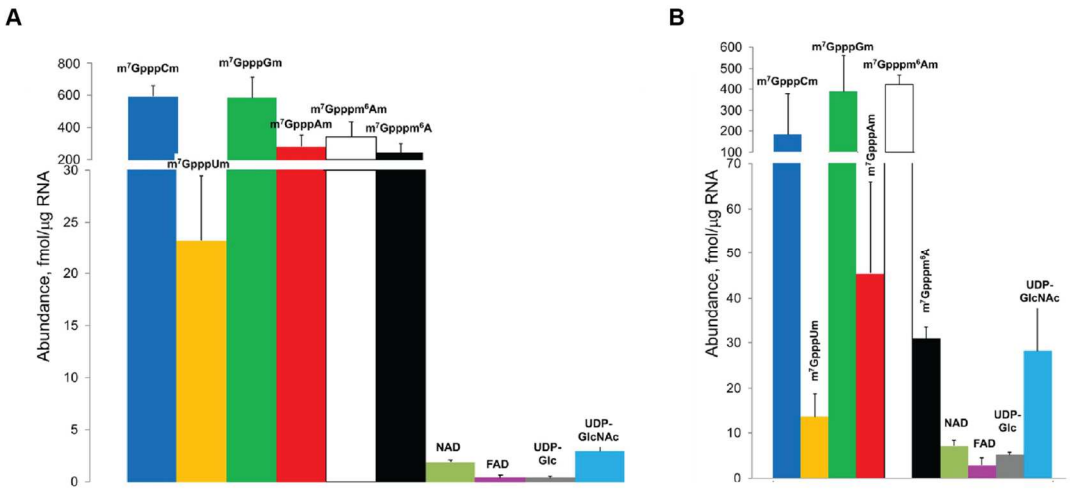

Figure 10. Quantitative analysis of the cap landscape by CapQuant.(A) In human CCRF-SB cells. (B) In mouse liver tissue. Adapted from J. Wang *et al.,* 2019.

1.3.2.2 Sequence-based analysis of NADylated RNAs

Although mass spectrometry-based methods allow the detection and quantification of NADylated RNAs, they do not allow the identification of the transcript sequence. The development of the specific enrichment of NADylated RNAs coupled to next generation-sequencing was a crucial asset for profiling NADylated RNAs. All current capture approaches of NADylated RNAs rely heavily on the use of the *Aplysia californica* adenosine diphosphate-ribosylcyclase (ADPRC) to modify NADylated RNAs combined with click chemistry. Click chemistry is term coined by Kolb *et al.*, (2001) describing efficient and fast chemical reactions that ligate ("click") two molecules together with few or no byproducts.

Cahová *et al.,* (2015) were the first to develop a chemo-enzymatic approach that allows a specific enrichment of NADylated RNAs. First, they used ADPRC to catalyze the replacement of the nicotinamide moiety of NADylated RNAs with a clickable alkynyl group. Then, through a copper-catalyzed, azide–alkyne cycloaddition (CuAAC) reaction, this clickable moiety is conjugated ("clicked") to a biotin-azide derivative (Figure 11A) or to a biotinylated RNA tag-azide (Figure 11B). Finally, the generated biotinylated RNAs can be enriched using streptavidin and sequenced by next-generation sequencing (NAD captureSeq, Cahová *et al.,* 2015). Alternatively, the enrichment step can be bypassed and the samples can be subjected to direct nanopore sequencing (NAD tagSeq, Zhang *et al.,* 2019).

However, later studies highlighted two main shortcomings of this ADPRC-catalyzed, CuAAC-based reaction capture method. First, the use of copper ions as catalyst during the cycloaddition reaction step induces RNA fragmentation (Winz *et al.*, 2017). This led to an accumulation of 5'-ends of abundant RNAs and to the erroneous conclusion that most NADylated RNAs were short and 3'-end truncated (Hu *et al.*, 2021). Therefore, an alternative protocol was developed using a copper-free, strain-promoted, azide-alkyne cycloaddition (SPAAC) reaction. The use of copper ions was avoided to preserve RNA integrity and increase the yield of full-length RNA transcripts. In this case, the ADPRC reaction is carried out with a clickable azide group. This clickable moiety is then clicked to a highly reactive ("strained") biotin-alkyl derivative (Figure 11C) or to a biotinylated RNA-tag-alkyl (Figure 11D). Similarly to the CuAAC-based approach, the biotinylated RNAs can be streptavidin-enriched and

sequenced by next-generation sequencing (SPAAC-NAD-Seq, Hu *et al.,* 2021; NADcapPro, Sharma *et al.,* 2023), or they can be subjected to direct nanopore sequencing when an RNA tag is used (NAD tagSeq II, Zhang *et al.,* 2021).

More recently, the use of a chemical compound containing both a primary alcohol group and biotin allowed to combine the two chemo-enzymatic steps into a single enzymatic reaction, resulting in the biotinylation of the NADylated RNA (ONE-seq, Niu *et al.,* 2023).

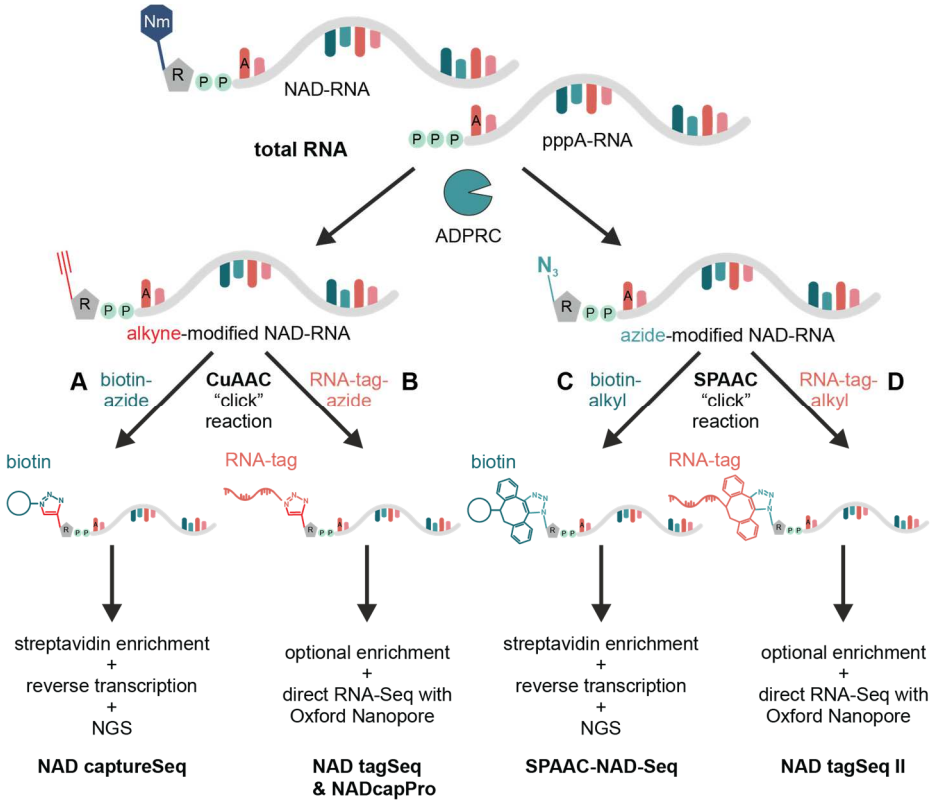

Figure 11. Overview of the main available NADylated RNA capture protocols. (A) NAD captureSeq (Cahová *et al.,* 2015). (B) NAD tagSeq (Zhang *et al.,* 2019). (C) SPAAC-NAD-Seq (Hu *et al.,* 2021) & NADcapPro (Sharma *et al.,* 2023). (D) NAD tagSeqII (Zhang *et al.,* 2021). ADPRC, adenosine diphosphate-ribosylcyclase; Nm, nicotinamide. Adapted from Wolfram-Schauerte and Höfer, 2023.

The second limitation is due to the promiscuous enzymatic activity of ADRPC that can react with m^7G-capped RNA. This side reactivity was not identified in the early development of NADcapture Seq, as this method was applied in a prokaryotic context. Hu *et al.,*(2021) and Zhang *et al.,* (2021) showed that the bond that links the base to the ribose can be subjected to the ADRPC-catalyzed reaction in both m^7G-capped and NADylated RNA. When investigating higher eukaryotic organisms, the low abundance of NADylated RNA compared to m^7G capped RNA needs to be taken into account, since this can lead to high background, false-positive results, and misidentification of

NADylated RNAs. To remedy this problem, recent methods either introduced the prior removal of m^7G-capped RNAs (Hu *et al.,* 2021; Sharma *et al.,* 2023) or a specific elution step of NADylated RNAs after the biotinylation enrichment (Niu *et al.,* 2023).

The ongoing evolution of NADylated RNAs capture methods renders difficult to compare their dataset and results. Past published findings must be carefully evaluated, in regards to the RNA species analyzed (polyA tail selection, RNA size selection) and to the reaction specificity of the method (CuAAC or SPAAC). Ideally, 5'-linked-NAD RNAs need to be validated by other ADPRC-independent methods. In summary, however, most of the identified NADylated across published studies (Table 1) are spliced and polyadenylated, although NADylated RNAs with intron retention have also been identified. Nuclear-, mitochondrial-, and chloroplast-encoded RNAs have been identified. The accumulation of 5'-shorter RNA might be due to a fragmentation bias of the CuAAC method, and with the use of the SPAAC method, full-length NADylated RNAs have been found.

Table 1. Overview of NADylated RNAs identified in eukaryotes and their characteristics. Adapted from Mattay 2022 and extended with data derived from the indicated references.

Organism	RNA type	Quantification	Characteristics	Method	References
Human (HEK293T)	mRNA	Large number, 1% 6%	Spliced, poly(A) tail	NAD captureSeq	(Jiao *et al.*, 2017)
	snoRNA	16 tr.	5'-processed ends	NAD captureSeq	(Jiao *et al.*, 2017)
	scaRNA	9 tr.	5'-processed ends	NAD captureSeq	(Jiao *et al.*, 2017)
	mRNA	188 tr.	Mitochondrial proteins, rRNA processing, histones	NAD captureSeq	(Grudzien-Nogalska *et al.,* 2019)
Mice (liver tissue)	Protein-encoding genes	1500-1631 tr.	Poly(A) RNA More for shorter genes More intron retention No mitochondrial-encoded RNA	ONE-Seq	(Niu *et al.,* 2023)
	ncRNA	117-141 tr.		ONE-Seq	(Niu *et al.,* 2023)
	pseudogenes	203-245 tr.		ONE-Seq	(Niu *et al.,* 2023)
Yeast (*S. cerevisieae*)	Pre-mRNA	37 151 tr.	Intron and exon reads	NAD captureSeq	(Walters *et al.,* 2017)
	mtRNA	4 tr.	5'-unprocessed ends	NAD captureSeq	(Walters *et al.,* 2017)
	mRNA	1460 -3810 tr.	short, 3'-truncated, alternative TSS, variable 5'-UTR	NAD captureSeq	(Zhang *et al.,* 2020)
	snoRNA	2 tr.		NAD captureSeq	(Zhang *et al.,* 2020)
	rRNA	1 tr.		NAD captureSeq	(Zhang *et al.,* 2020)

	mRNA			NAD capture Seq	(Sharma *et al.,* 2022b)
	mRNA	268 tr.	nuclear-encoded mitochondrial protein Poly(A) tail	SPAAC NAD seq	(Sharma *et al.,* 2023)
	mRNA	769 tr.	nuclear-encoded mitochondrial protein Poly(A) tail	NADcapPro seq	(Sharma *et al.,* 2023)
	mtRNA	5 tr.		NADcapPro seq	(Sharma *et al.,* 2023)
Plant (*A. thaliana*)	mRNA	600 tr.	Spliced, poly(A) tail, protein-coding, truncated 5 UTR, no chloroplast-encoded RNA	NAD captureSeq	(Wang *et al.,* 2019b)
	Protein-coding gene	188 tr.	Rubisco most abundant	NAD captureSeq	(Wang *et al.,* 2019b)
	mtRNA	1 tr.		NAD tagSeq	(Zhang *et al.,* 2019)
	rRNA	1 tr.		NAD tagSeq	(Zhang *et al.,* 2019)
	lncRNA	1 tr.		NAD tagSeq	(Zhang *et al.,* 2019)
	mRNA	5642 tr.	M^7G -depleted mRNA, low abundant tr., poly(A), reads distributed along gene bodies, full-length	SPAAC NAD Seq	(Hu *et al.,* 2021)
	mtRNA	8 tr.		SPAAC NAD Seq	(Hu *et al.,* 2021)
	mRNA	3683 tr.	M^7G-depleted mRNA, poly, read enrichment at the 5′ end	CuuAC-NADseq	(Hu *et al.,* 2021)
	mtRNA	4 tr.		CuuAC-NADseq	(Hu *et al.,* 2021)
	mRNA	951 tr.		NAD captureSeq	(Yu *et al.,* 2020)
	snRNA	49 tr.		NAD captureSeq	(Yu *et al.,* 2020)
	snoRNA	7 tr.		NAD captureSeq	(Yu *et al.,* 2020)
	lncRNA	26 tr.		NAD captureSeq	(Yu *et al.,* 2020)
	rRNA	1 tr.		NAD captureSeq	(Yu *et al.,* 2020)

Abbreviations: mRNA, messenger RNA; mtRNA, mitochondrial RNA; ncRNA, non-coding RNA; rRNA, ribosomal RNA; scaRNA, small Cajal body-specific RNA; snRNA, small nuclear RNA; snoRNA, small nucleolar RNA; tr, transcripts.

1.3.3 Biosynthesis, translation potential, and degradation of eukaryotic NADylated RNAs

1.3.3.1 Stochastic process or functional capping of NADylated RNA?

Two mechanisms have been considered for the biosynthesis of NADylated RNA: *ab initio* capping and post-transcriptional capping.

Initiation of transcription with NAD instead of adenosine triphosphate (ATP) by DNA-dependent RNA polymerase is considered as the main pathway for generating cellular NADylated RNAs, and this mechanism is supported by several *in vitro* studies. The ability of *E. coli* RNA polymerase (RNAP) to use adenosine-derived coenzymes as initiating nucleotides for *in vitro* RNA synthesis has been known for a few decades already (Malygin and Shemyakin, 1979). The authors highlighted at that time the striking similarity of the 5'-end structure between a 5'-NAD-RNA and a m^7G-capped RNA, and they suggested that cytoplasmic nucleotide-containing coenzymes could be involved in RNA synthesis initiation in *E. coli*. However, it is only thirty years later that their work gained significance with the discovery of NADylated RNAs *in vivo* (Chen *et al.,* 2009). Bird *et al.,* (2016) showed that NAD can not only be used by *E. coli* RNAP to initiate transcription, but also that the resulting initial RNA product can be extended to a full-length RNA product. This incorporation is promotor-dependent and sequence-specific: because NAD share the same Watson-Crick base pairing preference as ATP, initiation occurs with a +1A promotor (Bird *et al.,* 2016). This ability to incorporate nucleotide-containing metabolites at the 5'-end is shared by eukaryotic RNA polymerases. *S. cerevisiae* RNA Pol II can initiate *in vitro* transcription with NAD (Bird *et al.,* 2016). Both yeast and human single-subunit mitochondrial RNAP (mtRNAP) are able to initiate transcription with NAD *in vitro* too, and with a higher efficiency than their nuclear equivalents (Bird *et al*, 2018). In line with these *in vitro* data, Bird *et al.,* (2016) could demonstrate that transcription initiation with NAD as the non-canonical initiating nucleotide occurs *in vivo* in *E. coli*, and that the efficiency of initiation is determined by the promoter sequence.

It is still unclear whether transcription initiation with NAD occurs simply for stochastic reasons or whether it is a regulated event. It could be that the ratio of intracellular ATP to other ATP-analogues might affect the chance for NAD entry into the active site of the polymerase. For example, in *E. coli* the intracellular concentration of NAD (2.3 mM) is higher than its affinity for initiation transcription by RNAP (100–400 µM) (Julius and Yuzenkova, 2017). In yeast, changes in the NAD levels were reflected by changes in mitochondrial NADylated RNA levels; the same outcome was observed in human cells (Bird *et al.,* 2018). To be noted, only one chloroplast-encoded NADylated RNA has been detected up to date (from a rRNA gene in *A. thaliana*, (Zhang *et al.,* 2019)), which could be either explained by the weak ability of the chloroplast

RNA polymerases to use NAD as an initiating nucleotide or by the low level of free NAD in chloroplasts. In human cells, results are more conflicting: the increase or decrease of the cellular NAD concentration led to a similar effect on the level of NADylated RNAs (Grudzien-Nogalska *et al.,* 2018), however in a later report (Grudzien-Nogalska *et al.,* 2019) observed that upon environmental stress, some NADylated RNAs increased while cellular NAD levels did not show a similar increase. This would suggest that, in part, not all NADylated RNAs are a result of NAD concentration.

The existence of a post-transcriptional capping mechanism with NAD has been hypothesized due to the identification of intron-encoded NADylated snoRNAs and scaRNAs (Jiao *et al.,* 2017). Since these RNAs are intronic and their processing generates a 5'-monophosphorylated end, their enrichment could not be explained by the promiscuous activity of ADRPC on a m^7G cap, yielding a false positive result. In addition, the identification of spliced RNAs or 5'-UTR truncated RNAs in several sequencing experiments (Table 1) also raised questions about the existence of a cytoplasmic NADdylation event. However, no dedicated enzyme or complex able to modifying post-transcriptionally RNAs to NADylated RNAs has been identified up to date.

1.3.3.2 Translatability potential of NADylated RNAs

Considering the critical role of the m^7G cap in recruiting various cap-binding factors, the presence of NAD at the 5'-end of the RNA raises questions whether or how NADylated RNAs could interact with the RNA processing and translation machineries.

To investigate the translatability potential of NADylated RNA, Jiao *et al.,* (2017) co-transfected *in vitro* generated NADylated and m^7G-capped luciferase RNA into human cells, and performed a luciferase assay. No luciferase activity was detected for the NADylated RNA. In line with these results, a luciferase assay performed by incubating *in vitro* generated NADylated RNA in a cell-free yeast extract did not show translation either (Zhang *et al.,* 2020). Surprisingly, Wang *et al.,* (2019) detected NADylated RNAs in actively translating polysomes in plants. However, this was only characterized by using an ADPRC-dependent method, and therefore a promiscuous activity of ADPRC on m^7G-capped RNA cannot be ruled out. In yeast, mass spectrometry analysis of

proteins associated with the 5'-NAD cap upon pulldown did not reveal any proteins involved in cellular translation (Sharma *et al.,* 2022b). Furthermore, Sharma *et al.,* (2023) detected cellular polyadenylated NADylated RNA only in the free pool of ribosomes by polysome profiling. Although a cap-independent translation mechanism cannot be excluded (alternative mechanisms are reviewed in Shatsky *et al.,* 2018), collectively these data rather suggest that cytoplasmic NADylated RNA are not engaged in translation in eukaryotes.

Interestingly, mitochondrial protein-coding NADylated RNA has been found to be associated with translationally active mitochondrial ribosomes in yeast by Sharma *et al.,* (2023). Mitochondrial RNAs are transcribed into a single long polycistronic transcript that is further cleaved and processed. They do not possess a 5'-cap, and therefore, contrary to cytoplasmic mRNA translation, there is no requirement for cap binding factors for translation initiation (Kummer and Ban, 2021). Sharma *et al.,* (2023) suggested that that might explain why NADylated RNAs are engaged by mitochondrial ribosomes and could be at least tolerated, if not translated.

1.3.3.3 A diverse decapping machinery for NADylated RNAs

Unlike the m^7G cap, which protects and stabilizes the RNA, the 5'-NAD modification appears to act as a targeting signal for RNA degradation. The canonical decapping enzyme Dcp2 is not able to cleave within the pyrophosphate linkage of NADylated RNA (Jiao *et al.,* 2017). Instead, two main classes of conserved proteins have been identified that are able to remove the 5'-NAD from NADylated RNA by different mechanisms: on the one hand, the Nudix hydrolase Nudx in bacteria, its yeast homolog Npy1 and its mammalian homolog Nudt12; on the other hand, the DXO/Rai1 proteins in yeast and mammals (Figure 12).

NudC, Npy1, and Nudt12 belong to the Nudix hydrolase family, and are thus related to the canonical decapping enzymes Dcp2, Nudt16 and Nudt3 (1.2.4.1.). NudC, Npy1 and Nudt12 cleave the pyrophosphate bond within NAD, generating a 5'-monosphosphorylated RNA that starts with an adenosine and releases NMN (Höfer *et al.*, 2016b; Zhang *et al.*, 2016; Grudzien-Nogalska *et al.*, 2019; Wu *et al.*, 2019; Zhang *et al.*, 2020). The decapping enzymes Rai1 and Dxo1 in yeast, and DXO in mammals are already known for being involved in 5'-end capping quality control (see 1.2.4.3)

(Jiao *et al.,* 2010, 2013; Chang *et al.,* 2012). They remove the entire NAD moiety by hydrolyzing the phosphodiester link between NAD and the first nucleotide of the RNA, generating a 5'-monophosphorylated RNA and releasing NAD (Jiao *et al.,* 2017; Grudzien-Nogalska *et al.,* 2018).

In yeast, Zhang *et al.,* (2020) proposed a surveillance mechanism against NADylated RNAs, relying on the Rai1, Dxo1, and Npy1 deNADding proteins. Rai1 is known to be associated with the RNA Pol II elongation complex in the nucleus (Harlen and Churchman, 2017a) and Dxo1 is localized both in the nucleus and in the cytoplasm (Chang *et al.,* 2012). NAD captureSeq sequencing in mutant yeast strains showed that these three enzymes target both different and overlapping subsets of NADylated RNA (Zhang *et al.,* 2020). These data and the different subcellular localization of the identified deNADding enzymes led (Zhang *et al.,* 2020) to suggest a hierarchical surveillance model in which nuclear Rai1 and Dxo1 would target NADylated RNAs in the nucleus, and cytoplasmic Dxo1 and Npy1 would target NADylated RNAs that would be present in the cytoplasm.

While this spatial and temporal hierarchical pathway has not yet been formally demonstrated in mammals, these enzymes and their deNADding activity are conserved and their subcellular localization is similar. DXO also has deNADding activity (Jiao *et al.,* 2017). Nudt12, the homolog of the bacterial deNADding enzyme NudC (Grudzien-Nogalska *et al.,* 2019; Wu *et al.,* 2019) was initially characterized as a peroxisomal protein when overexpressed with a C-terminal GFP tag (Abdelraheim *et al.,* 2003). However, in human cells, Wu *et al.,* (2019) identified a complex formed between Nudt12 and Bleomycin Hydrolase (BLMH) in a few cytosolic granules. BLMH is a cysteine peptidase (Akiyama *et al.,* 1981) but its role beyond binding Nudt12 is unclear, since human BLMH does not bind nucleic acids (O'Farrell *et al.,* 1999) and has no influence on Nudt12 activity (Wu *et al.,* 2019). Transfected NADylated RNA in human Nudt12 and DXO knockout cells were found to be more stable, while m^7G-capped RNA stability remained unchanged compared to control and knockout conditions (Jiao *et al.,* 2017). NADcapture Seq analysis of Nudt12 and DXO knockout cells indicated that DXO and Nudt12 target different populations of NADylated RNA, with DXO targeting more snoRNAs and scaRNAs, and Nudt12 preferentially

deNADding histones mRNAs and nuclear-encoded mRNAs coding for mitochondrial proteins (Jiao *et al.,* 2017).

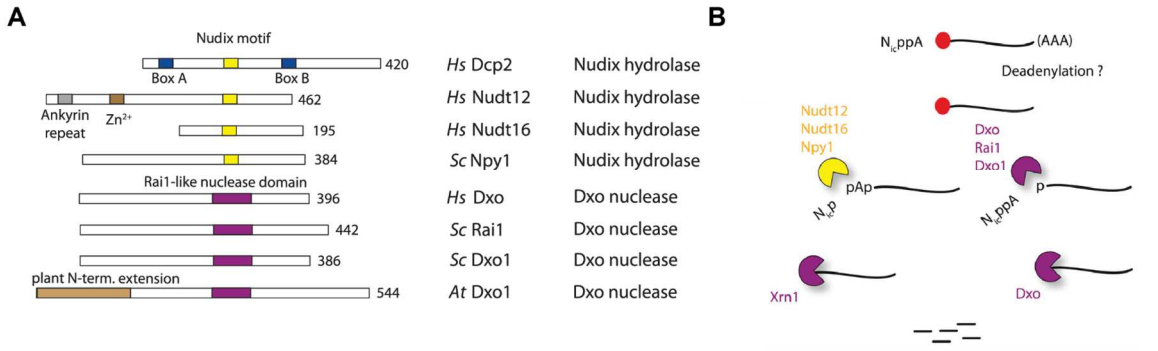

Figure 12. Eukaryotic NADylated RNA turnover. (A) Schematic representation of deNADding enyzmes mentioned in the text. Proteins with decapping activity are aligned relative to their Nudix motif or Dxo nuclease domain. The canonical decapping enzyme Dcp2 is indicated as a comparison. (B) Decay of NADylated RNAs proceeds through either Nudix hydrolases or Dxo exoribonucleases. Nudix hydrolases cleave within the diphosphate link of NADylated RNA, generating a monophosphorylated RNA, and releasing NMN. Dxo proteins remove the entire NAD moeity, generating a monophosphorylated RNA and releasing NAD. Monophosphorylated RNA can be degraded either by the 5'-3' exoribonucleoase activity of Dxo proteins or XRN1. In yellow, Nudix hydrolase domain; in violet, Dxo nuclease domain. *At, Arabidopsis thaliana; Hs, Homo sapiens; Sc, Saccharomyces cerevisiae.* Adapted from Mattay 2022.

Furthermore, mouse Nudt16 was shown to possess *in vitro* deNADding enzymatic activities (as well as deFADing and dpCoAping activities) and Nudt16 knockout human cell lines exhibited a moderated increase in NADylated RNA levels; however, its specific targets are not known (Sharma *et al.,* 2020). Recently, Sharma *et al.,* (2022) identified a deNADding activity for the yeast Xrn1 upon high concentration in addition to its canonical 5'-3' exoribonuclease activity (Sharma *et al.,* 2022; 2023). Thus, the identification of enzymes able to cleave NADylated RNAs and their specificity is still ongoing.

1.4 AIM OF THIS THESIS

The cap structure at the 5'-end of cellular RNAs plays a crucial role in post-transcriptional gene regulation. Recently, the presence of coenzymes, including the redox cofactor NAD, at the 5'-end of RNA in bacteria and eukaryotes has been uncovered. The biological significance and function of these so-called "cap-like structures" remains poorly understood. The detection and identification of NADylated RNAs have been made possible by the continuous development and improvement of capture methods. However, the most commonly used identification and sequencing

methods rely on the prior modification of the NAD moiety, which is associated with several limitations and biases. Therefore, this thesis aims to explore alternative approaches to enrich NADylated RNAs and investigate their biological functions in a relevant context.

2 RESULTS

2.1 SYNTHESIS OF MODEL NADYLATED RNA

For the establishment and testing of different RNA capture methods, sufficient amounts of NADylated RNA were needed. However, unlike other 5'-end modifications, 5'-NAD-modified RNAs were not commercially available. Therefore, we set out to generate NADylated RNA in the lab. So far, no enzyme that catalyzes the modification of 5'-NAD has been identified that would allow a post-transcriptional enzymatic capping of an RNA body, as can be easily done for the m^7G cap by the vaccinia capping enzyme complex (Fuchs *et al.,* 2016). NADylated RNA can be generated by two methods: either by co-transcription (Huang, 2003) or by chemical synthesis (Höfer *et al.,* 2016).

2.1.1 Co-transcriptional incorporation of NAD

In vitro transcription by T7 RNA polymerase produces RNA transcripts from a DNA template harboring a 5'-T7 RNA polymerase promoter. The use of the T7 class II (ϕ2.5) promotor allows transcription to be initiated by ATP, instead of the most commonly used GTP-initiating class III (ϕ6.5) promotor (Dunn *et al.,* 1983). Due to its adenosine group, NAD can be used as an initiating nucleotide in place of ATP by the T7 RNA polymerase for transcription, generating 5'-NAD-linked RNA (Huang, 2003). When supplementing a mix of nucleotides with NAD, the transcription by the T7 polymerase generates a mixture of triphosphorylated and NADylated RNAs (Figure 13A). In contrast, N^7-methylguanosine-capped RNA can be easily obtained by post-transcriptional capping with the commercially available Vaccinia Capping System (NEB), based on the heterodimer vaccinia virus capping enzyme.

Separation of the different RNA species according to their 5'-ends can be achieved by boronate affinity electrophoresis (Nübel *et al.,* 2017). Boronic acids form reversible covalent bonds with *cis*-diol groups (Figure 13B). This property can be exploited to study the RNA ends, when acryloylaminophenyl boronic acid (APB) is co-polymerized into a standard denaturing urea polyacrylamide (PAA) gel (Igloi and Kössel, 1987).

Transient interactions occurs between the supplemented boronyl groups and the free diol groups of the ribose moiety present in the 5'-NAD or the diols of m^{7}G cap structure (Figure 13C). Thus, NADylated RNA and m^{7}G-capped RNA have lower electrophoretic mobility on a APB gel compared to a triphosphorylated RNA of the same sequence (Igloi and Kössel, 1987; Nübel *et al.,* 2017).

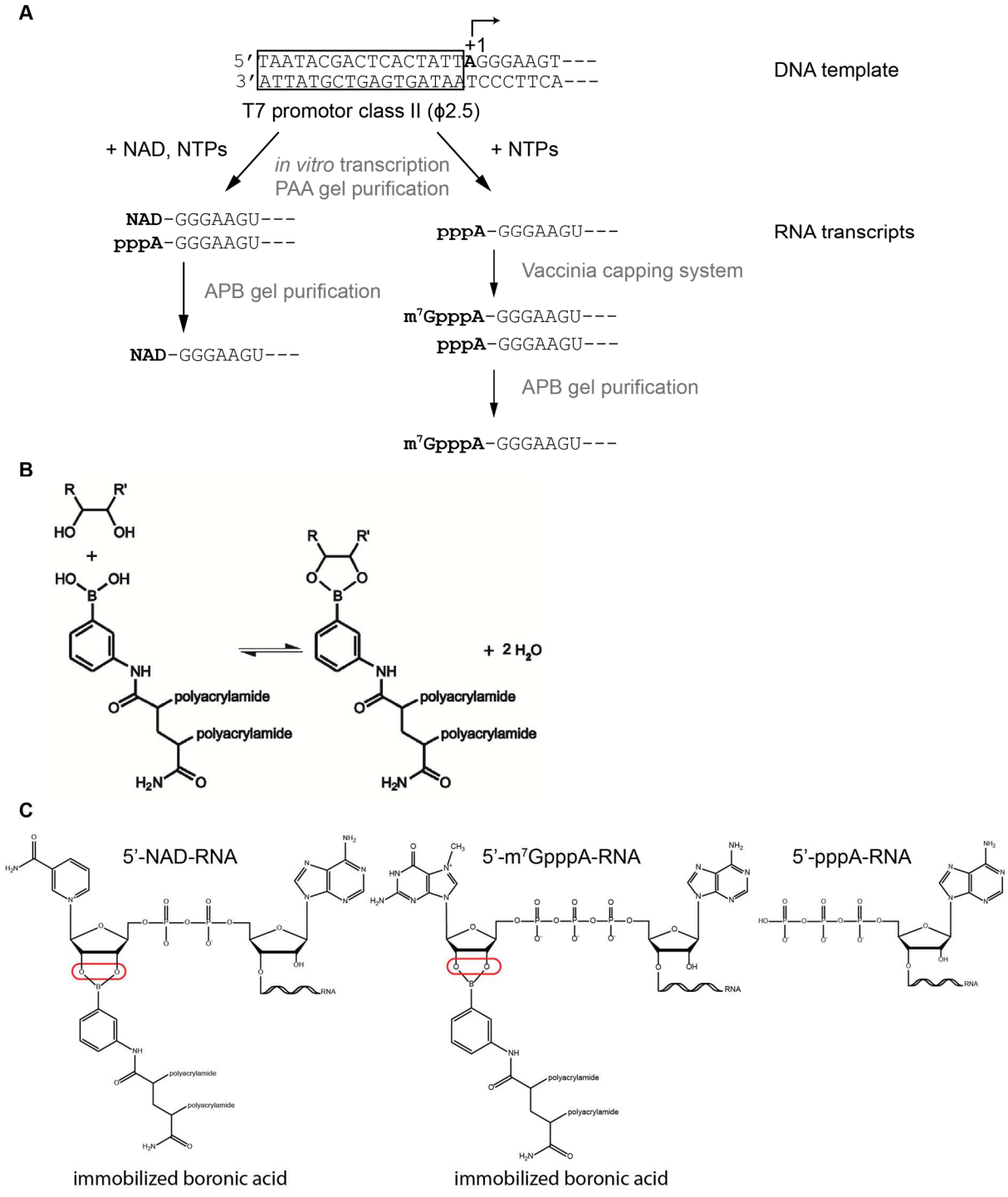

Figure 13. *In vitro* transcription of 5'-NAD-RNA, m^{7}G-capped RNA and 5'-ppp-RNA. (A) With the addtion of NAD in the transcription reaction mix, in vitro transcription by the T7 class II promoter produces a mixture of

NAD-RNA and pppA-RNA. RNA is purified according to size by standard denaturing polyacrylamide (PAA) gel electrophoresis. The m7G cap structure is added by the Vaccinia capping system to the ppp-RNA. The different RNA species are separated according to their 5'-end by acryloylaminophenyl boronic acid (APB) gel electrophoresis. (B) Interaction of immobilized aminophenyl boronic acid with cis-diols. Adapted from (Nübel et al., 2017). (C) Interaction (in red) of immobilized aminophenylboronic acid with the cis-diol groups present in the NAD moeity of a NADylated RNA and in the cap structre of a m7G-capped RNA, but not with a triphosphorylated RNA.

We synthesized our model RNA by *in vitro* transcription of a synthetic double-stranded DNA template containing the T7 ϕ2.5 promotor containing an adenosine at the transcription start and encoding for a 62-nucleotide long transcript sequence (T7ϕ2.5-A-62 DNA as designed in Winz *et al*, 2017). NAD was supplemented (lane 1) or ATP was only used (lane 2) as the initiating nucleotide in the transcription mix. The *in vitro* transcription reaction products were purified by PAA gel electrophoresis to separate the RNA of interest from other by-products (Figure 14A), then run on a APB gel to separate NADylated RNAs from triphosphorylated RNAs (Figure 14B) The purified triphosphorylated RNAs were capped with the Vaccinia Capping System (NEB), then run on a APB gel to separate between m^7G-capped RNAs and triphosphorylated RNAs (Figure 14C). Finally, the different purified RNA species were evaluated on a standard denaturing gel and a APB gel (Figure 14D). While the samples ran at the same size on a standard denaturing polyacrylamide gel (Figure 14D, top panel), a shift in their mobility due to their different 5'-end was observed by APB gel electrophoresis (Figure 14D, bottom panel), with NADylated RNA exhibiting the strong retard (lane 1), followed by the m^7G-capped RNA (lane 2), then their triphosphorylated counterpart (lane 3).

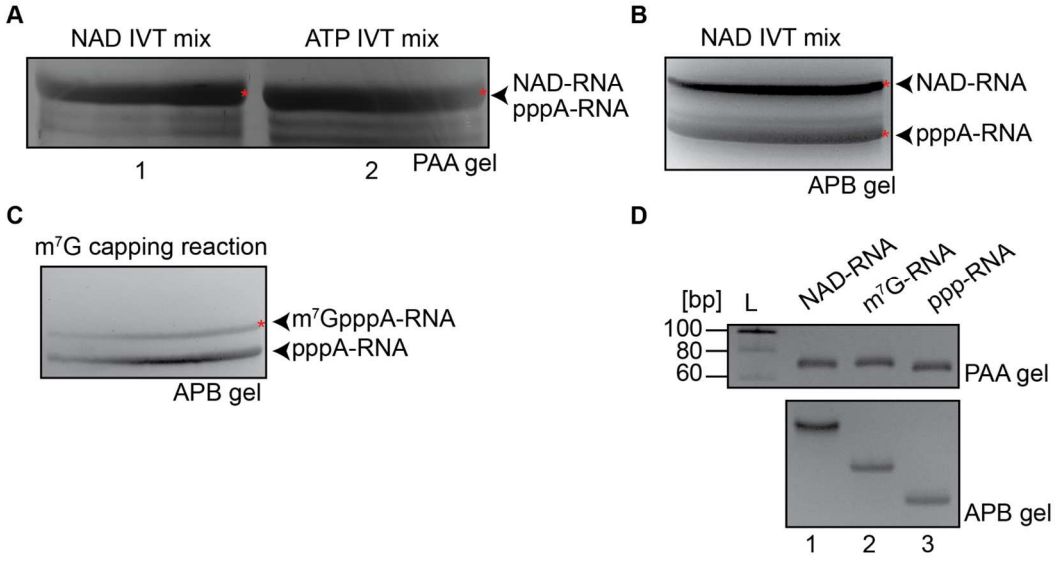

Figure 14. Gel purification and analysis of *in vitro* transcribed RNAs. (A) Separation of crude *in vitro* products on a preparative 12% PAA gel, vizualized by UV shadowing. (B) Separation of purified NAD-/ppp-RNA mixture on

a 0.2% APB preparative gel, stained with ethidium bromide. (C) Separation of m^7G-/ppp-RNA after capping on a 0.2% APB preparative gel, stained with ethidium bromide. (D) Purification and integrity of RNA are checked on 8% PAA (top) and 0.2% APB analytical gels (bottom) by ethidium bromide staining. NAD-RNA, m^7G-RNA and ppp-RNA show the same mobility on a PAA gel, while exhibiting differential retardation on a APB gel. Red (*) indicate gel bands that were excised for RNA elution.

To be noted, the first denaturing PAA gel step (Figure 14A) can be bypassed and the crude *in vitro* reaction can be run directly on an APB gel, as we did in our first attempts. However, this prevents to separate the possible abortive or run-off in vitro transcribed products, and therefore, we recommend to always perform a first denaturing polyacrylamide gel purification step.

2.1.2 Chemical synthesis of NADylated RNA

An alternative way to attach a nicotinamide riboside to an existing RNA molecule can be achieved by phosphorimidazolide chemistry. This method was developed by Höfer *et al.,* (2016) and is based on the reaction of 5'-monophosphate RNA with an activated nicotinamide mononucleotide (Im-NMN) (Figure 15A).

The implementation and optimization of chemical NAD-RNA synthesis and HPLC analysis were performed by R. Hett. A 5'-monophosphorylated RNA 5-mer (obtained by solid-phase synthesis) was converted to a 5'-NAD-RNA by reacting with Im-NMN. The total length of the RNA was small enough that the HPLC analysis of the product could detect the conversion from 5'-p-RNA to 5'-NAD-RNA (Figure 15B). This could also be applied to a monophosphorylated RNA produced by *in vitro* transcription. By using a DNA template containing the T7ϕ2.5 promotor with an adenosine at the transcription start site and encoding an A-less sequence (T7 ϕ2.5 A-31, as designed in Hu *et al.*, 2021), while using adenosine monophosphate (AMP) as an initiating nucleotide in the nucleotides mix, we ensured the transcription of a 5'-monophosphorylated RNA starting with an adenosine. After running the product obtained by imidazolide reaction on a APB gel, a shift due to the addition of 5'-NAD to the monophosphorylated RNA was observed (Figure 15C, lane 2).

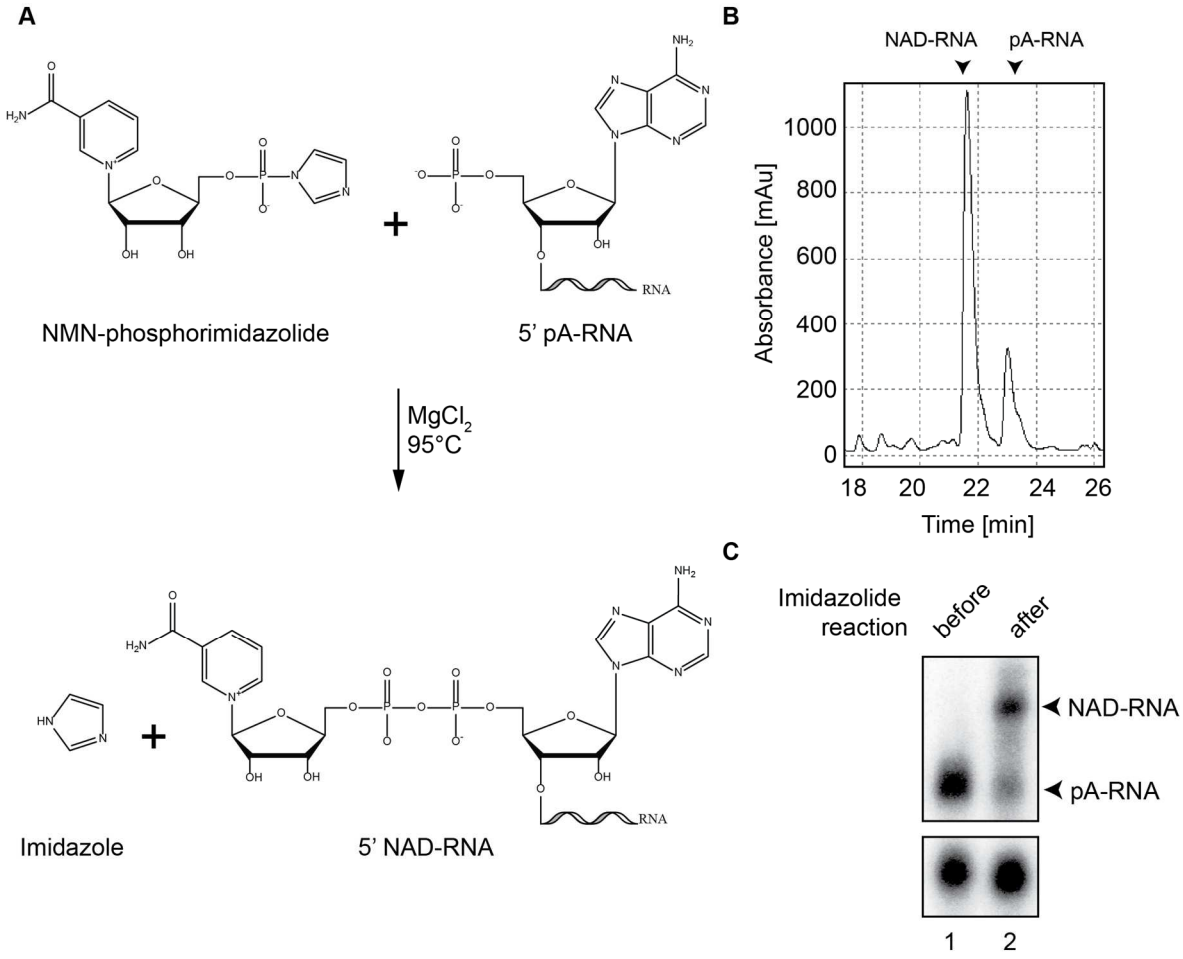

Figure 15. Chemical synthesis of 5'-NAD-RNA by phosphorimidazolide coupling. (A) Schematic of the coupling reaction of NMN-phosphorimidazolide with the free phosphate of a 5'-p-RNA in aqueous solution in the presence of $MgCl_2$. (B) HPLC analysis of the the reaction product. Peak at 21.9 min correspond to 5'-NAD-5mer RNA. (C) Gel analysis of 30-mer RNA 3'end-radiolabeled on 0.2% APB gel (top) and 8% PAA gel (bottom). The mobility shift corresponding to the addition of 5'-NAD to the p-RNA was detected after the imidazolide reaction (lane 2).

However, for the chemical addition of NAD onto longer RNAs containing internal adenosines, two points need to be considered. First, the triphosphorylated RNA obtained by IVT needs to be enzymatically converted to a monophosphorylated form prior to coupling. Second, the phosphorimidazolide coupling reaction requires subsequent clean-up, either by APB gel purification or enzymatic digestion of unreacted monophosphate RNA. For handling reasons, we decided to produce the further RNAs used in this thesis with the IVT-based strategy.

2.1.3 Validation of 5'-NAD-linked RNA

Next, we confirmed that we produced 5'-NADylated RNA by assays independent of an APB gel electrophoresis to rule out the possibility that the observed mobility shift was

due to other factors (such as heterogeneity in the RNA sequence or interactions from the 3'-end).

First, we performed 5'-end analysis of our *in vitro* RNA generated by sequential treatment with RNA 5' Polyphosphatase (Rpp) and XRN-1. Rpp processes 5'-triphosphorylated RNA to 5'-monophosphorylated RNA by cleaving the phosphodiester bond between α and β phosphates. XRN-1 is a 5'-3'-exonuclease that digests 5'-monophosphorylated RNA (Figure 16A).

Rpp treatment followed by XRN-1 digestion degraded the triphosphorylated RNA sample (Figure 16B, lane 7) while the NADylated RNA sample was protected from XRN-1 degradation by its 5'-NAD modification (lane 2).

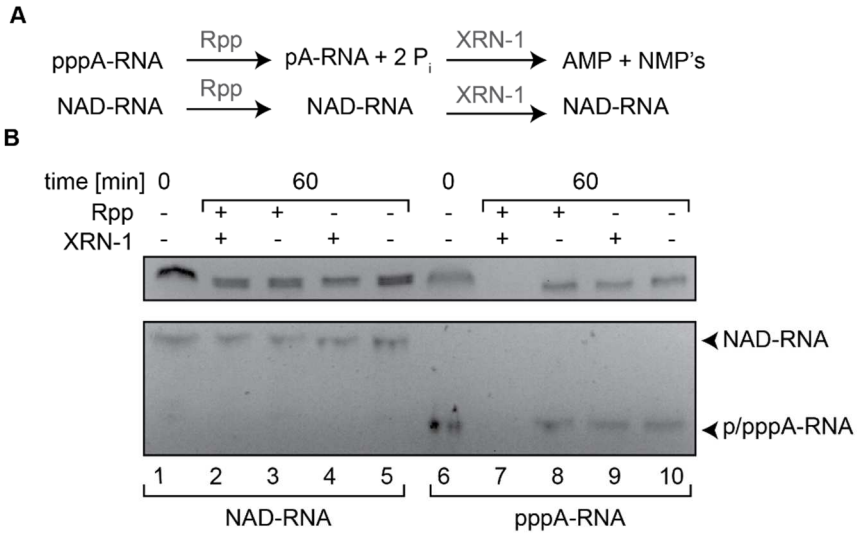

Figure 16. Analysis of the 5'-ends of RNA generated *in vitro*. (A) Schematic representation of RNA 5' Polyphosphatase (Rpp) processing and XRN-1 degradation of 5'-NAD-RNA and 5'-ppp-RNA. (B) NAD-RNA and ppp-RNA were treated sequentially by Rpp/XNR-1 for 1 h each. The reaction was split in two and RNA were resolved on a 8% PAA gel (top) and a 0.2% APB gel (bottom).

Second, we wanted to confirm that this 5'-end protection was indeed due to the incorporation of NAD. The reaction of *N*-alkylpyridinium with ketone molecules followed by heating in excess acid produces a fluorescent compound. Therefore, NMN and NAD can be converted into a highly fluorescent derivative, a strategy that has previously been applied to monitor the enzymatic activity of NAD-consuming enzymes (Putt and Hergenrother, 2004). The fluorescence reaction has a linear correlation with the NAD concentration and can be detected by a spectro-fluorometric readout.

We adapted this derivatization approach for a fluorometric detection of NADylated RNA upon reaction with acetophenone/NaOH and formic acid (Figure 17A). Upon derivatization, a fluorescent signal was detected for the NADylated RNA sample, which increased proportionally with the amount of input NAD-RNA. The signal detected in triphosphorylated RNA sample was indistinguishable from the background signal (Figure 17B).

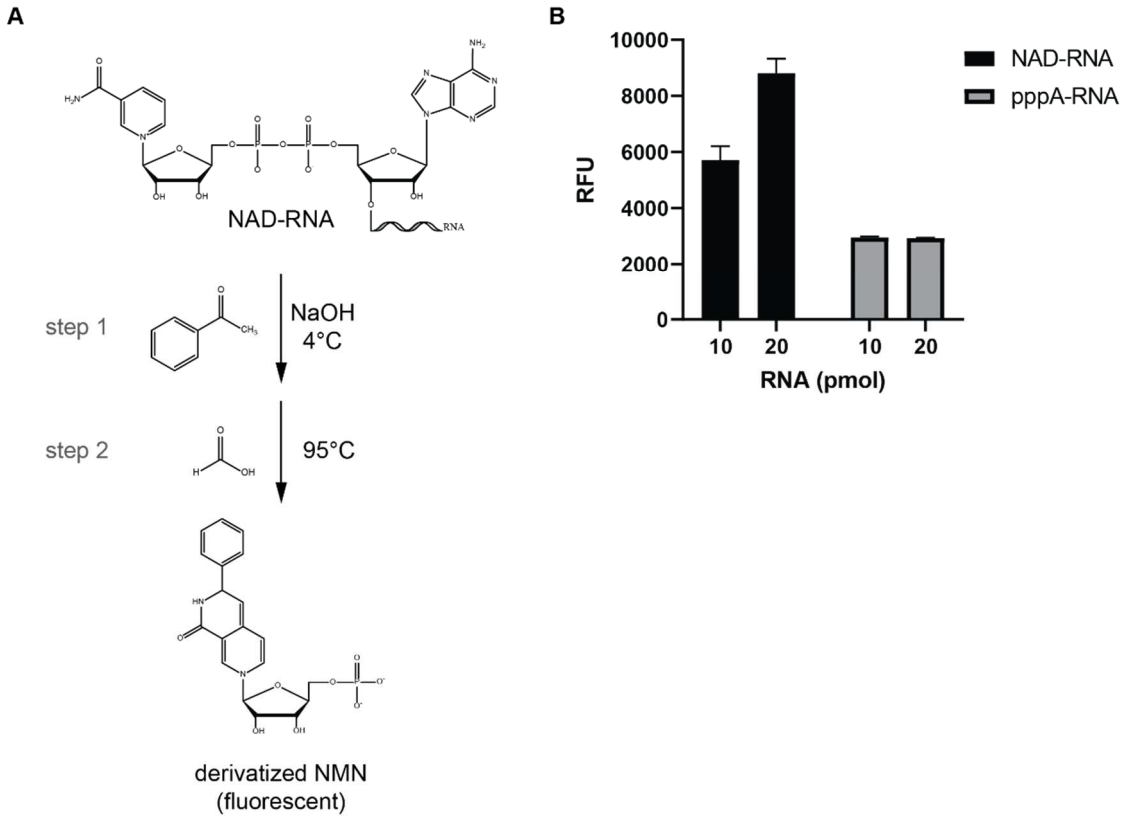

Figure 17. Fluorescent derivatization of NAD-RNA. (A) The NMN moety is converted into a fluorescent compound upon reaction with acetophenon followed by heating in excess of formic acid. (B) Fluorometric analysis of NAD-RNA (black) and ppp-RNA (gray) generated in vitro.

Taken together, these assays allowed us to confirm that we successfully generated and purified 5′-NAD-modified RNAs that can be used for further studies.

2.2 DEVELOPMENT OF A NADYLATED RNA CAPTURE METHOD

One of the issues encountered in current NADylated RNA enrichment protocols is specificity (covered by (Möhler and Jäschke, 2023). We aimed to develop a protocol that would combined capture and deNADding approaches (Figure 18), by first

enriching NADylated RNAs, then performing an enzymatic treatment of enriched NADylated RNAs would yield a 5'-monophosphate RNA. This phosphate group could then be used for the 5'-ligation of an adapter and subsequent preparation of a NGS library for the identification of NADylated RNA sequences.

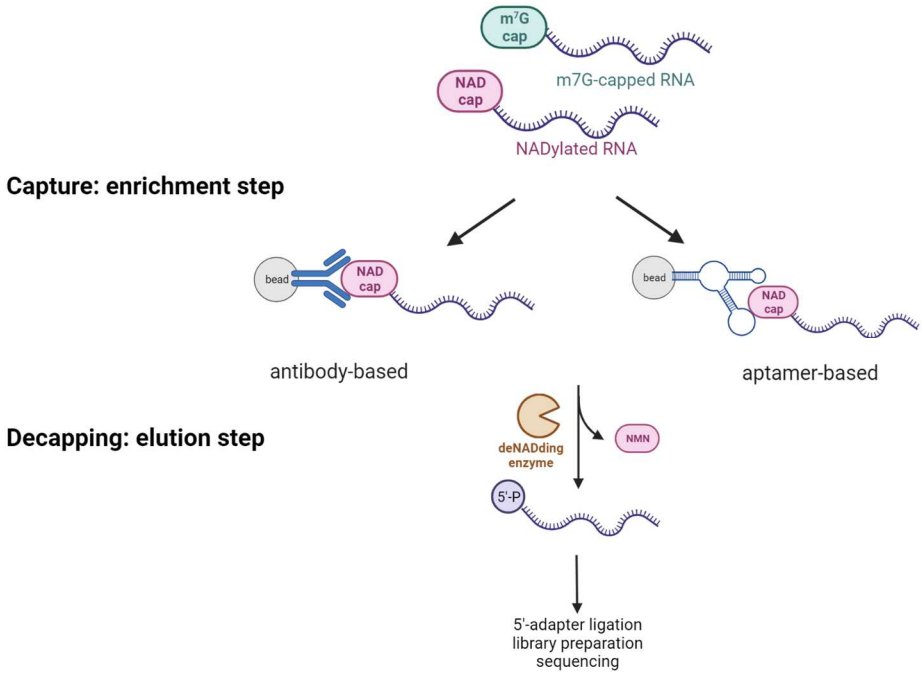

Figure 18. Overview of the NADylated capture-decapping approach. We aimed to establish a method to specifically capture NADylated RNAs over m^{7}G-capped RNAs either by an antibody or an aptamer that recognizes and binds the NAD moeity. The enriched RNA could then be eluted by cleaveage with a specific deNADding enzyme, which would generated a 5'-monophosphorylated RNA that could be available for subsequent preparation of NGS libraries.

2.2.1 Decapping approach

2.2.1.1 Selection of a suitable deNADding enzyme

Several decapping enzymes that cleaves NADylated RNA *in vitro* have been identified in recent years. They can be divided into three classes depending on their substrate and mode of cleavage. Among them, we wanted to select an enzyme that would specifically cleave 5'-NAD and generated a 5'-monophosphorylated RNA. Several enzymes caught our attention (Table 2, Figure 19).

Table 2. DeNADding enzymes identified to date and their *in vitro* decapping activity on capped-RNA.

Class	Substrate → Product	Enzyme	Decapping activity on capped-RNA *in vitro*					References
			NAD-	FAD-	dpCoA-	m^{7}GpppA-	GpppA-	
1	NRppA-RNA → NRppA + pRNA	Rai1 (*Sp*)	++	++	+	-	nt	(Jiao *et al.*, 2017; Doamekpor *et al.*, 2020b;

	and NRppA → NRp + pA						Sharma *et al.,* 2022b, 2022a)
		Npy (*Sc*)	++	nt	++	-	nt	(Zhang *et al.,* 2016, 2020; Zhou *et al.,* 2021)
		Dxo1 (*Kl*)	++	++	++	+	nt	(Jiao *et al.,* 2017; Doamekpor *et al.,* 2020b)
		Dxo1 (*At*)	++	nt	nt	-	nt	(Pan *et al.,* 2020)
		Dxo (*Mm*)	++	++	++	+	nt	(Jiao *et al.,* 2017; Doamekpor *et al.,* 2020b; Sharma *et al.,* 2020)
		Rat1 (*Sp*)	++	+	nt	-	nt	(Sharma *et al.,* 2022a, 2022b)
		Xrn1 (Hs)	+	+	nt	nt	nt	(Sharma *et al*, 2022b, 2022a)
		Xrn1 (Sc)	++	nt	nt	nt	nt	(Sharma *et al.,* 2022)
		Xrn1 (Kl)	++	++	nt	-	nt	(Sharma *et al.,* 2022b, 2022a)
2	NRppA-RNA → NRp +pA-RNA	NudC (*Ec*)	++	nt	++	+	nt	(Cahová *et al.,* 2015; Höfer *et al.,* 2016b; Zhang *et al.,* 2016; Grudzien-Nogalska *et al.,* 2019; Zhou *et al.,* 2021)
		Nudt12 (*Hs*)	++	nt	nt	+	+	(Grudzien-Nogalska *et al.,* 2019; Wu *et al.,* 2019)
		Nudt12 (*Ms*)	++	-	++	+	+	(Song *et al.,* 2013; Grudzien-Nogalska *et al.,* 2019; Sharma *et al.,* 2020)
		Nudt16 (*Hs*)	nt	nt	nt	++	++	(Song *et al.,* 2010; Grzela *et al.,* 2018)
		Nudt16 (*Ms*)	++	++	++	++	++	(Sharma *et al.,* 2020)
3	NRppA-RNA → NRp + pA-RNA	Rpph (*Ec*)	++	nt	nt	++	nt	(Frindert *et al.,* 2018; Grudzien-Nogalska *et al.,* 2019)
		Rpph (*Bs*)	++	nt	nt	nt	nt	(Frindert *et al.,* 2018)

Abbreviations: *Ec, Escherichia. coli; Sv, Streptomyces venezuelae; Bs, Bacillus subtilis; Sa, Staphylococcus aureus; Sc, Saccharomyces cerevisiae; Sp, Schizosaccharomyces pombe; At, Arabidopsis thaliana; Hs, Homo sapiens; Mm, Mus musculues; Kl, Kluyveromyces lactis*; NR, nicotinamide riboside; nt, not tested; X– indicates 3'-single stranded RNA.

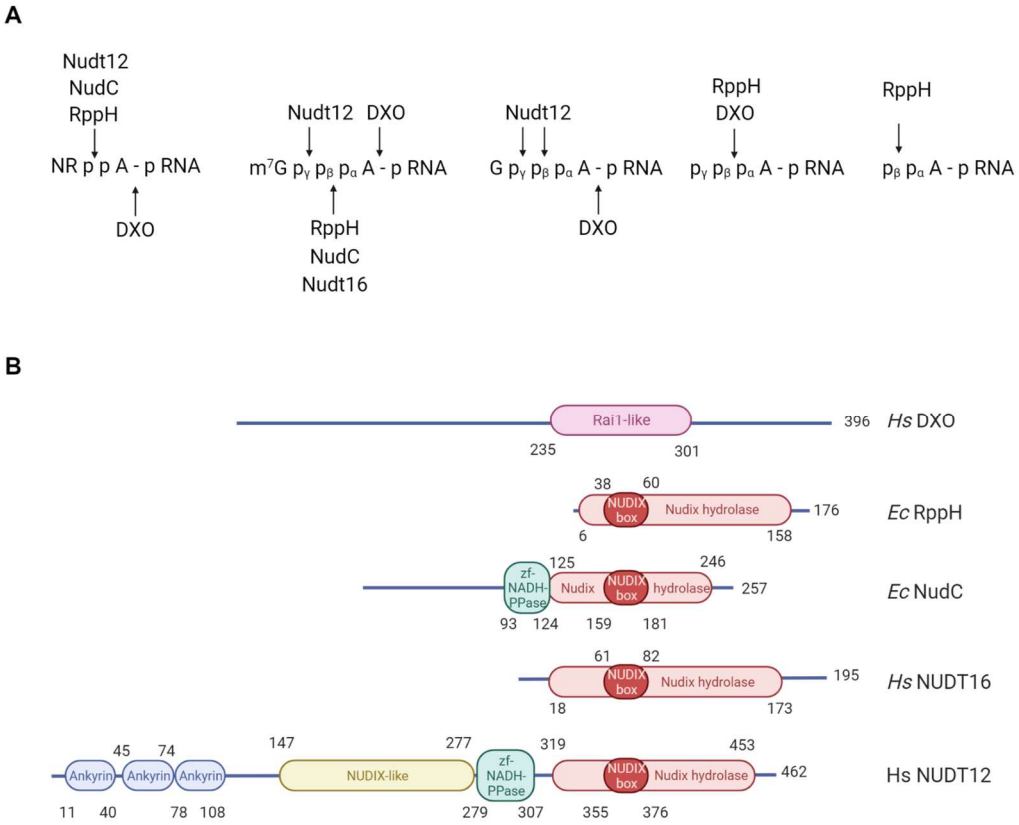

Figure 19. DeNADding enyzmes and decapping activities. (A) Schematic overview of the main substrates and *in vitro* cleavage sites for the decapping enzymes mentioned in the text. Cleavage sites indicated by an arrow. Rpph, another bacterial Nudix pyrophosphohydrolase, is indicated for comparison. (B) Schematic representation of the domain organization of the aforementioned decapping enzymes. Proteins are aligned relative to their Nudix motifs when relevant. Color domain: red, nudix hydrolase; purple, DXO family; green, NADH pyrophosphatase zinc ribbon domain. Abbreviations: NR, Nicotinamide riboside; *Ec, Escherichia. Coli; Hs, Homo sapiens*.

NudC, the first enzyme reported with a deNADing activity in *E. coli*, was a promising candidate. NudC efficiently hydrolyzes NADylated RNA by cleaving within the pyrophosphate of NAD and generates 5'-monophosphorylated RNA (Cahová *et al.,* 2015; Höfer *et al.,* 2016b; Zhang *et al.,* 2016). However, other reports highlighted a broad pyrophosphatase activity of NudC towards other types of metabolite-derived caps such as FADylated and CoAlated RNA (Bird *et al.,* 2016; Vvedenskaya *et al.,* 2018; Zhou *et al.,* 2021).

The mammalian Decapping and Exoribonuclease protein (DXO) generates a 5'-monophosphate RNA by cleaving the phosphodiester link after the first adenosine and hence removing the entire NAD moiety (Jiao *et al.,* 2017). However, DXO is a highly versatile enzyme with decapping activity towards various 5'-ends of RNA: it displays activity toward incomplete m^7G cap structures (Jiao *et al.,* 2013), pyrophosphohydrolase activity (Jiao *et al.,* 2013), and hydroxyl-dinucleotide hydrolase activity (Doamekpor *et al.,* 2020a). A later publication showed that DXO is

also active towards FADylated and dpCoAylated RNA (Doamekpor *et al.,* 2020b). Because all these enzymatic activities generate a monophosphorylated RNA, DXO is an unsuitable candidate for our purposes.

Nudt16, a mammalian Nudix hydrolase, has also been identified as a deNADing enyzmes (Sharma *et al.,* 2020), however Nudt16 also cleaves FADylated RNA (Sharma *et al.,* 2020) and was already known to decaps m^7G-capped RNAs as well (Song *et al.,* 2010).

Nudt12, the mammalian homologue of NudC, hydrolyzes NADylated RNA in the same way by cleaving within the pyrophosphate of NAD and thus generates 5'-monophosphorylated RNA (Grudzien-Nogalska *et al.,* 2019; Wu *et al.,* 2019). Although human Nudt12 can also cleave m^7G-capped RNA, it hydrolyzes the cap between α- and β-phosphates (Wu *et al.,* 2019), generating diphosphorylated RNA. Furthermore, human Nudt12 exhibits a marked preference and stronger binding to 5'-NAD compared to a m^7G cap (Ray and Frick, 2020). Considering these characteristics and, compared to the other enzymes with deNADing activities *in vitro*, human Nudt12 appeared to be our best candidate for specifically cleaving NADylated RNAs and generating monophosphorylated RNAs for subsequent adaptor ligation.

2.2.1.2 Expression and purification of recombinant human Nudt12

Based on our deNADding enzymes comparison, we decided to express and purified the recombinant human Nudt12 with two different tags (GST- and His_6-tag). The NUDT12 sequence was amplified from HEK293T cells cDNA and cloned in expression vectors pGEX-4T-1 and pCold I, so that the protein would be expressed with a N-terminal GST-tag or His_6-tag. The constructs were transformed into *E. coli* Rosetta(DE3) and the recombinant tagged-Nudt12 protein was purified from large-scale culture using GSTrap Column or Ni-NTA column for the His_6-tag protein. The purity of the recombinant proteins was analyzed by SDS-PAGE and Coomassie staining (Figure 20) and the identity of the proteins was confirmed by mass spectrometry for GST-Nudt12 and His_6-Nudt12 (performed by AG Bruckmann).

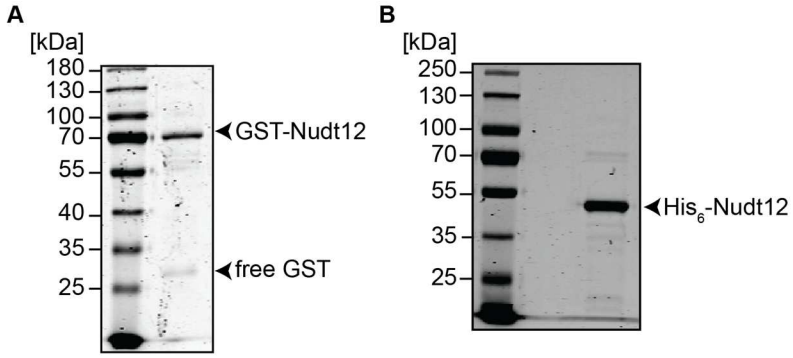

Figure 20. Expression and purification of recombinant Nudt12. Recombinant purified N-terminally tagged GST-Nudt12 (A) and His_6-Nut12 (B) proteins were separated by SDS-PAGE followed by Coomassie blue staining. Molecular-weight size markers are depicted on the left of the gels.

2.2.1.3 Recombinant human Nudt12 hydrolyzes free NAD and NADylated RNA

We wanted to test whether our recombinant purified enzymes were catalytically active.

First, we tested the capacity of GST-tagged Nudt12 to hydrolyze NAD to NMN and AMP (Figure 21A). NAD was incubated with GST-tagged Nudt12 and the reaction was monitored by HPLC (HPLC analysis performed by R. Hett). The disappearance of NAD (substrate) was accompanied by the appearance of AMP (product) over time, confirming the successful hydrolysis of free NAD (Figure 21B). NMN (presumed product) could not be detected by UV absorption with a C18-column, due to its both negative and positive charges.

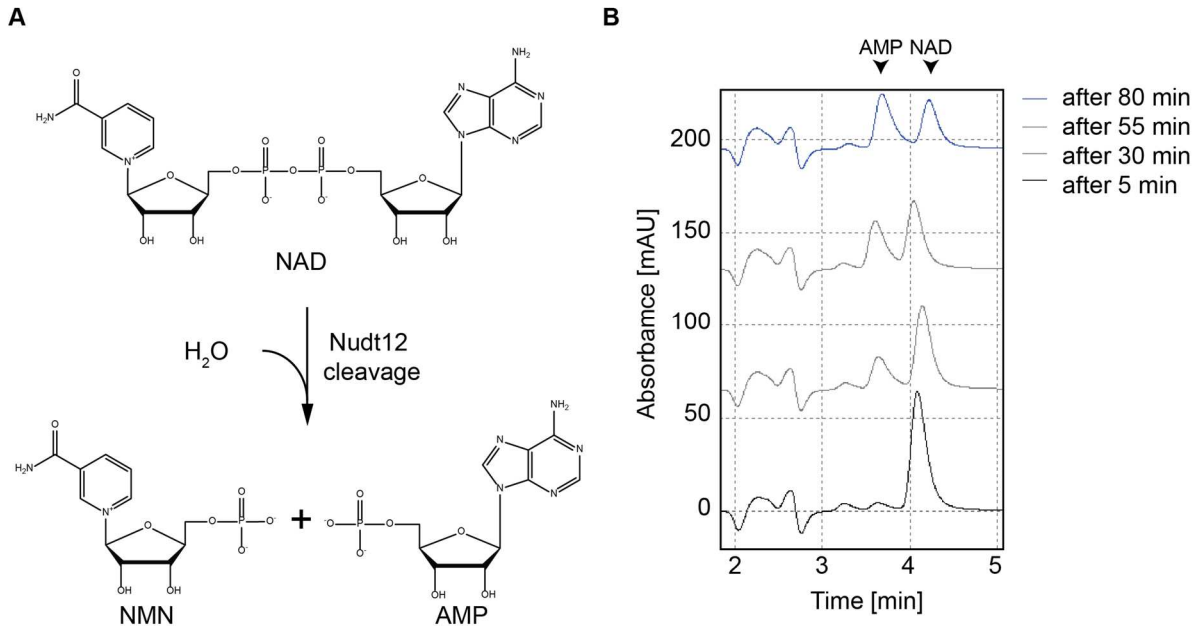

Figure 21. GST-Nudt12 hydrolyzes NAD to NMN and AMP. (A) Schematic of NAD hydrolysis reaction by Nudt12 and the reaction products. (B) NAD was incubated in the presence of Nudt12 at 25°C and aliquots of reaction mixture taken at the indicated time points were separated by HPLC on a C-18 column. TheAMP peak could be detected after 30 min and its intensity increased over time while the NAD peak decreased.

Second, we tested the deNADding activity of recombinant GST- and His-tagged Nudt12 on NADylated RNA.

We generated an *in vitro* transcribed ^{32}P-labeled NADylated RNA (from the T7ϕ2.5 AG-51CU DNA), which contains a starting adenosine at the +1 position and a unique guanosine at the +2 position, and carries a single ^{32}P at the phosphodiester linkage between the first and second transcribed nucleotides (NRppA*pGp-RNA) (Figure 22A). We subjected this RNA substrate to deNADding with the recombinant Nudt12 proteins followed by RNase T1 digestion. RNase T1 is an endoribonuclease that specifically cleaves RNA after guanine residues. Therefore, cleavage of the NRppA*pGp-RNA transcript by RNase T1 would generate NRppA*pGp. However, hydrolysis of the disphosphate linkage within the 5'-NAD moiety by Nudt12 would first generate pA*pGp-RNA and subsequently a pA*pGp product following RNase T1 digestion.

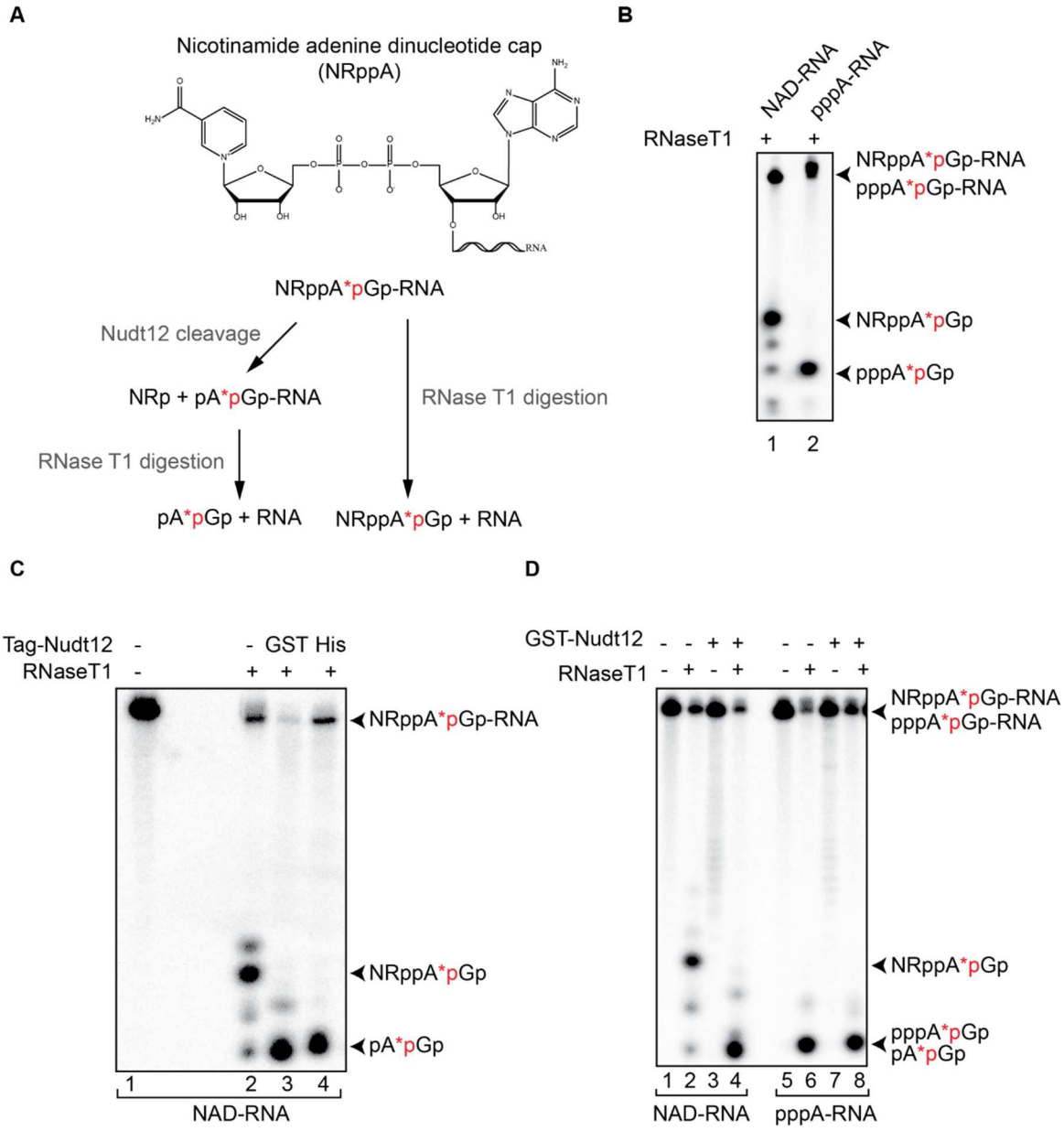

Figure 22. GST-Nudt12 and His$_6$-Nudt12 have *in vitro* deNADding activity on NADylated RNA. (A) Schematic of NADylated RNA (NRpppA-RNA) and the expected cleavage products by the indicated enzymes. Nudt12 cleaves within the pyrophosphate link within the NAD (NRpppA), liberating nicotinamide mononucleotide (NRp) and generating monophosphorylated RNA (pApGp-RNA). RNase T1 specifically cleaves single-stranded RNA at G residues. (B) Acrylamide gel-based analysis of RNA digestion products. NRppA*pG and pppA*pG were released from ^{32}P-labeled NAD-RNA and ppp-RNA respectively after incubation with T1 at 37°C for 30 min. (C) Acrylamide gel-based analysis of RNA decapping products upon GST-Nudt12 and His$_6$-Nudt12 incubation with NAD-RNA. (D) Acrylamide gel-based analysis of RNA decapping products after GST-Nudt12 incubation with NAD-RNA and ppp-RNA. The pA*pGP and ppppA*pGp dinucleotides migrated similarly. All reactions were run on a 20% PAA gel. The star (*p) indicates the position of the ^{32}P labeling.

Upon RNase T1 treatment, *in vitro* transcribed ^{32}P-labeled NADylated and triphosphorylated RNA released detectable NRppA*pG (lane 1) and pppA*pG (lane2), respectively (Figure 22B). To compare the activity of the two enzymes, *in vitro* transcribed ^{32}P-labeled NAD-capped RNA was incubated with GST-tagged and His-

tagged Nudt12, followed by RNase T1 digestion (Figure 22C). Both enzymes successfully released the expected pA*pGp cleavage product. However, GST-tagged Nudt12 appeared to cleave more efficiently than His-tagged Nudt12 (lane 3). The cleavage assay of NADylated and triphosphorylated RNA (Figure 22D) generated pA*pGp and pppA*pGp products that migrate similarly (lanes 4 and 8), confirming that the cleavage occurred at the diphosphate link.

Finally, we compared the activity of GST-Nudt12 on NADylated RNA to its m^{7}G-capped equivalent with a RNA body containing of all four nucleotides. Both transcripts were generated from the T7ϕ2.5-A-62 DNA template. Treatment of NADylated RNA with Nudt12 would generate monophosphorylated RNA, while similar treatment of m^{7}G-capped RNA would generate diphosphorylated RNA. The loss of *cis*-diol groups from the 5'-NAD or m^{7}G structure after cleavage would affect their mobility on APB gel electrophoresis.

After incubation with GST-Nudt12, the samples were divided in two and ran on a APB gel (Figure 23, top panel) and on a PAA gel (lower panel). A mobility shift on APB gel was observed after GST-Nudt12 treatment for the NADylated RNA (top, lane 4). This shift was due solely to the cleavage of NMN since the corresponding sample showed no degradation on the PAA gel (bottom, lane 4). Under the same experimental conditions, no cleavage was observed for m^{7}G-capped RNA, or at a level undetectable by our assay (Figure 23, lane 8).

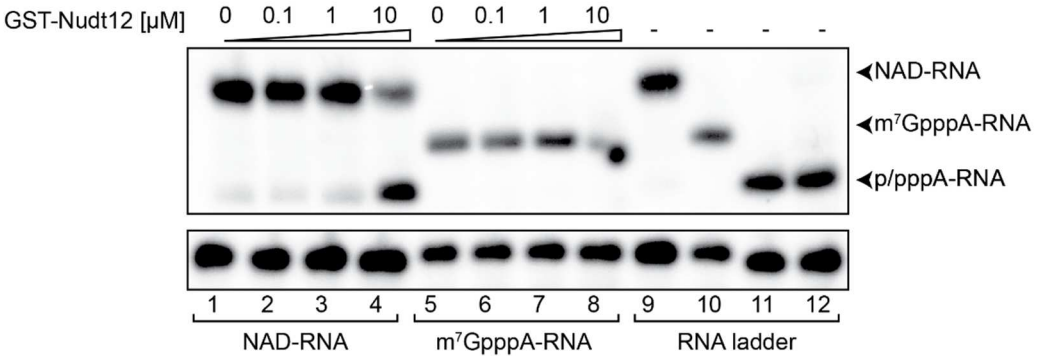

Figure 23. GST-Nudt12 cleaves NADylated RNA but not m^{7}G-capped RNA. 3'-end-labeled 5'-NAD- and m^{7}G-RNA were incubated with the indicated concentration of GST-Nudt12 for 1 h at 37°C. Reaction products were split in two and resolved on 0.2% APB (top) and 8% PAA (bottom) gels. The RNA ladder is made up of untreated NAD-, m7G-, and ppp-RNA. p-RNA (lane 12) was generated by digestion with Rpp .

In summary, we have expressed and purified a recombinant human Nudt12 enzyme that is active *in vitro* on free NAD and NADylated RNA.

2.2.2 Capture approach

2.2.2.1 Antibody-based approach

Monoclonal antibodies against nucleobases have found diverse scientific applications such as immunofluorescence or ELISA. More recently, immunoprecipitation of modified nucleotides by monoclonal antibodies can be coupled with next-generation sequencing to map, quantify, and characterize modifications across the transcriptome (reviewed in Schwartz and Motorin 2017; Yan Zhang, Lu, and Li 2022). However the generation of monoclonal antibodies with high affinity and specificity against nucleobases is challenging, because they are non-immunogenic small molecules that differ only slightly in terms of their chemical structure from one to another. Thus, it requires a prior coupling to an immunogenic carrier to elicit an efficient immune response (reviewed in Feederle and Schepers 2017).

Our lab has previous expertise in developing antibodies against modified ribonucleosides by modifying a nucleobase-coupling protocol (Erlanger and Beiser, 1964), that allows the conjugation of nucleobases sensitive to oxidation or reduction. Application of this modified protocol has successfully led to the generation of monoclonal antibodies against N6-methyl-Adenosine (m^6A), 5-methylcytosine (m^5C) and N6, N6-dimethyladenosine (m_2^6A) suitable for various applications (Weichmann *et al.,* 2020).

At the time of this thesis, no monoclonal antibodies against NAD, NADH or NMN were available yet, and we attempted to generate such antibodies that would allow the specific enrichment of NADylated RNAs.

2.2.2.1.1 Synthesis of antigen for immunization and generation of hybridomas

NAD and NMN are molecules too small to elicit an efficient immune response by themselves. Thus, they required a prior coupling to a carrier protein, in our case ovalbumin (OVA), which is often used as an immunogenic carrier for nucleosides (Plescia and Braun, 1967). The antigens were generated by conjugating NADH and NMN to ovalbumin by an oxidation-reduction method described by Erlanger and Beiser (1964), to form NAD-OVA and NMN-OVA (Figure 24A). Similarly, NAD or NMN were coupled to bovine serum albumin (BSA) as carrier protein. The coupling was performed by R. Hett.

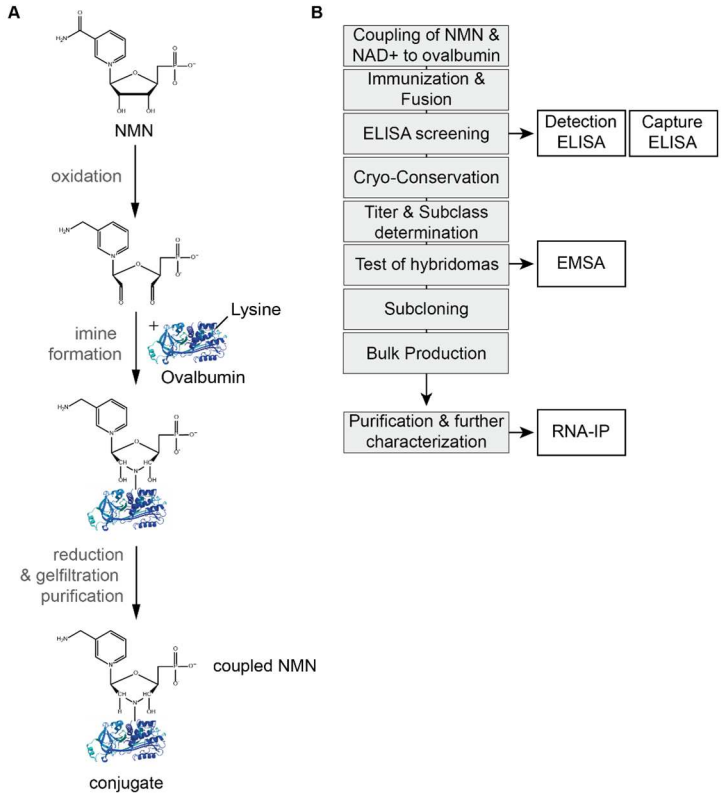

Figure 24. Synthesis of antigens for immunization. (A) Coupling of ovalbumin to NMN. The first chemical reaction oxidizes and opens the ribose ring between the 2′ and 3′ position. An amino group of a lysine side chain of ovalbumin is used as a reactive group, resulting in covalent coupling to the protein. (B) Overview of antibody generation workflow. Adapted from Weichmann et al., 2020.

NAD and NMN conjugated with OVA were used to immunize rats and mice. The immunization, fusion of splenocytes and myeloma cell lines, selection of hybridoma cells, and primary screening were carried out by our collaborators (R. Feederle, Helmholtz Munich). Hybridoma supernatants were tested by detection ELISA on BSA-conjugated NMN and BSA-conjugated NAD, and positive candidates on BSA-coupled NAD were sent to us for further validation (Figure 24B).

2.2.2.1.2 Screening of hybridoma clones

A common strategy to screen large numbers of hybridoma clones against their antigens is to perform dot blot, a method in which oligonucleotides are spotted, immobilized onto a nylon membrane, and incubated with potential antibody candidates. However, this requires a large amount of modified oligonucleotides, from 5 to 10 µg per spot (Matsuzawa *et al.,* 2019; Weichmann *et al.,* 2020). Since 5'-NAD-modified RNA are not commercially available, we had to rely solely on home-made synthesis (see 2.1.1), with such a total yield not easily reachable.

To identify possible hybridoma supernatants binding to 5'-NAD-modification, we performed electrophoretic mobility shift assay (EMSA) by incubating a 3'-end radiolabeled NADylated RNA with an increasing amount of hybridoma supernatants. When RNA is bound to the antibody, the complex migrates more slowly than free RNA. The use of a negative control during antibody generation screening is important to rule out cross reactivity; thus, a triphosphorylated RNA of identical sequence was used as a negative control.

Out of 62 supernatants, clones 26D11 and 28C11 showed a shifted band upon incubation with the NADylated RNA (Figure 25A, lanes 2,3, 8 and 9), which was not present for its negative triphosphorylated RNA equivalent (lanes 5, 6, 11 and 12). Such shift was not observed with any other hybridoma supernatants (Figure 25A, right panel). This shift could be repeated with an increased range of dilution of hybridoma and another batch of *in vitro* transcribed RNAs (Figure 25B). To be noted, this EMSA screening was performed with RNA purified with only one-step gel purification with a preparative APB gel (2.1.1), which could explain the multiple bands observed. In addition, since the hyridoma supernants are not purified, others contaminants could also binds to the labeled RNA and give non-specific signals. Finally, the RNAs used in these EMSA exeriments were relatively long (~ 60 nt). Even though they were denatured before the incubation with the hybridoma supernatants, it could be possible that the RNA could have re-folded in different conformations that would affect its migration on the native gel used in the EMSA.

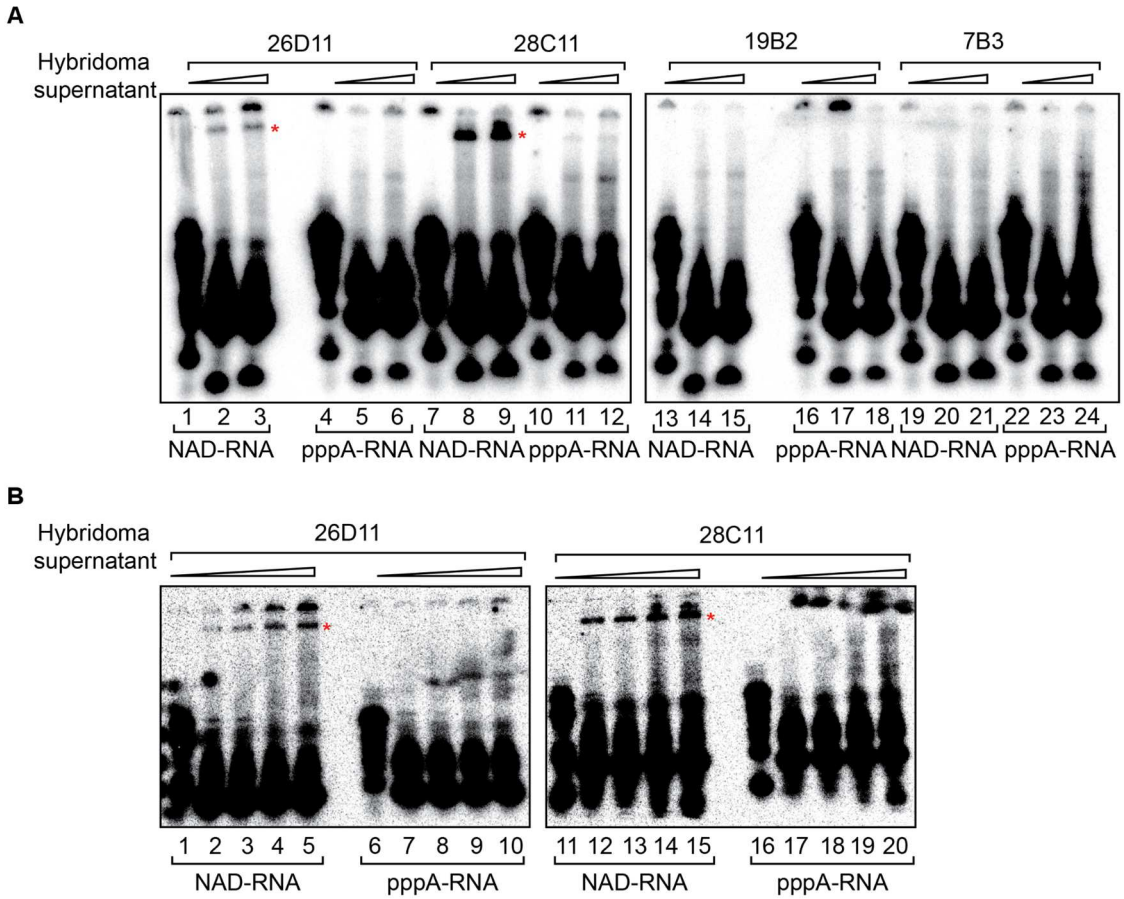

Figure 25. EMSA screening of hybridoma supernatants with NAD-RNA and ppp-RNA. (A) EMSA performed with 3-end radiolabeled NAD- and ppp-RNA and sequential dilution (0, 1:4 and 1:2) of hybridoma supernatant. Negative clones 19B2 and 7B3 are presented as comparison. (B) EMSA repeated with an wider range of sequential dilution (0, 1:16, 1:8, 1:4 and 1:2) and a different batch of *in vitro* transcribed RNA. Stars (*) indicate shifted bands of interest.

2.2.2.1.3 Purified antibodies showed little to no affinity to free NAD and NADylated RNA

To estimate the general performance of the antibodies, we wanted to determine their affinities to free NAD.

Equimolar mixtures of NAD and adenosine (as an internal standard) were incubated with purified 26D11 or 28C11 antibody. Subsequently, the mixture was centrifuged through a filter allowing molecules smaller than 10 kDa to pass through. This procedure separates antibody-bound from -unbound NAD. The input samples and filtrates were further analyzed and quantified by HPLC. Antibody purification and HPLC analysis were performed by Robert Hett.

To our dismay, HPLC analysis revealed little to no binding of 26D11 or 28C11 to NAD (Table 3). A single-point estimation for the apparent dissociation constant (K_D) gave the range of 50-100 µM. This implies that these antibodies do not have high affinity in solution for NAD.

Table 3. Quantification of the integrated area of the NAD/A ratio peaks normalized to input.

Sample	Peak area NAD	Peak area adenosine	Ratio NAD/A	Changes relative to input (%)
Input	522748	561941	0,9303	NA
26d11	414315	466714	0,8877	-4,57
28c11	430125	460606	0,9338	0,38

Nonetheless, we still wanted to evaluate whether purified antibodies would recognize and bind NAD in an RNA context, as the EMSA assay might have indicated hybridoma supernatant binding NAD when 5'-linked to a RNA body rather than free NAD.

To this end, we performed RNA immunoprecipitation by coupling the purified antibodies to agarose beads and incubating them with a 3'-end radiolabeled RNA to see if the antibody would bind and capture the NADylated RNA (Figure 26A). However, when incubating NADylated RNA with 26D11 or 28C11 antibody-conjugated beads, no NADylated RNA was immunoprecipitated (lanes 6 and 18), and they remained unbound in the supernatant (lanes 2 and 14). In addition, we performed EMSA with the purified antibodies (Figure 26B). No visible shift was observed for NADylated RNA upon incubation with 26D11 or 28C11 antibodies (lanes 6 and 18) compared to unbound NADylated RNA (lanes and lane 13).

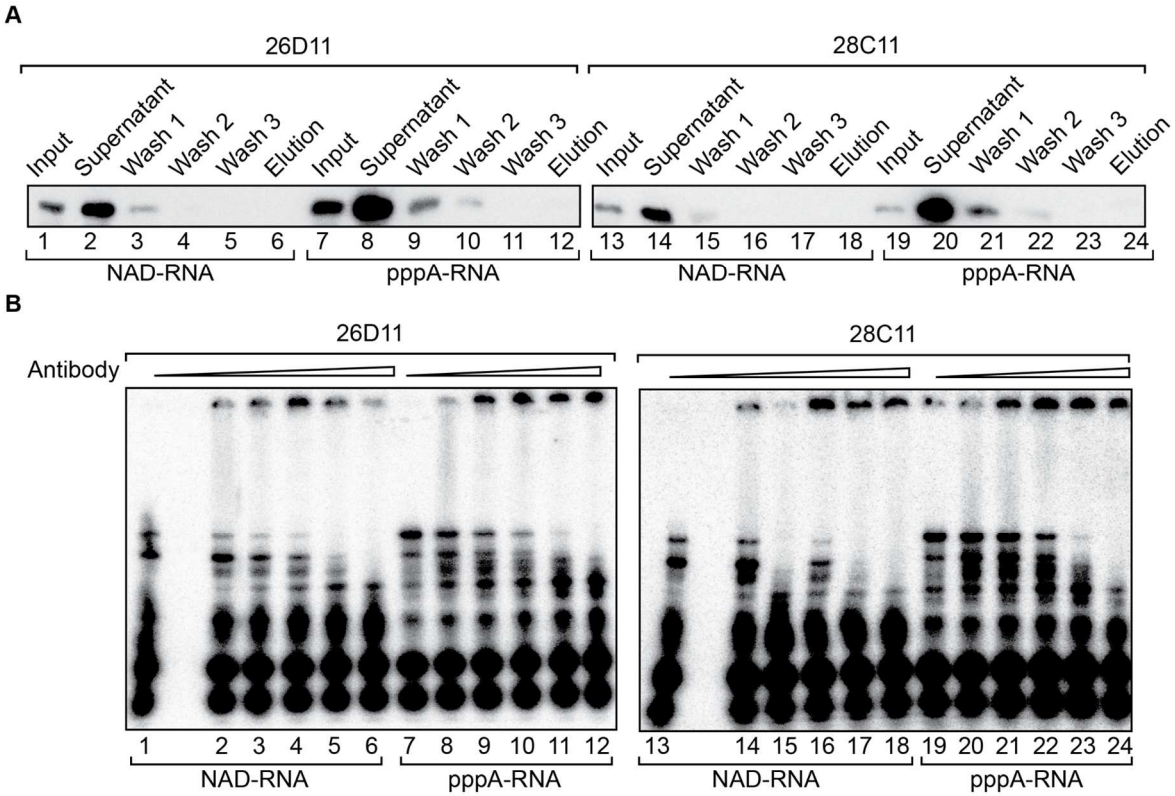

Figure 26. The purified 26D11 and 28C11 antibodies do not specifically enrich NADylated RNA. (A) Immunoprecipitation of NAD-RNA and ppp-RNA using purified 26D11 or 28C11 antibodies. RNA was separated on a denaturing PAA gel and analysed by northern blotting with radiolabeled probes against the RNA transcripts. (B) EMSA was performed with 3'-end radiolabeled RNA incubated with sequential dilution (0, 1:4, 1:2) of antibodies.

We repeated the EMSA to compare the remaining hybridoma supernatant used for the preliminary screening and the new hybridoma supernatant received in large scale for antibody purification (Figure 27). Although this shifted band pattern for NADylated RNA was observed when incubated with the old hybridoma (lanes 3 and 15), no such shift was observed with the new supernatant (lanes 9 and 21). This led us to think that the observed shift might have come from other impurities in the unpurified old supernatant reacting with NAD-RNA, and not from antibody binding itself.

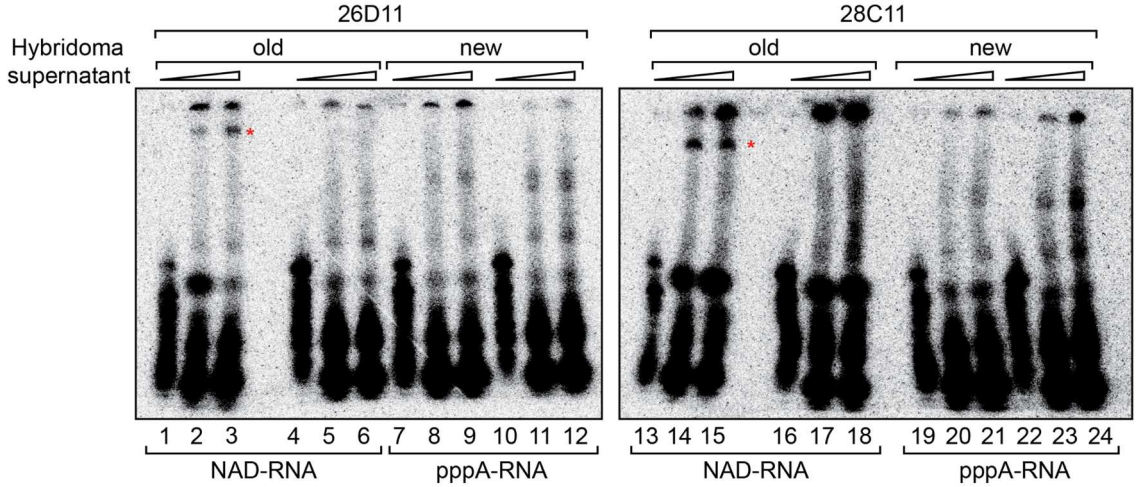

Figure 27. EMSA comparison between old and new hybridomas supernatant. EMSA was performed with 32P-labeled RNA and sequential dilution (0, 1:4, 1:2) of hybridoma supernatants. Stars (*) indicate shifted bands of interest.

In summary, we were unsuccessful in our attempt to generate monoclonal antibodies against NADylated RNAs.

2.2.2.2 Aptamer-based approach

Aptamers are single-stranded oligonucleotides, usually of small size (15 to 100 nucleotides), whose three-dimensional conformation upon folding forms as binding pocket for a ligand. They can bind to a wide range of targets (from metal ions to proteins) with high affinity and recognition, thus providing an alternative to traditional antibodies (reviewed in Walter *et al.*, 2012, and in Ali *et al.*, 2019).

Aptamer candidates can be generated through an *in vitro* selection strategy, namely systematic evolution of ligands by exponential enrichment (SELEX), in which libraries of oligonucleotides of random sequence are screened for their binding properties towards a specific target (Ellington and Szostak, 1990; Tuerk and Gold, 1990). Aptamers can also occur naturally: c*is*-regulatory structured RNA element called riboswitches can be found in the 5'-UTR regions of bacterial RNA. They contain two domains: an aptamer domain and an expression platform adjacent to it. Specific binding of a metabolite to the aptamer domain induces structural changes that affect the folding of the expression platform, which regulates the expression level of the downstream encoded gene (reviewed in Micura and Höbartner 2020).

Their ability to bind ligands in a way comparable to antibodies prompted us to reviewed the existing literature to identify an aptamer or riboswitch binding NMN or NAD that could be used for our capture approach.

2.2.2.2.1 The NMN aptamer and the NAD riboswitches

Although the first attempt by Burgstaller and Famulok (1994) to isolate RNA motifs that bind to NMN and NAD was unsuccessful, Lauhon and Szostak, (1995) were able to select RNA aptamers specific to the nicotinamide ribose portion of the NAD. The minor clone they identified binds to NAD with a dissociation constant (K_D) of 2.5 µM and was able to distinguish between the oxidized and reduced form of NAD. Upon reselection, they identified mutations that contribute to additional specificity for NMN over NMNH. The predicted secondary structure consists of two interacting stem-loop domains, depending on Mg^{2+} for its stability. They hypothesized that the small loop could interact with the stem in the tertiary structure of the aptamer (Figure 28A).

Two classes of NAD-sensitive riboswitches have been identified. The NAD class I riboswitch is based on the *nadA* motif in *Acidobateria* species (Malkowski, Spencer and Breaker 2019) and have been found upstream of genes involved in NAD biosynthesis (Weinberg *et al.,* 2017). The consensus secondary structure is composed of two almost similar domains in tandem, consisting in a single hairpin structure with an internal bulge. The first domain binds NAD and NADH; however, it does not interact with the NMN moiety or the nicotinamide ring on its own, but binds to the adenosine diphosphate moiety (Chen *et al.,* 2020; Huang *et al.,* 2020). The second domain also bind ADP derivatives, although with a much lower affinity (Chen *et al.,*

2020). Because of this lack of specificity towards NAD or NMN, this riboswitch was not suitable for capturing NADylated RNA.

The NAD-class II riboswitch derives from the *pnuC* motif associated with genes encoding a putative transporter of nicotinamide riboside in several bacteria, including *Streptococcus* (Panchapakesan *et al.,* 2021). The consensus secondary structure consists of two stems connected by a large internal loop (Figure 28B). In-line probing reactions show conformational change upon incubation with NAD, NMN, and NR, but not NADH. The K_D value with NAD was estimated to be approximately 100 µM, NMN was found to bind three-fold more tightly than NAD to the RNA by in-line probing (Panchapakesan *et al.,* 2021). Xu *et al.,* (2023) measured a K_D of 41.1 µM with NMN for this riboswitch. Together, this indicates that this motif recognizes the NMN moiety of NAD, contrary to the class I riboswitch, and makes it an interesting candidate for our purposes.

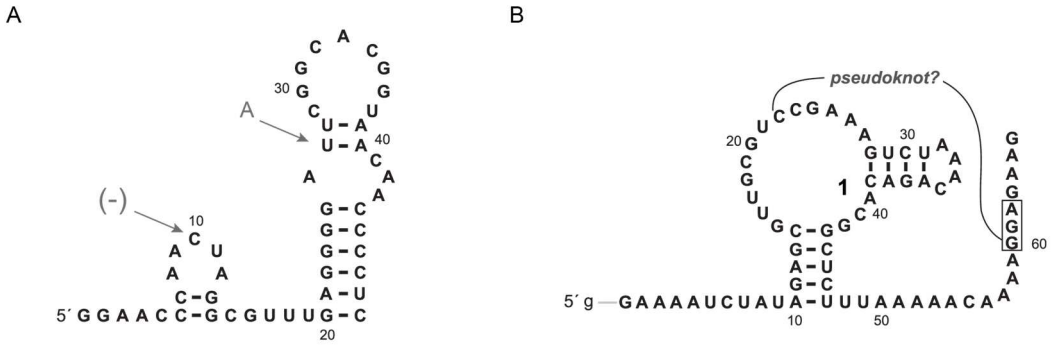

Figure 28. Sequence and proposed secondary structure of the NMN aptamer and NAD-II-ribsowitch investigated in this thesis. (A) Shortened NMN aptamer with major conserved mutations indicated by grey arrows upon reselecting for differential binding between NMN and NMNH. Deletions are indicated by (-). (B) NAD-II riboswitch based on 65 *pnuC* RNA construct. Adapted from Lauhon and Szostak 1995; Panchapakesan et al., 2021.

2.2.2.2.2 Immobilization strategy

A few factors must be considered to ensure that the immobilization of the aptamer on a support does not interfere with its optimal folding and thus its binding activity. For instance, minimization of the steric hindrance between the aptamer and the surface of the support can be achieved by the use of spacers. The choice of covalent or non-covalent interactions to immobilize the aptamer depends on downstream processing (reviewed in Peyrin 2009; Walter, Stahl, and in Scheper 2012).

We opted for a non-covalent binding strategy based on biotin-streptavidin interaction, because of the rapidity and the simplicity of the immobilization. We took

advantage of a RNA bait-pull-down method already established in our lab (Treiber *et al.,* 2018) and adapted it to our purpose: a leader sequence is added to the 5'-end of the RNA aptamer of interested that is complementary to a 3′-biotinylated 2′-*O*-methyl-modified RNA adaptor sequence, and the 3'-biotin allows the immobilization of the adaptor to magnetic beads coated with streptavidin (Figure 29).

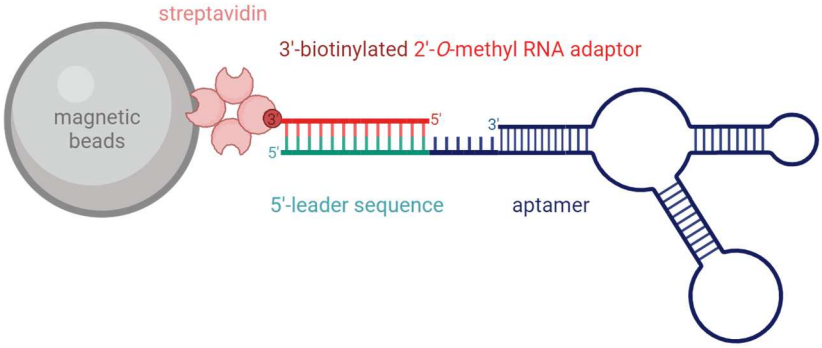

Figure 29. Schematic representation of the aptamer-based capture. The *in vitro* transcribed aptamer contained an added 5'-leader sequence complementary to a 3'-biotinylated 2′-O-methyl-modified adaptor that is immobilized on strepatvidin-coated magnetic beads.

Folding conditions include multiple variables, such as aptamer concentration, temperature, buffer composition, or incubation time. We used the respective selection buffer conditions for the folding of the aptamers and the capture assays. The divalent cation Mg^{2+} is known to play an important role into stabilizing RNA tertiary structure of RNA (Misra and Draper, 1998; Sengupta *et al.,* 2014; Fischer *et al.,* 2018). We selected a magnesium concentration of 20 mM, since this concentration has been shown to increase the stability of the shortened NMN aptamer sequence (Lauhon and Szostak, 1995). This magnesium concentration is also associated with increased binding affinity between the NAD-II riboswitch and NMN (Xu *et al.,* 2023). Before immobilization on beads, the aptamers were denatured and refolded by cooling down in presence of the adaptor in their respective selection buffers (Lauhon and Szostak, 1995; Panchapakesan *et al.,* 2021). Since metal ions promote RNA hydrolysis at high temperature (Dallas *et al.,* 2004; Guth-Metzler *et al.,* 2023), magnesium was added to the mix only when the temperature was below 65°C.

2.2.2.2.3 Aptamer-based enrichment of NADylated RNA

To test the feasibility of this approach, the aptamers of interest were denatured, incubated with the adaptor and cooled down in the presence of Mg^{2+} to promote the folding of the aptamers and the hybridization of the complementary sequence

between the aptamer and the adaptor. The resulting hybridized aptamer-adaptor was coupled to streptavidin beads. The 30-mer NADylated RNA and monophosphorylated RNA produced by chemical synthesis (2.1.2) were 3'-end radiolabeled. These RNA contained no internal adenosine, had identical sequence and differed only by their 5'-end (5'-NAD or 5'-monophosphorylated adenosine). The RNAs were incubated with the set-up, washed with the folding buffer, eluted in RNA loading buffer, and analyzed by denaturing urea-PAGE gel (Figure 30).

No unspecific binding to the beads was observed when the RNA was incubated with the magnetic streptavidin beads only (lanes 2, 9, 16 and 23). For the capture performed with the NMN aptamer, a stronger signal can be detected for the NADylated RNA (lane 7) compared to the monophosphorylated RNA (lane 14). However, a similar signal was detected for both RNA species for the NAD-II riboswitch (lanes 21 and 28), which can be interpreted as non-specific enrichment.

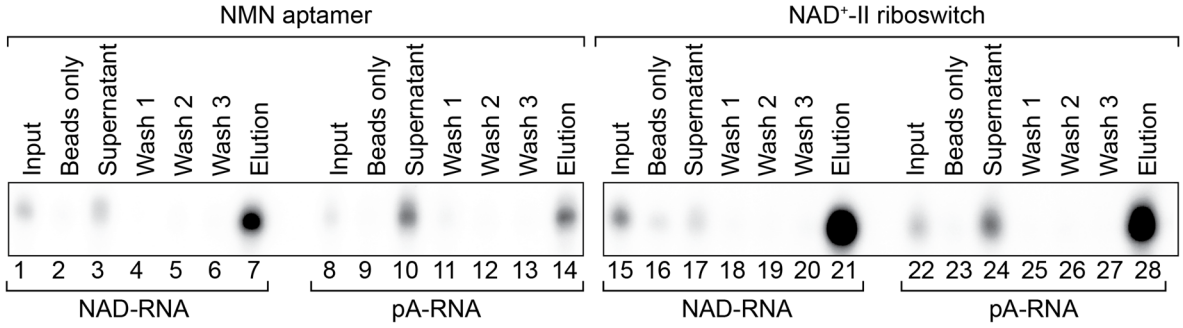

Figure 30. Aptamer-based capture with 30-mer A-less NADylated RNA and monophosphorylated RNA. An equimolar amount of adaptor and aptamer were hybridized together and coupled to magnetic streptavidin beads. The set-ups were incubated with 30-mer NAD-RNA or pA-RNA 3'end-radioabeled for 1h at 4°C. After incubation, beads were washed three times in folding buffer, supernatant and washes were collected and precipitated. Samples were eluted with 2X RNA loading dye. The RNA were resolved on a denaturated PAA gel and exposed overnight to a phosphoscreen.

We then repeated the capture with the 62-mer NADylated and triphosphorylated RNA generated by *in vitro* transcription (see 2.1.1). These RNAs contained internal adenosines, had identical sequences, and only differed by their 5'-end. We added a previous denaturation step to linearize these RNA just before incubating them with the aptamer adaptor set-ups. The RNAs were incubated with the set-up, and analyzed by denaturing urea-PAGE gel (Figure 31). As previously, we detected a stronger signal for the NADylated RNA enriched with the NMN aptamer (lane 5) compared to the triphosphorylated RNA (lane 8). Uncaptured NADylated RNA was detected in the supernatant (lane 3). In this case, upon incubation with the NAD-II riboswitch, the

NADylated and triphosphorylated RNA were detected in the supernatant (lanes 9 and 12), and barely any signal was detected from the eluted beads (lanes 11 and 14).

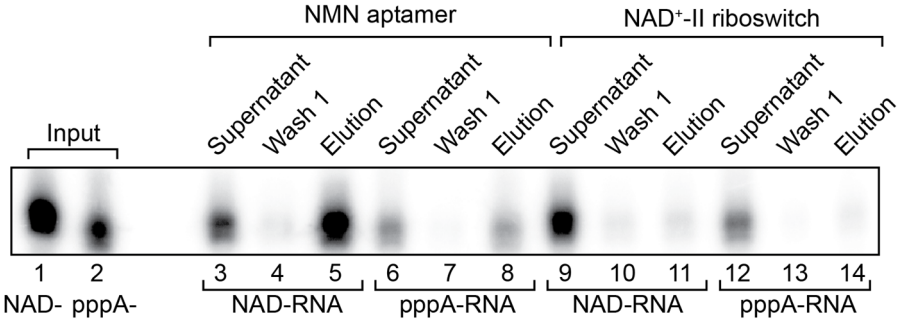

Figure 31. Aptamer-based capture with 62-mer NADylated RNA and triphosphorylated RNA. An equimolar amount of adaptor and aptamer were hybridized together and coupled to magnetic streptavidin beads. The set-ups were incubated with 62-mer NAD-RNA or pppA-RNA 3'end-labeled with for 1h at 4°C. After incubation, beads were washed three times in folding buffer, supernatant and washes were collected and precipitated. Only the first wash was loaded. Samples were eluted with 2X RNA loading dye. RNA were resolved on a denaturated PAA gel and the gel was exposed overnight to a phosphoscreen.

Finally, we compared aptamer-based enrichment between NADylated RNA and m^7G-capped RNA (Figure 32, top panel). After the capture, we performed a competitive elution by adding NAD in excess to the set-up and incubating for another hour, in order to displace bound NADylated. Aliquots of the supernatant after coupling the hybridized aptamers-adaptor were also saved and run alongside the other samples (lanes 1 and 16). For the NMN aptamer, as previously, uncaptured NADylated RNA was detected in the supernatant after capture (lane 3). Faint signal could be detected upon NAD elution at the conditions used, and since the signal was of similar intensity as the washes, we concluded the elution was not successful. The enriched NADylated RNA was eluted with RNA loading dye (lane 8). In comparison, barely any m7G-capped RNA was captured (lane 15). For the NAD-II riboswitch, similar results were observed, with a stronger signal from unspecific binding m^7G-capped RNA to the beads (lane 30).

Afterwards, the coupling of the aptamer to the beads was assessed by northern blotting as control, with probes specific for the NMN aptamer and the NAD-II riboswitch (Figure 32, bottom panel). Unbound aptamers in excess could be detected in the supernatant after the coupling step to the beads (lanes 1 and 16). Since the elution from the beads after the immobilization was performed with RNA loading dye, the hybridization between the aptamers and the adaptor was disrupted, and aptamers can be detected in the eluate. A signal of similar intensity was detected from all

coupled set-ups (lanes 8 and 15, lanes 23 and 30), confirming that the difference observed in the enrichment was indeed due to the capture of NADylated RNA over m^{7}G capped-RNA. Some remaining signals from the 3'-end radiolabeled NADylated and m^{7}G-capped RNA could still be detected (lane 2, 3, 9, and 10, and lanes 17,18, 24, and 25). To be noted, the NMN aptamer and the RNA are of similar length (~60 nt) and run at the same size, making it difficult to distinguish the individual signals.

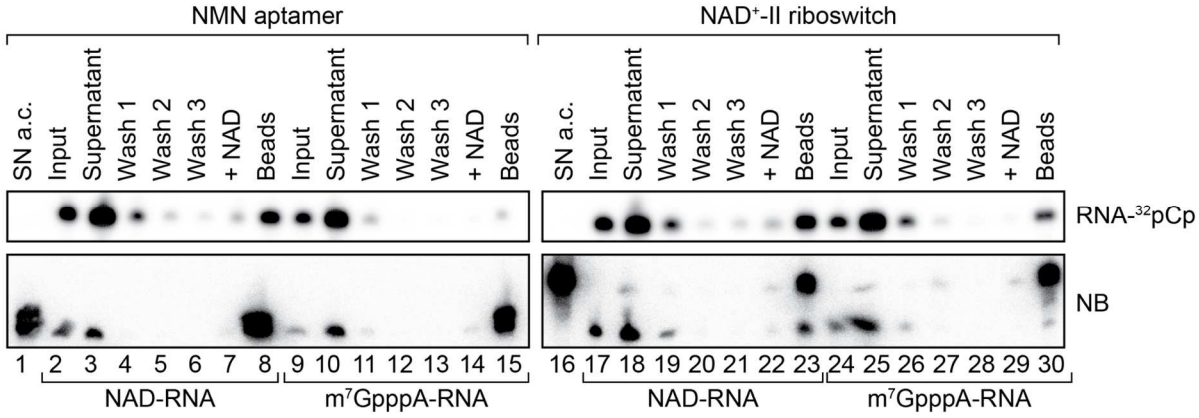

Figure 32. Aptamer-based capture with 62-mer NADylated RNA and m^{7}G-capped RNA. An equimolar amount of adaptor and aptamer were hybridized together and coupled to magnetic streptavidin beads. Aliquot of the supernatant after coupling (SN a.c.) was preleved . The set-ups were incubated with 62-mer NAD-RNA or m^{7}G-capped RNA 3'end radiolabeled for 3h at 4°C. NAD in excess was added for elution and incubated for another hour. After incubation, beads were washed three times in folding buffer, supernatant and washes were collected and precipitated. Samples were eluted with 2X RNA loading dye. RNA were resolved on a denaturated PAA gel and the gel was exposed 4h to a phosphoscreen to detect signal of labeled NAD- or m^{7}G-RNA (top panel). Afterwrds, the gel was blotted and aptamers were detected by nothern blotting with a complentary radiolabeled probes specific for their respective sequences (bottom panel). Some residual signal from the hot NAD and m^{7}G-RNA could still be slightly detectable.

We decided to focus on the NMN aptamer and the elution conditions of the bound NADylated RNAs.

We repeated the competitive elution with NMN and NAD in excess after enrichment of NADylated RNA (Figure 33). However, NADylated RNA was not eluted either under these conditions (lanes 2 and 4). Finally, we tried to elute by incubating with our purified recombinant Nudt12 to cleave specifically NADylated RNAs as per our original approach combining NADylated RNA capture to deNADding (Figure 18). However, by incubating the set-up at the optimal temperature and buffer for the enzyme (37°C), both RNAs were collected in the eluate (lane 6 and 13) and no m^{7}G-capped RNA was retained on the beads (lane 14), which would be the case if the elution by cleavage was specific for NADylated RNAs. This suggests that the temperature or buffer composition disrupted the stability and folding of the aptamer,

and the captured RNAs were released. Therefore, it would be necessary to assess the ability of the enzyme to cleave at a lower temperature maintaining the aptamer folding; in this case longer enzymatic treatment time might be necessary.

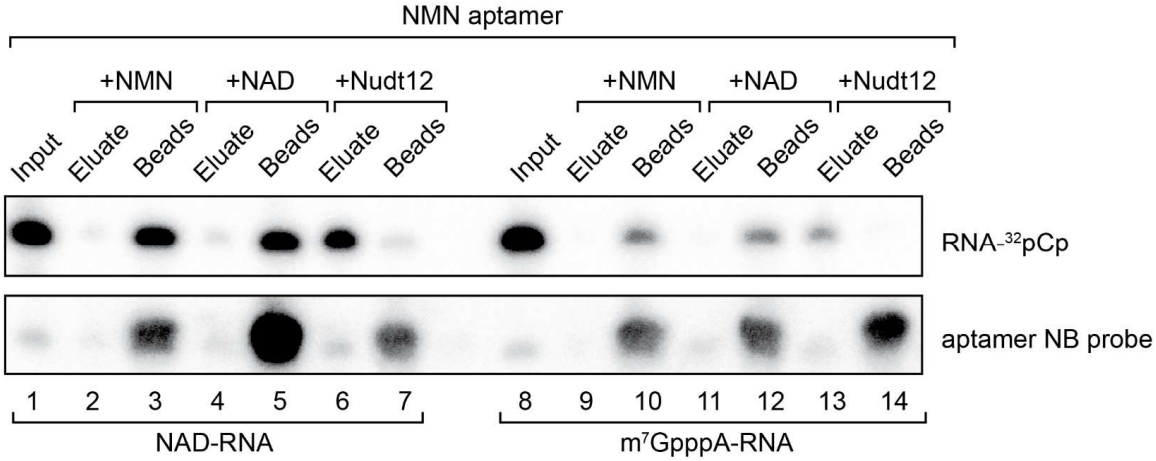

Figure 33. Elutions conditions of aptamer-based capture of NADylated RNA. An equimolar amount of adaptor and aptamer were hybridized together and coupled to magnetic streptavidin beads. The set-ups were incubated with 62-mer NAD-RNA or m^{7}G-capped RNA 3'end-radiolabeled for 3h at 4°C. After incubation, the set-ups were washed three times in folding buffer and were divided in three samples and underwent different elutions conditions. 100 µM NAD or NMN added for elution and incubated for another hour. Purified recombinant Nudt12 was added and the set-up was incubated for 30 min at 37°C. After incubation, the eluates were collected and precipitated. RNA on beads were eluted with 2X RNA loading dye. Samples were resolved on a denaturated PAA gel and the gel was exposed 4h to a phosphoscreen to detect signal of labeled NAD- or m^{7}G-RNA (top). Afterwrds, the gel was blotted and aptamers were detected by nothern blotting with complementary radiolabeled probes specific for their respective sequences (bottom). Some residual signal from the hot NAD and m^{7}G-RNA could still be slightly detectable.

Taken together, we could enrich NADylated RNAs by a capture approach based on a NMN-binding aptamer.

2.3 INVESTIGATION OF NADYLATED RNAS IN AN RELEVANT BIOLOGICAL CONTEXT

2.3.1 Establishment of a luminescent-based NAD cap levels detection assay

We wanted to establish an assay allowing us to detect endogenous NAD cap levels, more suitable to the low NADylated RNA levels in eukaryotes (Wang *et al.,* 2019a). We built on the NAD-capQ protocol, a two-step enzymatic assay that detects and quantifies NAD cap levels in total RNA (Grudzien-Nogalska *et al.,* 2018). We replaced the detection step performed originally with a commercially available colorimetric kit

(Sigma-Aldrich, limit of detection of 400 nM) with a luminescent detection kit (Promega, limit of detection of 1 nM). The adapted NAD-capQ luminescence-based assay consists of two steps (Figure 34). In the first step, enzymatic treatment of RNA with NP1 cleaves within the phosphodiester bonds of the RNA and releases 5'-NAD and nucleotides. In the second step, NAD is detected by a bioluminescent assay (NAD/NADH-Glo Assay, Promega). NAD is converted into NADH by a NAD cycling enzyme. In the presence of NADH, a proluciferase substrate is reduced to luciferin, which is used as a substrate by a recombinant luciferase. The light signal produced is proportional to the starting amount of NAD and NADH in the sample; the cycling of the coupled enzymatic reactions increases the sensitivity of the assay.

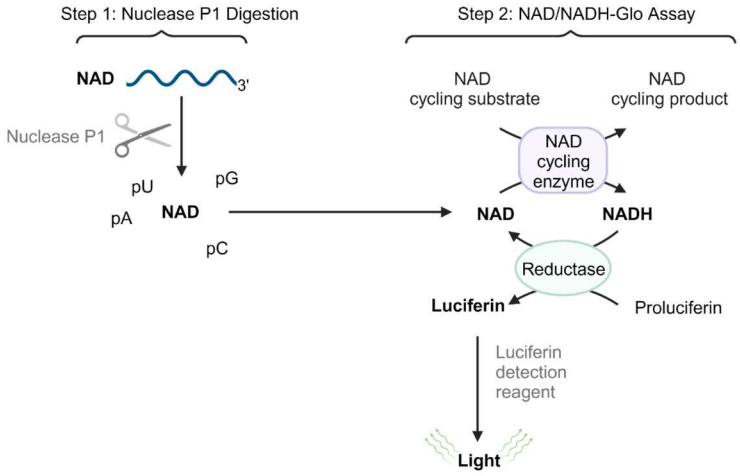

Figure 34. Schematic of NAD-capQ luminescence-based detection assay. Step 1: enzymatic treatment of RNA with nuclease P1 (NP1) releases 5'-NAD and nucleotides. Step 2: detection by a commercially NAD/NADH bioluminescent assay. NAD is converted to NADH by a NAD cycling enzyme. In the presence of NADH, a proluciferase substrate is reduced to luciferin, which in turn is used as a substrate by a recombinant luciferase. The light signal can be easily detected by a luminometer and the light produced is proportional to the starting amount of NAD and NADH in the sample. Adapted from Grudzien-Nogalska *et al.,* 2018 and Promega NAD/NADH-Glo™ Assay technical manual.

To validate the assay, we incubated *in vitro* transcribed NADylated and triphosphorylated RNA in presence and in the absence of NP1, performed the enzymatic cycling reaction, and measured the luminescence in each sample (Figure 35A). The signal detected in the sample containing NADylated RNA treated with NP1 was above background level of luminescence detected in the untreated sample. On the contrary, the signal in the samples containing triphosphorylated RNA was barely distinguishable with or without NP1 digestion, indicating that the signal detected in the analysis of NADylated RNA was derived from the NAD released.

We then performed our assay with NADylated RNA and m^{7}G-capped RNA. By plotting the net luminescence values of the samples against a standard curve generated using NAD, we could convert the luminescence (in RLU) to the concentration of NAD and interpolate the amount of NAD in the experimental samples (Figure 35B).

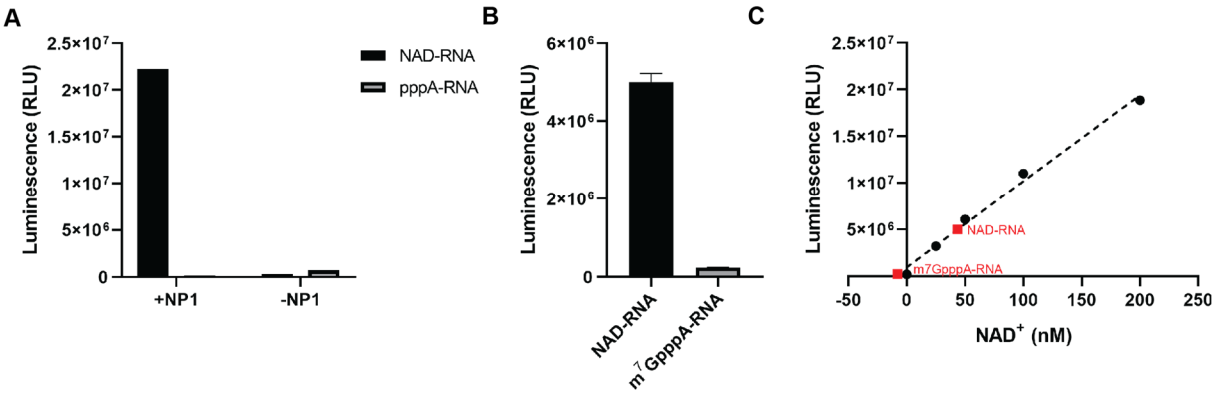

Figure 35. NAD-capQ luminescence-based analysis of RNA generated *in vitro*. (A) 1 µg of generated *in vitro* NADylated RNA (black) and triphosphorylated RNA (grey) with or without Nuclease P1 (NP1) digestion. (B) Net luminescence value for NADylated RNA (black) and m^{7}G-capped RNA (grey) obtained by difference between NP1-digested and NP-1 non-digested luminescent values. (C) Quantitation of NADylated RNA and m^{7}G-capped RNA (red data-points) plotted on a NAD standard curve generated by linear regression analysis of background corrected NAD standards (black data-points).

We tested our method on total RNA from HEK293T cells to detect endogenous NAD cap levels. Unfortunately, we have repeatedly observed that when using total RNA, we obtained a background signal higher in the control samples without NP1 than in the RNA sample digested with NP1. In fact, this trend could already be observed when using *in vitro* generated triphosphorylated RNA only (Figure 35A); however, the amount of NAD liberated upon digestion of the NADylated RNA equivalent was high enough to allow quantification. We tried to use heat-inactivated NP1 for the negative control instead of omitting the enzyme or replacing it with glycerol, but we still observed this same high signal (Figure 36A) that renders impossible to quantify endogenous NADylated level (Figure 36B). Although we cannot explain why such as high luminescence signal occurs in non-digested NP1 samples, we could hypothesize that the endogenous level of NADylated RNAs in mammalian cells is too low and the digestion by NP1 generated too few free NAD to be detected by the assay. It may be necessary to perform additional purification steps of the samples (e.g. size-selection or poly(A) selection of RNA) to increase the NADylated RNA content and allow detection of released NAD upon NP1 digestion.

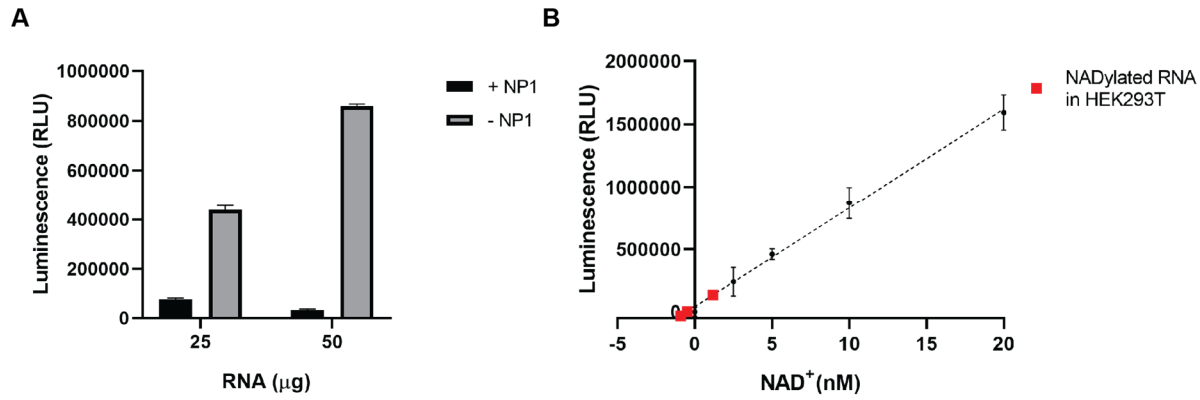

Figure 36. NAD-capQ luminescence-based analysis of cellular NADylated RNA levels in HEK293T. (A) 25 or 50 µg of total RNA extracted from HEK293T cells and precipitated prior the assay with ammonium acetate to remove residual free NAD was digested with (black) or without (grey) Nuclease P1 (NP1) digestion.) (B) Plotted value of 50 µg of total RNA extracted from three independent biological replicates of HEK293T cells (red data-points) on a NAD standard curve generated by linear regression analysis of background corrected NAD standards (black data-points).

2.3.2 Is U1 snRNA NADylated?

Benoni *et al.,* (2022) reported in a preprint that the U1 spliceosomal RNA is 5'-NADylated and that the 5'-NAD modifications increase the efficiency of splicing of HIV-1 and cellular RNA upon HIV-1 viral infection. Considering the highly regulated synthesis of the trimethylated cap of snRNAs, as well as its crucial role for nuclear reimport and for the formation of the spliceosome (see 1.2.2.2, but also Hamm *et al.,* 1990; Marshallsay and Lührmann, 1994), we were curious about the possibility of a NADylated U1 being incorporated in a mature spliceosome contributing to splicing *in vivo*. Therefore, we wanted to investigate the presence of NADylated snRNA in conditions favorable to NADylated U1 detection and to evaluate whether a NADylated U1 was incorporated in a functional spliceosome

2.3.2.1 Validation of CuAAC-NAD biotinylation

We implemented the ADPRC-catalyzed, CuAAC-based biotinylation reaction of NADylated RNA in the lab (Cahová *et al.,* 2015). In short, ADPRC modifies the nicotinamide moiety of a NADylated RNA with a clickable alkyl group, and in turn this group is linked by copper-catalyzed cycloaddition (CuAAC) reaction to a biotin-azide derivative, generating a biotinylated RNA (Figure 37) (see 1.3.2.2).

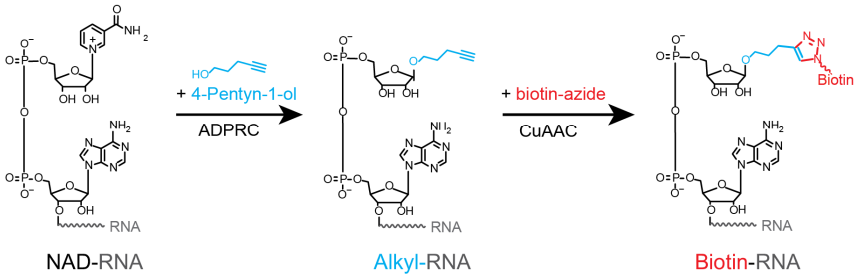

Figure 37. Schematic of the chemo-enzymatic CuAAC-NAD biotinylation reaction. In the first step, adenosine diphosphate-ribosyl cyclase (ADPRC) catalyzes the replacement of the nicotinamide moeity of the NADylated RNA with 4-pentyl-1-ol. In the second step, the biotin-PEG3-azide is attached to the introduced alkyne moeity by copper-catalyzed cycloaddition (CuAAC) reaction. Adapted from Cahová et al., 2015.

First, we subjected *in vitro* generated NADylated, m^{7}G-capped and triphosphorylated RNAs to CuAAC-NAD biotinylation reaction and samples were processed in presence (+) or absence (-) of ADPRC, where –ADPRC samples underwent all treatments except the addition of the enzyme. A dot blot assay was used to assess the biotinylation of RNA (Figure 38A). The biotinylation of NADylated RNA was successfully detected with fluorescent dye-labeled streptavidin in the presence of ADPRC (Figure 38A, top panel, lane 1), while m^{7}G-capped RNA displayed low reactivity upon CuAAC-NAD (lane 2), as previously reported (Hu *et al.,* 2021). The triphosphorylated RNA was not biotinylated (lane 3). Reactions performed in the absence of ADPRC did not show any biotinylation signals (lanes 4, 5, and 6). For control, RNA on the membrane was subsequently detected with a radiolabeled probe (Figure 38B, bottom panel). Only the triphosphorylated RNA sample without ADPRC was partially lost or degraded during the process (lane 6).

Second, we subjected total RNA extracted from HEK293T mixed with spike-in NADylated RNA to CuAAC-NAD biotinylation and incubated the reaction samples with streptavidin beads. Aliquots were saved after each step and capture RNA was eluted from the beads. Northern blot analysis of the samples revealed that the NADylated RNA spike-in was carried out in all the steps, but was only enriched by streptavidin beads in the reaction in the presence of ADPRC (Figure 38B, top panel, lane 5). Slight degradation can be observed due to RNA fragmentation in the presence of copper ion during the CuAAC reaction step (Figure 38B, lower panel, lanes 3 and 7).

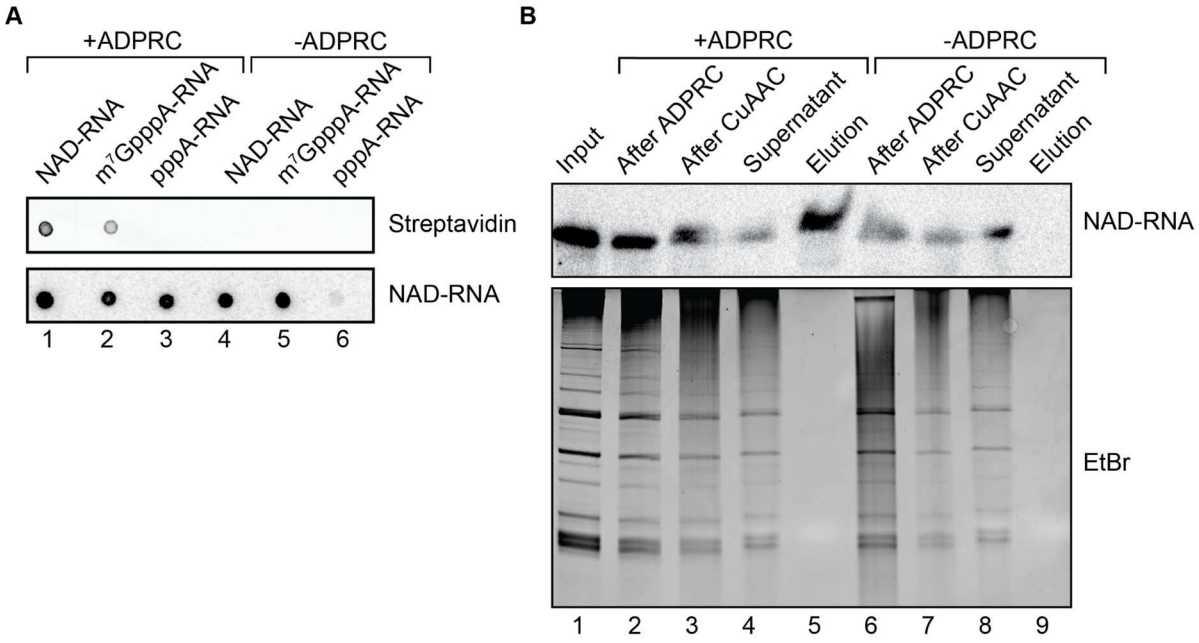

Figure 38. Validation of ADPRC-catalyzed, CuAAC-based biotinylation of NADylated RNA. (A) Dot blot assay of *in vitro* generated NAD-, m^{7}G- RNA and ppp-RNA after chemo-enyzmatic biotinylation reaction in the presence or absence of ADPRC. Biotin-labeled RNA were detected with streptavidin IRdye (top) and afterwards by northern blot with a radiolabeled probe (bottom). (B) 50 ng of NAD-RNA generated *in vitro* was spiked in 50 µg of total RNA prior to the biotinylation reaction in the presence or absence of ADPRC. Biotinylated RNA was purified on streptavidin magentic beads and eluted in 2x RNA loading dye. RNA was resolved on a denaturing PAA gel, analysed by northern blot with a radiolabeled probe against RNA spike-in (top). Ethidium bromide (EtBr) staining of the gel before blotting served as control for RNA quality (bottom).

2.3.2.2 Isolation of NADylated U1 under 3'-5' degradation altered conditions

The low abundancy of NADylated RNAs in eukaryotes (Wang *et al.,* 2019a) renders difficult the investigation of their biological relevance. A preprint reported that the U1 spliceosomal RNA was 5'-NADylated, and that this modification increased the efficiency of RNA splicing upon HIV-1 viral infection (Benoni *et al.*, 2022). We hypothesized that a NADylated U1 snRNA may be recognized as a faulty snRNA due to the NAD cap. The NAD cap would prevent the degradation of U1 snRNA via decapping and XNR1-mediated 5′-3′ degradation, as it occurs normally for defective U1 snRNAs in mammals (Shukla and Parker, 2014). Thus, degradation could only occurs in a 3'-end dependent manner by the TUT-DIS3L2 surveillance pathway (see 1.2.3.2). The 3'-5' exoribonuclease DIS3L2 degrades misprocessed pre-snRNAs and defective snRNA without the Sm Ring (Pirouz *et al.,* 2016; Łabno *et al.,* 2016b; Ustianenko *et al.,* 2016; Roithová *et al.,* 2020). In addition, the 3'-5' exoribonuclease DIS3 of the exosome complex (reviewed in Chlebowski *et al.,* 2013) has been reported to play a role in snRNA synthesis (Allmang *et al.,* 1999). Thus, we reasoned that blocking 3'-5' degradation pathway of snRNAs would lead to an accumulation of

NADylated U1 snRNA. With a higher, and thus detectable, level of NADylated U1 snRNA, we could then investigate its possible incorporation in a mature and functional spliceosome.

DIS3L2 KO and its parental HEK293T cell line were kindly provided by Z. Warkocki (Polish Academy of Sciences, Poland). Since DIS3 is essential for human cells (Davidson *et al.,* 2019), we relied on a conditional DIS3 knockout cell line in Flp-In T-REx-293 (generated by C. Latini, our lab) consisting in a stable cell overexpressing DIS3 upon doxycycline induction and in which the PIN domain of endogenous DIS3 was targeted by CRISPR/Cas9. The mild leaky expression of exogenous DIS3 allows the cells to survive. Expression of DIS3 and DIS3L2 in wild-type and mutants cell lines was assessed by Western blot (Figure 39A).

We isolated U1 snRNA from DIS3 KO, DIS3 overexpressed, DIS3L2 KO and WT cell lines using biotinylated oligonucleotides. After two consecutive purification steps, the U1 snRNA was highly enriched (Figure 39B, lanes 3, 6, 9 and12), and was then subjected to CuAAC-NAD biotinylation. Retained RNAs were eluted on streptavidin beads and analyzed by northern blotting (Figure 39C). Only a weak signal was detected in U1 from HEK293T (lane 7). Considering that the bond linking the base to the ribose can be targeted by ADPRC in both NAD-RNA and m^7GpppA-RNA (Hu *et al.,* 2021; Zhang *et al.,* 2021), we cannot exclude the possibility that the hypermethylated cap present on mature snRNAs ($m_3^{2,2,7}$G) could also be modified by ADPRC, biotinylated and enriched. However, we did not detect any signal in the other samples (lane 5, 6, and 8), as it should be the case if m^3G-capped U1 was enriched. In the future, we would advise to first test if m^3G-capped-RNAs are targeted by ADPRC, as this has not been shown yet, to repeat the assay with NADylated RNA and m^3G-capped RNA spike-ins to evaluate the enrichment specificity, and, if necessary, to add a prior m^3G-RNA depletion step (e.g. by an antibody against the TMG cap (Bochnig *et al.,* 1987). Altogether, this renders difficult to draw any further conclusions about the potential presence of 5'-NAD on U1 snRNA.

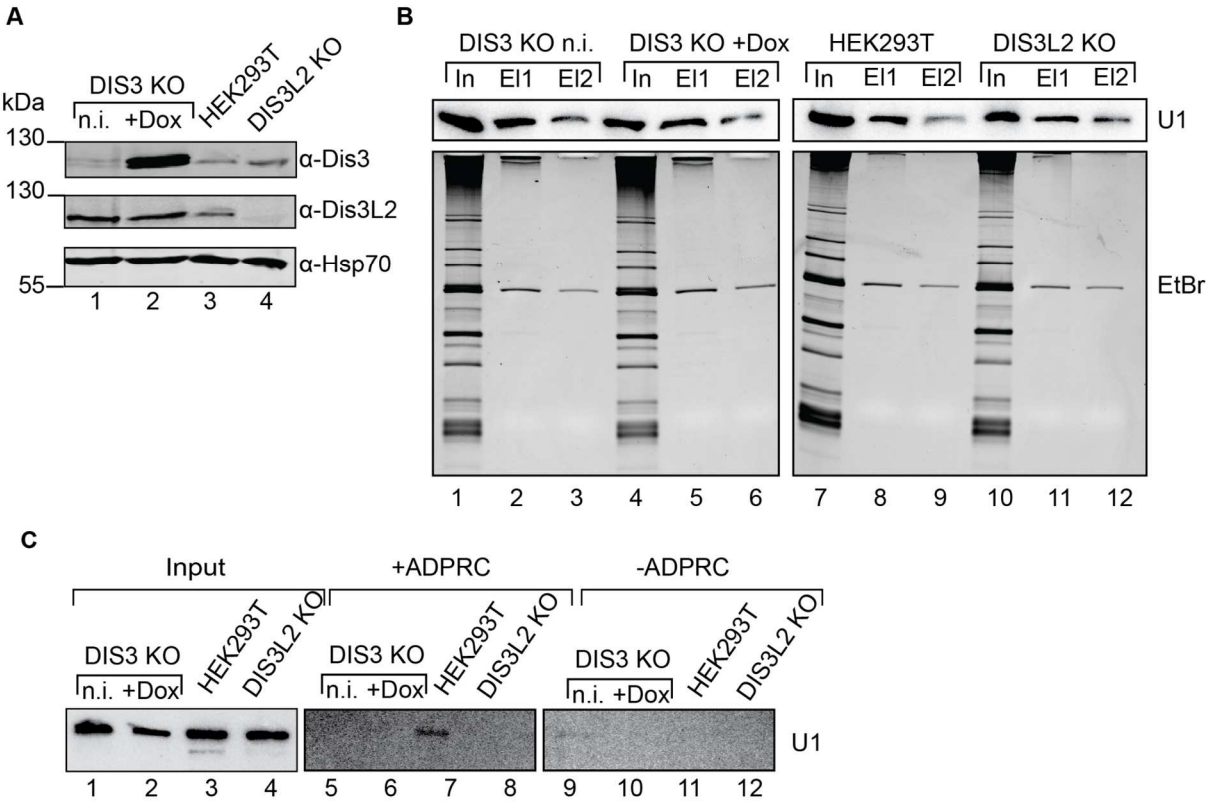

Figure 39. Analysis of NADylated U1 upon enrichment with CuAAC-NAD biotinylation. (A) Validation of the cell lines by Western blot. DIS3 and DIS3L2 expression was detected with specific antibodies. Leaky expression of the exogenous DIS3 was detected in the conditional knockout cell line (DIS3 KO) under non-induced conditions (n.i.). Overexpressed DIS3 in DIS3 KO was detected upon induction with doxycycline (+dox) for 48 h. Detection of Hsp70 served as a loading control. Molecular size marker weights are depicted on the left. (B) Analysis of U1 snRNA enrichment. U1 snRNA was isolated using biotinylated antisense oligonucleotidese in two consecutive purification rounds from total RNA extracted from each cell line. Inputs (In), and aliquots saved after each eluated rounds (El1 and El2) were analyzed by nothern blotting using a complementary radiolabeled probe to detect isolated U1 snRNA (top) Ethidium bromide staining of the gel before blotting served as a control for RNA quality (bottom). (C) Isolated U1 was subjected to CuAAC-NAD biotinylation in the presence (+) or absence (-) of ADPRC and analyzed by norther blotting. The input before the reaction and enriched biotyinlated RNA eluted from magnetic streptavidin beads with 2X RNA loading dye were resolved on a denaturating PAA gel. U1 snRNA was detected by northern blotting using a complementary radiolabeled probe

.

3 DISCUSSION

The m^7G cap structure that can be present at the 5'-end of RNA is crucial for RNA metabolism (Pelletier *et al.,* 2021). Recently, the nucleotide-containing coenzyme NAD was discovered to be covalently linked to the 5'-end of some RNA species (Doamekpor *et al.,* 2022; Mattay, 2022). This discovery has been made possible by the development of high-throughput techniques. However, these methods heavily rely on the enzymatic modification of the NAD moiety prior to their enrichment, and this gives rise to specificity biases (Möhler and Jäschke, 2023). Therefore, we explored the possibility to directly target NADylated RNAs, and coupled it to a deNADding step for higher specificity. To establish our assays, we first implemented the synthesis of NADylated RNAs in our laboratory (2.1), we expressed and purified a deNADding enzyme (2.2.1), we explored the possibility of NADylated RNA-capture by using antibodies or aptamers as NAD-binding structures (2.2.2), and we began investigating endogenous NADylated RNAs in a relevant biological context (2.3).

3.1 ADVANTAGES AND LIMITATIONS OF DIFFERENT SYNTHESIS METHODS FOR NADYLATED RNAS

The study of non-canonically capped RNA currently suffers from the lack of mass manufacturing of such RNAs. Thus, our first step was to synthesize NADylated RNAs, as 5'-NAD-modified RNAs are notyet commercially available yet. We implemented two methods in the laboratory: co-transcriptional incorporation of NAD by T7 RNA polymerase (Huang 2003), and chemical synthesis of NADylated RNAs (Höfer *et al.*, 2016a), both presenting their advantages and limitations.

3.1.1 Co-transcriptional incorporation of NAD

The use of T7 class II (ϕ2.5) promotor allows transcription to be initiated by adenosine-containing nucleotides (Huang 2003). When NAD is added to the reaction mix, the *in vitro* transcription from a DNA template containing internal adenine generates a mixture of NADylated RNA and triphosphorylated adenosine-starting

RNA. Although the RNA production can be nudged towards 5'-NAD-modified RNAs by using a higher amount of NAD as initiating nucleotide in the reaction mix, the transcription of triphosphorylated RNAs cannot be avoided. Therefore, the subsequent separation of these two species is required, which can be achieved by acryloylaminophenyl boronic acid (APB) polyacrylamide gel electrophoresis (Nübel *et al.,* 2017).

During our first tests, we directly ran the crude *in vitro* transcription reaction mixture on an APB gel containing appropriate polyacrylamide percentages to simultaneously separate the RNA according to their 5'-end and on their size (data not shown), minimizing time and handling steps as suggested by Nübel *et al.,* (2017). However, we realized in later experiments that this can still lead to the copurification of abortive products, which can be detected under sensitive measurement conditions (e.g. ^{32}P-labeling), but not by ethidium bromide staining.

Therefore, we switched to a two-step purification of the transcription mixture, first by resolving the RNAs on a PAA gel, to ensure the purification of RNAs homogenous in size, followed by APB affinity gel electrophoresis, to separate the RNAs based on their 5'-end modification (Figure 14A). The size, purity, and integrity of the RNAs were confirmed on an analytical PAA gel, and their 5'-ends on an analytical APB gel before further use (Figure 14B). However, high purity and homogeneity were obtained at the expense of yield, because of two consecutive gel purifications leading to an inevitable loss of material. However, this method presents the advantage of being easily implemented in a laboratory familiar with T7 *in vitro* transcription and urea-PAGE electrophoresis.

Interestingly, Niu *et al.,* (2023) took advantage of the boronic acid affinity binding properties to develop an enrichment method based on boronic acid beads. This method allowed them to enrich NADylated RNA over 5'-monophosphorylated RNA, and could also be used to separate NADylated RNAs from triphosphorylated RNA after *in vitro* transcription. However, it does require the blocking of the diol of the ribose at the 3'-end of the RNA that could otherwise also interact with boronic acid.

The use of the T7 class II (ϕ2.5) promotor, which requires an adenosine-containing initiating nucleotide, allows the easy substitution of NAD by synthetic NAD analogs. NAD analogs could become an important chemical tool to study NADylated RNA, by

modulating the resistance of the NAD group to enzymatic cleavage or its affinity to binding proteins, or by allowing to monitor the modified NADylated RNA. For instance, Mlynarska-Cieslak *et al.,* (2018) synthesized new di- and tri-nucleotides NAD analogs possessing modifications at the pyrophosphate bridge of NAD or within the phosphodiester bond between NAD and the third nucleotide. They could be recognized and incorporated into RNA 5'-ends by T7 Polymerase, some of them with very high efficiency. These NAD analogs altered the susceptibility of the modified NADylated RNAs to enzymatic cleavage, making them a useful tool to study deNADding enzymes. The increased stability of these modified NADylated RNAs could thus also be useful in a cellular context to study the turnover of NADylated RNA. As another example, fluorescent NAD analogs could allow real-time monitoring of cleavage activity, a property that has been exploited by Abele *et al.,* (2020) in a high-throughput screening approach to discover new deNADding enzymes. Additionally, incorporation of fluorescent NAD could also allow visualization or tracking of NADylated RNA molecules in cells upon transfection. As a prior inspiration, m^7G cap analogs have become invaluable assets in investigatating m^7G-capped RNA translation, localization, stability, turnover, and cap-binding partners (Ziemniak *et al.,* 2013; Warminski *et al.,* 2017, 2023; Bollu *et al.,* 2022; Shanmugasundaram *et al.,* 2022).

3.1.2 Chemical synthesis of NADylated RNA

As an alternative to *in vitro* transcription, we implemented the synthesis of NADylated RNAs using a phosphorimidazolide chemistry-based approach, in which an imidazole-activated NMN is coupled to a 5'-monophosphorylated RNA (Höfer *et al.*, 2016a). We applied this chemical method to RNAs of different lengths; however, yield, separation and purification remain an issue to consider.

The small size of a 5-mer RNA allowed to follow the conversion of the 5'-monophosphorylated RNA to a NADylated RNA by HPLC analysis (Figure 15B). However, the longer size of a 30-mer RNA prevented such a single-nucleotide resolution, which does not allow to monitor the addition of one NAD group to a monophosphorylated RNA. Therefore, we separated the reaction by APB gel electrophoresis, which allowed us to assess the success of the conversion of the 5'-

end (Figure 15C). The reaction was not fully complete under the conditions used, but was similar to the synthesis yield of 45% observed by Höfer *et al.*, (2016a). Therefore, the separation of NADylated RNAs from uncapped RNAs after synthesis and 5'-end modification steps remains necessary regardless of the applied method (*in vitro* transcription or chemical).

Höfer *et al.*, (2016a) used an enzymatic approach to remove unreacted 5'-monophosphorylated RNA by digestion with the 5'-3' exoribonuclease XRN-1, which recognizes 5'-monophosphate. However, when testing this approach in our earlier trials with commercially available XRN-1, we observed incomplete digestion and unspecific RNA degradation (data not shown). Furthermore, enzymatic digestion requires an additional cleaning step to remove the enzyme, and digestion conditions need to be optimized to ensure the complete digestion of the unwanted 5'-monophosphorylated RNA. Thus, we decided to pursue the APB gel-based purification approach for our synthesized NADylated RNAs. Nevertheless, enzymatic digestion could still be considered for RNAs of longer size that would not be able to be resolved by APB gel electrophoresis.

The phosphorimidazolide chemistry-based method can be applied to any 5'-monophosphorylated RNA. A 5'-monophosphorylated RNA that starts with an adenosine (5'-pA-RNA) can be easily obtained by *in vitro* transcription when using a DNA template containing a single adenosine at the starting position, and AMP in the nucleotide mix. However, a DNA template containing internal adenines requires the use of ATP in the nucleotide mix, and therefore 5'-triphosphorylated RNAs are also generated as a side product. Thus, the transcribed RNAs require first the removal of the 5'-pyrophosphate moieties before being subjected to chemical capping. This step could be performed enzymatically with the use of the Rpp for instance, however, this would add another enzymatic and associated clean-up step with potential loss of material. Therefore, considering the additional cost and handling reasons, we decided to pursue the synthesis of the NADylated RNA used in our studies by *in vitro* transcription.

Nevertheless, the chemical approach presents two advantages that the co-transcriptional synthesis approach cannot offer. First, an additional labeling step could be introduced (including a radioactive label, a fluorophore, an affinity tag or

other small molecules) on the gamma phosphate of the 5'-monophosphorylated RNA before the reaction. The coupling would then result in an internally-labeled NAD cap with versatile uses for decapping studies. For example, ^{32}[P]NAD is very expensive, and this is an alternative way to produce ^{32}[P]-labeled NADylated RNA (NRp*pA-RNA) with a lower cost (Höfer *et al.,* 2016a). Second, this chemical capping enables the preparation of long NADylated RNAs that cannot be run on an APB gel due to their size. Additionally, this limitation could be circumvented by combining the ligation of a short chemically NAD-capped oligonucleotide to a longer RNA body generated by *in vitro* transcription, as it can already be done for other 5'-end modifications (Depmeier *et al.,* 2021).

The study of NADylated RNA would benefit from the discovery or the development of an enzyme or protein complex capable of covalently adding a NAD or NMN moiety to the 5'-end of an RNA in a sequence-independent manner. Wiedermannová, *et al.,* (2021) suggested different possible post-transcriptional mechanisms of NADylation: first, that some enzymes involved in the NAD biogenesis pathway could catalyze the transfer of a nicotinamide ribonucleotide to a 5'-ATP-ending RNA (pppA-RNA), second, by the covalent binding of a NAD molecule to a triphosphorylated RNA, and finally, by the transfer of nicotinamide to an ADP-ribosylated RNA. Wiedermannová, *et al.,* (2021) tested whether the bacterial nicotinamide mononucleotide adenylyl-transferases (NMNAT) NadD and NadR could use NMN to modify a triphosphorylated RNA *in vitro*, but they did not observe any capping activity. Thus, a post-transcriptionally acting NADylating-enzyme remains yet to be discovered.

3.1.3 Validation of 5'-NAD-linked RNA

We validated the presence of NAD linked to the 5'-end of the RNA after *in vitro* transcription or chemical synthesis using by two methods that did not rely on boronic acid affinity binding.

First, we used Rpp, which removes the gamma and beta phosphate of a triphosphorylated RNA but has no effect on the 5'-end of protected NADylated RNA, followed by a treatment with XNR-1, which degrades RNAs carrying a 5'-monosphophate (Figure 16). By this assay, we were able to confirm that the 5'-end of our synthesized NADylated RNA was protected from degradation. However, the

enzymes used in decapping and degradation assays should be carefully selected. For instance, the *E. coli* RNA 5´-Pyrophosphohydrolase (RppH) is commercially available and is used to convert 5'-triphosphorylated RNAs into 5'-monophosphorylated RNAs (Almeida *et al.,* 2019). RppH was originally reported to be inactive on NADylated RNAs (Cahová *et al.,* 2015; Bird *et al.,* 2016), however, later reports showed its cleavage activity on NADylated RNAs too (Grudzien-Nogalska *et al*, (2019). This activity may be explained by the RNA substrate sequence used in their decapping studies, since the *B. subtilis* homolog of RppH has a preference for RNA carrying a guanosine residue at the +2 position (Hsieh *et al.,* 2013; Piton *et al.,* 2013; Gao *et al.,* 2020). Furthermore, Sharma *et al.,* (2022b) recently uncovered a deNADding activity of the yeast Xrn1, and the XRN-1 exoribonuclease provided by NEB is purified from a plasmid overexpressing the yeast XRN-1 gene. Although we did not observe NAD removal or degradation of our NADylated RNA by XRN-1, all together, this highlights the need to be cautious when considering the activity of 5'-processing enzymes on novel or uncharacterized cap structures.

Second, we modified a fluorometric NAD detection assay (Putt and Hergenrother, 2004) to confirm the presence of NAD on our synthesized NADylated RNAs by a rapid and simple procedure (Figure 17). Interestingly, a preprint study developed a method based on this fluorescence reaction, namely FluorCapQ, to quantify bulk NADylated RNA levels in bacteria (Wiedermannova *et al.,* 2023).

3.2 CHALLENGES OF DEVELOPING NADYLATED RNA IDENTIFICATION METHODS

The main obstacle to the identification of NADylated RNAs lie in their low abundance, especially in higher eukaryotes compared to bacteria, and the lack of tools to specifically enrich them. Several protocols have been developed over the years to identify and sequence NADylated RNAs and can be classified in two groups: decapping approaches and capture approaches (reviewed in Möhler and Jäschke, 2023).

3.2.1 Decapping approach

The identification of the deNADding enzyme NudC and its mechanism of action i.e. cleaving NADylated RNAs within the diphosphate bridge of NAD (Cahová *et al.,* 2015; Höfer *et al.,* 2016b; Zhang *et al.,* 2016), quickly led to the idea of taking advantage of this function. By yielding 5'-monophosphate products, direct 5'-ligation of an adapter could be performed for the preparation of a sequencing library and the identification of NADylated RNA sequences. CapZyme-Seq (Vvedenskaya *et al.,* 2018) was based on this idea, and used a combination of two decapping enzymes, the bacterial NudC (Cahová *et al.,* 2015) and the fungal Rai1 (Xiang *et al.,* 2009). However, NudC and Rai1 are not specific for NADylated RNAs and exhibit cleavage activity toward other nucleotide-containing metabolites that harbor a diphosphate bridge (Table 2). Thus, this method could only contribute to the identification of RNAs with different 5'-ends, but not of the specific nature of the 5'-cap (NAD, FAD, dp-CoA or yet other uncovered non-canonical caps). Therefore, a standalone decapping approach cannot be used as a *de novo* identification method of NADylated RNAs, because all the deNADding enzymes characterized so far possess a lack of specificity toward the NAD cap to some extent (Table 2).

However, we reasoned that, under the condition of adding a first step of enrichment of NADylated RNAs (3.2.2), we could still take advantage of the yielded 5'-monophosphate for sequencing. Thus, we selected Nudt12 (2.2.1.1), the human homolog of NudC, expressed and purified it (Figure 20). We assessed its activity on NADylated RNAs of different sequences (Figure 22 and Figure 23) and did not observe a cleavage activity on m^7G-capped RNAs (Figure 23) as previously reported by Wu *et al.,* (2019). However, this could have resulted from the sensitivity of the assay we used (APB gel electrophoresis and 3'-end labeled RNAs). In fact, resolution of decapping reactions by thin-layer chromatography has revealed a slight activity of human Nudt12 on m^7G-capped RNAs (Wu *et al.,* 2019). However, these thin-layer chromatography assays have also shown that human Nudt12 cleaved m^7G-RNA between the gamma and beta phosphate, liberating m^7GMP and a 5'-diphosphorylated RNA. There 5'-adaptor ligation would fail with such products, and

cleavage of m^{7}G-capped RNA would not alter the specific generation of NADylated RNA libraries.

Interestingly, Wu *et al.,* (2019) have mutated residues in the conserved catalytic Nudix motif of a shortened version of human Nudt12 and generated an enzyme exclusively active on NADylated RNAs. However, the cleavage activity of the shortened mutant Nudt12 has not been tested on other non-canonically capped RNAs substrates. This could be important, since the mouse homolog of Nudt12 possesses deCoAping activity *in vitro* (Sharma *et al.,* 2020). Nevertheless, the engineering of decapping enzymes that are only active on specific 5'-cap structures could renew the interest of decapping approaches that are directly coupled to sequencing.

3.2.2 Capture approach

All capture strategies available to date rely on the prior chemo-enzymatic modification of NADylated RNAs. Thus, we explored two binding approaches directly targeting the 5'-NAD moiety of NADylated RNAs: by antibodies (2.2.2.1) and aptamers (2.2.2.2).

3.2.2.1 Antibody-based capture

To date, no antibodies against non-canonical caps have been developed. Thus, we attempted to establish antibodies against 5'-NADylated RNAs. To this end, we accordingly synthesized antigens (R. Hett, our lab), and monoclonal antibodies against NAD and NMN were generated by our collaborators (R. Feederle, Helmholtz Munich). Antigens were synthesized by conjugating NADH or NMN to ovalbumin by oxidative coupling (Erlanger and Beiser, 1964). During this reaction, the ribose ring is opened between the 2' and the 3' position to allow the coupling to the immunogenic carrier. In the context of RNA modifications, this means that antibodies generated with this method do not discriminate between deoxyribose and ribose (thus between DNA and RNA) or additional modifications of the hydroxyl group of the ribose (e.g. 2'-*O*-methylation). Therefore, in the case of NMN or NAD, this could influence the specificity of recognition of the antibody to 5'-NADylated RNA. Other coupling methods could be considered. For instance, Matsuzawa *et al.,* (2019) crosslinked oligonucleotides containing the m^{6}A modification with keyhole limpet hemocyanin

(KLH) as an immunogenic carrier protein. This method allowed the ribose group to remain intact. The resulting KHL-conjugated m^6A-oligo was used for immunization, and monoclonal antibodies against m^6A were successfully generated. However, in the case of a 5'-NADylated RNA, using a 5'-modified oligonucleotide could cause the generate of antibodies with a bias towards the employed RNA sequence and not the 5'-modification itself.

When testing the hybridoma supernatants we received from our collaborators by EMSA to compare their binding affinity with NADylated RNAs next to triphosphorylated RNAs of identical sequence as a negative control, clones 26D11 and 28C11 showed an interaction with NADylated RNAs (Figure 25). However, with fresh hybridoma supernatants of larger scale, we could not repeat this effect, neither with the hybridoma supernatant (Figure 27), nor with the antibodies purified from them (Figure 26). Thus, the initially observed shift could have derived from a batch effect. We chose EMSA as an antibody screening method because of several advantages: the possibility to directly compare side-by-side bound NADylated RNAs and unbound triphosphorylated RNAs as negative control, the possibility of interaction detection with great sensitivity due to the radiolabeling of the RNAs, which benefited our situation of limited material at our disposal, and allowed the assay to take into account the RNA body context. Another approach could have been performed by immunoprecipitation after coupling the antibody to beads and incubating it with the NADylated RNAs. However, RNA immunoprecipitation with antibodies often requires condition optimization, such as testing of different antibody dilutions, buffer composition (e.g. salt and pH), incubation times, and washing conditions (Weichmann, 2019). Furthermore, the lack of abundant endogenous NADylated RNAs validated in HEK293T prevented us from testing and optimizing our antibodies in an *in vivo* context (Table 1) Indeed, only NAD captureSeq, with the known biases associated to this method (1.3.2.2), has been used in human cells (Jiao *et al.*, 2017; Grudzien-Nogalska *et al.*, 2019). Very recently, a one-step chemo-enzymatic method using a new reagent (ONE-seq, Niu *et al.*, 2023) has been performed in mice tissues, and the identified NADylated RNAs were further validated by an ADPRC-independent method. Thus, the human homologs of theses RNAs could be used as putative targets for further endogenous NADylated RNA capture assays.

While we were unable to identify robust NADylated RNA-binding antibody candidates, we remain convinced that establishing monoclonal antibodies against 5'-NAD structure would be beneficial for the study of NADylated RNAs. Antibody-based immunoprecipitation of NADylated RNA could be combined either to qPCR and mass spectrometry-based analysis to quantify them, or to transcriptome-wide sequencing to profile them, as this has been done for example for the TMG cap structure (Jia *et al.*, 2007; Martinez *et al.*, 2017b) or the RNA modifications m^6A (Dominissini *et al.*, 2012; Meyer *et al.*, 2012), m^5C (Edelheit *et al.*, 2013; Cui *et al.*, 2017) or internal m^7G (Zhang *et al.*, 2019b). To be noted, specificity and cross-reactivity remain an issue for many antibodies against RNA modifications, and can lead to false positive results (Mishima *et al.,* 2015; Grozhik *et al.,* 2019; Helm *et al.,* 2019). Thus, antibodies must be thoroughly validated before experimental use (Weichmann 2020).

3.2.2.2 Aptamer-based capture

Aptamers are single-stranded oligonucleotides that, upon folding, can bind ligands in a similar way to antibodies (reviewed in Walter, Stahl, and Scheper 2012, and in Ali, Elsherbiny, and Emara 2019). We tested whether aptamers binding NMN or NAD could be used to capture NADylated RNAs and we selected the NMN aptamer identified by Lauhon and Szostak (1995) and the NAD-class II riboswitch identified by Panchapakesan *et al.,* (2021) for our studies (2.2.2.2.1). The RNA aptamers were *in vitro* transcribed with the addition of a 5'-leader sequence complementary to a 3'-biotinylated 2′-*O*-methyl-modified adaptor. This allowed the aptamer to hybridize to the adaptor that has been previously coupled to streptavidin beads. This "RNA bait" method has been successfully used in our lab to identify RNA-binding proteins that bind to miRNA-hairpin sequences (Treiber *et al.*, 2017). Here, we performed a modified version with the NMN aptamer or the NAD-class II riboswitch to capture NADylated RNAs.

We observed a better enrichment of NADylated RNAs with the NMN aptamer than with the NAD-class II riboswitch (Figure 30, Figure 31 and Figure 32). This would reflect the difference in their dissociation constant, estimated at 2.5 µM for the NMN aptamer (Lauhon and Szostak, 1995) and at 41.1 µM for the NAD-class II riboswitch (Xu *et al.*, 2023). Very recently, Xu *et al.,* (2023) solved the crystal structure of the NAD-class II riboswitch in complex with NAD. This allowed them to design a

shortened sequence, retaining an affinity towards NMN comparable to that of the original riboswitch. Thus, the binding affinity of this minimized riboswitch for NADylated RNAs could also be interesting to test in the future.

When testing the NMN aptamer, we constated the preferential enrichment of NADylated RNAs compared to monophosphorylated RNAs (Figure 30), triphosphorylated RNA (Figure 31), and m^7G-capped RNAs (Figure 32 and Figure 33) of the same sequence. However, it would be important to repeat the capture assay under different conditions before concluding on a successful enrichment method usable in a biological context. First, a mixture of NADylated RNAs and m^7G-capped RNAs could be used to further assess specificity. Modulating the ratio of NADylated RNAs relative to m^7G-capped RNAs (for example 10%, 5%, or even 1%) would reflect the low abundancy of NADylated RNAs encountered *in vivo*. This would allow to assess the sensitivity of the capture method as it has been done by Niu *et al.*, (2023) when they had established ONE-seq. Second, RNAs with different lengths should be tested. Here, we used RNA of relatively short size (smaller than 100 nt), however, since SPAAC-NAD-Seq has allowed the identification of full-length NADylated RNAs, some even polyadenylated, (Hu *et al.*, 2021), it would be interesting to confirm that NADylated RNAs of several hundreds of nucleotides can also be enriched. Finally, repeating the capture assay with spike-in NADylated RNAs mixed with total RNA would allow to assess the specificity of the method within an RNA background context.

Unfortunately, we could not elute captured NADylated RNAs by competitive elution with NMN nor NAD (Figure 32 andFigure 33) under the conditions used in our assay. There could be two explanations. On the one hand, this could either mean that the aptamer binds NADylated RNAs with high affinity. In their selection experiments, Lauhon and Szostak, (1995) used different ligand concentrations: during the aptamer original selection, the NMN aptamers binding to the NAD column were eluted with 5 mM NMN, however, for column binding assays, the aptamer was eluted with a NAD concentration equal to the NAD portions bound to the column. Therefore, it is unclear whether we should expect the elution of capture NADylated RNAs under the conditions we used. On the other end, it could also signify that the enrichment of NADylated RNAs by the aptamer we observed was non-specific and thus cannot be

eluted by its ligand (NAD or NMN). However, competitive elution could also be performed with other small molecules or ions that interfere directly with the aptamer binding site. For instance, adenosine bound by a DNA aptamer was eluted by competitive binding of Ni^{2+} and Zn^{2+} (Deng *et al.*, 2003). Alternative elution strategies could also be considered, for instance by the use of chelating agents to remove the ions stabilizing the aptamer tertiary structure (Romig *et al.*, 1999).

Finally, we performed a Nudt12-catalyzed elution with the recombinant Nudt12 that we expressed an purified. However, both captured NADylated RNAs and unspecifically bound m^7G-capped RNAs were released after cleavage reaction (Figure 33). We hypothesized that the temperature or the buffer composition might have disrupted the stability and the folding of the aptamer. Unfortunately, the decapping step could not be further optimized due to time constraints. Nonetheless, if the elution of bound NADylated RNAs through Nudt12 cleavage could have been confirmed, we would have established an aptamer-based capture approach of NADylated RNAs with a deNADding-mediated elution. The 5'-monophosphates of the cleaved RNAs would allow for specific for adapter ligation for library preparation and subsequent sequencing analysis. To be noted, the two most recently published NADylated RNA capture protocols have added an enzymatic step to overcome the issue of the promiscuity activity of the ADPRC enzyme on m^7G-capped RNAs. NADcapPro (Sharma *et al.*, 2023) used Dcs1, the yeast homolog of the scavenger decapping enzyme DcpS, to decap m^7G-capped RNAs prior to the SPAAC-based capture of NADylated RNAs. ONE-Seq (Niu *et al.*, 2023) used the bacterial deNADding enzyme NudC to elute NADylated RNAs captured on streptavidin beads after ADPRC-catalyzed biotinylation. Thus, the combination of a decapping and a capture approach has been shown to contribute to increasing the specificity of the capture approach. So far, no other method offers the possibility to directly bind the NAD modification for enrichment of NADylated RNAs.

Additionally, this aptamer-based capture approach could be easily adapted to enrich other non-canonical caps. For instance, aptamers against coenzyme A (Burke and Hoffman, 1998) and flavine adenine dinucleotide (Burgstaller and Famulok, 1994; Lauhon and Szostak, 1995; Sengupta *et al.*, 2014; Merkle *et al.*, 2016) have been

identified. The sequences could thus be tested for the capture of CoAlated and FADylated RNAs.

3.2.3 Alternative identification approaches of NADylated RNAs

Although this thesis explored enzymatic treatment and antibody- and aptamer-based captures as potential methods to identify NADylated RNAs, other strategies could have been envisaged.

3.2.3.1 Protein-based capture

The binding affinity of a protein to an RNA of interest has been exploited by protocols based on the immuno-purification of RNA-binding proteins and their associated RNAs followed by RNA sequencing, such as RNA immunoprecipitation (RIP) or UV crosslinking and immunoprecipitation (CLIP) (reviewed in Hafner *et al.*, 2021). Immunoprecipitation of enzymes that install or read a specific RNA modification has been used to map RNA modifications, for instance, of the RNA methyltransferase NSun2 and its target site m^5C (Hussain *et al.*, 2013), or of the *E. Coli* Endonuclease V binding to inosine (Knutson *et al.*, 2020). Although there is no known enzyme capable to add a NAD cap to RNA transcripts, enzymes or proteins with binding affinity toward NAD or NMN could be used to directly target NADylated RNAs. A first possibility could be to use a known deNADding enzyme (Table 2), however, this might require point-mutations to disable the NAD cleavage activity and enhance the binding. A second possibility could be to use the NAD-binding domain of enzymes using NAD as cofactors (Bellamacina, 1996), for example, the NAD-binding domain of dehydrogenases (Lesk, 1995) or the Nudix homology domain (NHD) of the protein deleted in breast cancer 1 (DBC1) that binds NAD and NMN (Li *et al.,* 2017; Ou *et al.,* 2024).

3.2.3.2 Chemical-assisted approach

Chemical treatment coupled to sequencing is commonly used to detect and map internal RNA modifications (reviewed in Yoluç *et al.,* 2021; Zhang *et al.,* 2022; Motorin and Helm, 2024). Specific treatment can either cleave the RNA chain at the modification site or create a bulky chemical modification, which impairs the reverse transcription step during the library preparation and generates a detectable signature

(reviewed in Behm-Ansmant *et al.*, 2011; Motorin and Helm, 2024). In the case of the NAD modification, this would be irrelevant since the modification is located at the very end of the RNA and not internally. But a chemical approach could be used to specifically cleave the 5'-NMN or 5'-NAD of NADylated RNA, and be coupled to the ligation of a specific adapter followed by library preparation and sequencing. For instance, similarly to the decapping approach, a chemical treatment could induce a specific cleavage within the diphosphate bridge of the NAD, or immediately after the entire NAD moiety to yield a monophosphorylated RNA. The available 5'-monophosphate could then be used for adaptor ligation.

3.3 INVESTIGATION OF ENDOGENOUS NADYLATED RNAS

We tried to establish a luminescent-based assay to detect and quantify endogenous NAD cap levels. This two-step assay consisted of the digestion of RNA into nucleotides followed by the detection of free NAD with a luminescent detection kit. While the assay could be validated with our *in vitro* transcribed NADylated RNAs (Figure 35), unfortunately we could not establish its functionality *in vivo* when we applied it to analyze NADylated RNAs levels in total RNA from human cells (Figure 36). The available colorimetry-based assay NAD-capQ (Grudzien-Nogalska *et al.*, 2018) provided an accurate estimation of endogenous NAD-cap levels in procaryotes and yeast, however, its accuracy and sensitivity in mammals is more unclear (Wang *et al.*, 2019a). An assay allowing for the reliable quantification of levels of NADylated RNAs would be useful for screening and selecting *in vivo* conditions favorable for the study of endogenous NADylated RNAs. For instance, NADylated RNA levels have not been comparatively evaluated across all mice organs, but only in the liver and kidney (Wang *et al.*, 2019a; Niu *et al.*, 2023), neither across different types of human cells, but only in HEK293T cells (Grudzien-Nogalska *et al.*, 2018; Sharma *et al.*, 2020) and CCRF-SB cells (Wang *et al.*, 2019a). A tissue or cell line with higher levels of endogenous NADylated RNAs may provide a better context for investigating their biological roles.

Another way to increase endogenous NADylated RNA levels could be achieved by combining the deletion of decapping enzymes with the deletion of exonucleases, as we have initiated by investigating the NADylation status of U1 snRNA in DIS3 and

DIS3L2 knockout cell lines (Figure 39). Deletion of different deNADding enzymes has been done in yeast and unveiled a spatial and temporal hierarchical surveillance pathway of NADylated RNAs (Zhang *et al.*, 2020). However, only a double knockout cell line of Nudt12 and DXO has been generated in HEK293T cells and subjected to NAD-captureSeq (Grudzien-Nogalska *et al.*, 2019). Therefore, targeting the deNADding machinery in combination with 5'-3' or 3'-5' RNA degradation pathways could provide valuable insights on the regulatory mechanisms of NADylation and deNADding in mammals. For instance, considering the cytoplasmic subcellular localization of Nudt12 (Carreras-Puigvert *et al.*, 2017; Wu *et al.*, 2019), targeting together Nudt12 and XRN1 could prevent the decapping and 5'-3' degradation of NADylated RNAs in the cytoplasm. Furthermore, Nudt12 has been shown to hydrolyze *in vitro* a variety of dinucleotide cap structures with a marked preference for adenosine as one of the nucleotides (Song *et al.*, 2013; Lukaszewicz *et al.*, 2023). Thus, Nudt12 has the potential to act as a scavenging enzyme for NAD cap structures remaining after the degradation of NADylated RNAs in a 3'-5'-dependant manner, in a similar fashion to DcpS (Wang and Kiledjian, 2001).

In summary, the discovery of NADylated RNAs and RNA modified with other nucleotide-containing coenzymes provided a new link between RNA and energy metabolism as well as a novel addition to the cap epitranscriptome repertoire. However, numerous questions remain unanswered regarding their regulation and their biological roles in eukaryotes. The development of robust methods to detect, quantify, capture, and identify NADylated RNAs with high sensitivity, specificity, and reproducibility is strongly needed. Our aptamer-based capture approach, while requiring further optimization before *in vivo* applications, offers a new alternative for the enrichment of NADylated RNAs by directly targeting the NAD modification.

4 MATERIAL AND METHODS

4.1 MATERIAL

4.1.1 Antibodies

The antibodies used in this thesis are listed in Table 4.

Table 4. List of antibodies

Antibodies	Source	Identifier	Dilution
DIS3	Bethyl Laboratories	Cat#A303-765A; RRID:AB_11205807	1:1000
DIS3L2	Proteintech	Cat#67623-1-Ig; RRID:AB_2882825	1:5000
HSP70	Santa Cruz Biotechnology	Cat# sc-24; RRID:AB_627760	1:1000
Goat anti-Mouse IgG, IRDye 680RD conjugated antibody	LI-COR Biosciences	Cat#926-68070; RRID:AB_10956588	1:10000
Goat polyclonal anti-Mouse IgG, IRDye 800CW conjugated antibody	LI-COR Bioscience	Cat#925-32210; RRID:AB_2687825	1:10000
Goat polyclonal anti-Rabbit IgG, IRDye 800CW conjugated antibody	LI-COR Bioscience	Cat#926-32211; RRID:AB_621843	1:10000
Goat polyclonal anti-Rat IgG, IRDye 800CW conjugated antibody	LI-COR Bioscience	Cat#926-32219; RRID:AB_1850025	1:10000
IRDye® 800CW Streptavidin	LI-COR Bioscience	Cat#926-32230	1:10000

4.1.2 Bacterial strains

The bacterial strains used in this thesis are listed in Table 5.

Table 5. List of bacterial strains

Bacterial strains	Source
Escherichia coli Rosetta (DE3) competent cells	Our laboratory
XL1 blue competent cells	Our laboratory

4.1.3 Cell lines

The cell lines used in this thesis are listed in Table 6.

Table 6. List of cell lines

Cell Line	Source	Identifier
HEK293T	Our laboratory	ATCC CRL-3216, RRID:CVCL_0063
Flp-In™ T-REx™ 293 cell line	Invitrogen	Cat#R78007; RRID:CVCL_U427

4.1.4 Chemicals

Unless specified differently, all chemicals used were purchased in the highest standard (analytical grade) from the following suppliers: AppliChem (Darmstadt, Germany), Biorad (Hercules, USA), Merck (Darmstadt, Germany), Roche Diagnostics (Penzberg, Germany), Roth (Karlsruhe, Germany), Sigma-Aldrich (St. Louis, USA) and Thermo Fisher Science (Waltham, USA). Enzymes and their respective buffers were obtained from Thermo Scientific (Waltham, USA) and New England Biolabs (Ipswich, USA). Cell culture reagents were purchased from Sigma-Aldrich (St. Louis, USA). Radiochemicals were purchased from Hartmann Analytic GmbH (Braunschweig, Germany). Other consumables were purchased from the following suppliers: Sarstedt (Numbrecht, Germany), GE Healthcare (Buckinghamshire, UK), Biorad (Hercules, USA), Eppendorf (Hamburg, Germany), and Invitrogen (Carlsbad, USA).

4.1.5 Commercial kits

The commercial kits used in this thesis are listed in Table 7

Table 7. List of commercial kits

Kit	Company	Identifier
First-strand cDNA synthesis kit	Thermo Fisher Scientific	Cat#K1612
NAD/NADH-Glo™ Assay	Promega	Cat#G9071
NucleoBond Xtra, Midi kit	Macherey-Nagel	Cat#740422.50
NucleoSpin Gel and PCR Clean-up kit	Macherey-Nagel	Cat#740609.50
NucleoSpin Plasmid, Mini kit	Macherey-Nagel	Cat#740588.50
Oligo Clean & Concentrator	Zymo	Cat#D4060
Phusion™ High-Fidelity DNA Polymerase	Thermo Scientific	Cat#M0530L
T4 DNA Ligase kit	Thermo Fisher Scientific	Cat#EL0011
Vaccinia Capping System	New England BioLabs	Cat#M2080S

4.1.6 Instruments

The instruments used in this thesis are listed in Table 8.

Table 8. List of used instruments

Instrument	Company
ÄKTA purifier	GE Healthcare
Avanti J-20 XP Centrifuge	Beckman Coulter
Centrifuge 5415D	Eppendorf
Geiger Counter LB123 EG&G	Berthold
Gel Dryer Model 583	Bio-Rad
GeneAmp PCR System 9700	Applied Biosystems
HeraCell 240i CO2 Incubator	Thermo Fisher Scientific
HeraSafe KS	Thermo Fisher Scientific
Hybridization oven T 5042	Heraeus
Incubator Model B6200	Heraeus

Leica TCS SP8 MP	Leica Microsystems
Magnetic stirrer MR 300	Heidolph
Megafuge 40R	Thermo Fisher Scientific
Milli-Q PLUS	Millipore
Multimode-Microplate reader Mithras LB 940	Berthold Technologies
Nanodrop® spectrophotometer ND-100	Thermo Fisher Scientific
Odyssey Infrared Imaging System	LI-COR Biosciences
peqSTAR Thermocycler	PeqLab
Personal Molecular Imager	Bio-Rad
Polymax 2040	Heidolph
Power Supply EV233	Consort
Quantum ST4	PeqLab
Screen Eraser-K	Bio-Rad
Thermal Cycler 2720	Applied Biosystems
Thermomixer compact	Eppendorf
Trans-Blot SD	Bio-Rad
UV Stratalinker 2400	Stratagene
Vortexer REAX top	Heidolph

4.1.7 Oligonucleotides

Unless specified otherwise, all oligonucleotides used in this thesis were ordered from Metabion GmbH (Planegg, Germany).

4.1.7.1 DNA oligonucleotide sequences for cloning

The DNA oligonucleotide sequences used in this thesis for cloning are listed in Table 9.

Table 9. List of DNA oligonucleotide sequences for cloning

Name	Sequence
Nudt12 TEV BamHI	CCAGGATCCGAAAACCTGTATTTTCAGGGAATGTCTTCTGTAAAAAGAAGTCTGAA
Nudt12 SalI	AGCGTCGACTTAGAGATTAGGATTTATTCTAATCCAGTG

4.1.7.2 Biotinylated oligonucleotide sequences for RNA pulldowns

The biotinylated oligonucleotides used in this thesis are listed in Table 10.

Table 10. List of biotinylated oligonucleotide sequences for RNA pulldowns

Name	Sequence
3'-biotinylated 2'-O-methyl-RNA adaptor	AGGCUAGGUCUCCC–biotin
U1 pull down 3'-biotinylated oligo 1	GAAAACCACCTTCGTGATCA–biotin
U1 Pull down 3'-biotinylated oligo 2	GAGTGCAATGGATAAGCCTC–biotin
U1 Pull down 3'-biotinylated oligo 3	AGCGCGAACGCAGTCCCCCA-biotin

4.1.7.3 DNA oligonucleotide sequences for *in vitro* transcription

The DNA oligonucleotide sequences used in this thesis for in vitro transcription are listed in Table 11.

Table 11. List of DNA oligonucleotide sequences for *in vitro* transcription

Name	Sequence
Model-NAD-RNA template sense ϕ2.5 A-62	TAATACGACTCACTATTAGGGAAGTGCTACCACAACTTTAGCCATAATGT CACTTCTGCCGCGGGCATGCGGCCAGCCA
Model-NAD-RNA template antisense ϕ2.5 A-62	TGGCTGGCCGCATGCCCGCGGCAGAAGTGACATTATGGCTAAAGTTGTGG TAGCACTTCCCTAATAGTGAGTCGTATTA
Model-NAD-RNA template sense ϕ2.5 A-31	CTAATACGACTCACTATTAGGCCTCTCGCTCTGCTGGGTGTGCGCTTGC
Model-NAD-RNA template antisense ϕ2.5 A-31	GCAAGCGCACACCCAGCAGAGCGAGAGGCCTAATAGTGAGTCGTATTAG
Model-NAD-RNA template sense T7ϕ2.5 AG-51CU DNA	CTAATACGACTCACTATTAGTCCTCTCTCTCCTCTCTCTCCTCTTCCT TCTCTTCCTTCTCCTCTCC
Model-NAD-RNA template antisense T7ϕ2.5 AG-51CU DNA	GGAGAGGAGAAGGAAGAGAAGGAAGAGGAGAGAGAGGAGAGAGAGAGGAC TAATAGTGAGTCGTATTAG
NMN aptamer sens with leader sequence	TAATACGACTCACTATAGGGAGACCTAGCCTGGAACCCAATAGGCGTTTG AGGGGAATCGGCCACGGTAACAACCCCTC
NMN aptamer antisens leader sequence	GAGGGGTTGTTACCGTGGCCGATTCCCCTCAAACGCCTATTGGGTTCCAG GCTAGGTCTCCCTATAGTGAGTCGTATTA
NAD riboswitch2 sens with leader sequence	TAATACGACTCACTATAGGGAGACCTAGCCTGGAAAATCTATAGAGCGTT GCGTCCGAAAGTCTAAACAGACACGGCTCTTTAAAAACAAAAGGAGAAG
NAD riboswitch2 antisens leader sequence	CTTCTCCTTTTGTTTTTAAAGAGCCGTGTCTGTTTAGACTTTCGGACGCA ACGCTCTATAGATTTTCCAGGCTAGGTCTCCCTATAGTGAGTCGTATTA

4.1.7.4 Northern blot probe sequences

The Northern blot probes sequences used in this thesis for in vitro transcription are listed in Table 12.

Table 12. List of Northern blot probe sequences

Name	Sequence
Model-NAD-RNA template sense ϕ2.5 A-A62 NB	GCAGAAGTGACATTATGGCT
NMN Aptamer NB	GATTCCCCTCAAACGCCTAT
U1 snRNA NB	ATCCGGAGTGCAATGGATAA

4.1.8 Recombinant DNA

The plasmids used for molecular cloning or generated in this thesis are listed in Table 13.

Table 13. List of plasmids

Name	Insert	Source	Cloning enzymes	Identifier
pGEX-4T-1	N/A	GE Healthcare	N/A	28-9545-49
pGEX-4T-1-Nudt12	human NUDT12 (UniProtKB: Q9BQG2-1)	This thesis	BamHI/SalI	This thesis
pCold I	N/A	Takara bio	N/A	3361
pCold I-Nudt12	human NUDT12 (UniProtKB: Q9BQG2-1)	This thesis	BamHI/SalI	This thesis

4.1.9 Solutions

The solutions used in this thesis are listed in Table 14.

Table 14. List of solutions and composition

Solutions	Composition
10x native TB buffer	450 mM Tris base, 450 mM boric acid
10x TBE buffer	890 mM Tris-base, 890 mM boric acid, 20 mM EDTA pH 8.3
2X Nucleic Acids Binding Buffer	10 mM Tris-HCl pH 7.5, 2 M NaCl, 1 mM EDTA
2X RNA loading dye for APB gels	8 M urea, 10 mM Tris-HCl pH 8.0, 50 mM EDTA, 0.025% [w/v] xylene cyanol, 0.025% [w/v] bromophenol
2X RNA loading dye for PAA gels	90% (v/v) formamide, 0.025% [w/v] xylen cyanol, 0.025% [w/v] bromphenol blue in 1x TBE
50x Denhardts solution	1% Albumin Fraction V, 1% Polyvenylpyrrolidon K30, 1% Ficoll 400
50X TAE buffer	2 M Tris-base, 100 mM acetic acid, 50 mM EDTA pH 8.0
5x SDS Sample buffer	300 mM Tris-HCl pH 6.8, 10% [v/v] SDS, 62.5% [v/v] glycerol, 10% [v/v] β-mercaptoethanol, 0.05% [w/v] bromophenol blue
Biotinylation blocking solution	1 mM EDTA pH 8.0, 10% [v/v] SDS in 1X PBS
Biotinylation wash solution I	1 mM EDTA pH 8.0, 1% [v/v] SDS in 1X PBS
Biotinylation wash solution II	1 mM EDTA pH 8.0, 0.1% [v/v] SDS in 1X PBS
Coomassie destaining solution	10% [v/v] acetic acid, 30% [v/v] EtOH
Coomassie staining solution	10% [v/v] NaOAc, 30% [v/v] EtOH, 0.25% [w/v] Coomassie brilliant blue
EMSA buffer	50 mM Tris-HCl pH 7.5, 150 mM KCl, 5 Mm $MgCl_2$, 5% [v/v] glycerol, 1 mM DTT
EMSA sample buffer	20 mM Tris pH 7.5, 100 mM NaCl, 5 mM MgCl, 10% [v/v] glycerol
Gel filtration buffer	50 mM Hepes pH 7.4, 200 mM NaCl, 2 mM DTT
GST-Trap Buffer 1	1M NaCl in 1M PBS
GST-Trap Buffer 2	20mM Glutathion, 50mM Tris pH 8.0 in 1X PBS
His-Trap Solution A	50 mM NaPi pH 8.0, 300 mM NaCl, 10 mM imidazol
His-Trap Solution B	50 mM NaPi pH 8.0, 300 mM NaCl, 500 mM imidazol
Immobilization buffer	10 mM HEPES pH 7.5, 1 M NaCl, 5 mM EDTA
NAD-class II riboswitch buffer	50 mM Tris-HCl pH 8.3, 100 mM KCl
NET buffer	50 mM Tris, pH 7.5, 150 mM NaCl, 5 mM EDTA, 0.5 % [v/v] NP-40, 10 % [v/v] glycerol
NET wash buffer	50 mM Tris, pH 7.5, 300 mM NaCl, 5 mM EDTA, 0.5 % [v/v] NP-40, 10 % [v/v] glycerol
NMN aptamer buffer	20 mM HEPES pH 7.5, 200 mM KCl, 100 mM NaCl
Northern blot hybridization solution	5xSSC, 1x Denhardts solution, 20 mM NaPi pH 7.2, 7% [v/v] SDS
Northern blot wash solution I	5x SSC, 1% [v/v] SDS
Northern blot wash solution II	2xSSC, 1% [v/v] SDS
NP-40 lysis buffer	20 mM Tris-HCl pH 8.0, 137 mM NaCl, 0.3% [v/v] NP-40, 10 % [v/v] glycerol, 2 mM EDTA, 1 mM AESBF, 1 mM DTT
Nudt12 decapping buffer	10 mM Tris-HCl pH 7.5, 100 mM KCl, , 2mM $MgCl_2$, 2 mM $MnCl_2$,2 mM DTT
Phosphate-buffered saline (PBS)	1.37 M NaCl, 27 mM KCl, 100 mM Na_2HPO4, and 18 mM KH_2PO4
Saline sodium citrate buffer (20x SSC)	3 M NaCl, 0.3 M NaCitrate pH 7.0
SDS running buffer	25 mM Tris-HCl pH 7.5, 200 mM glycine, 25 mM SDS
Streptavidin wash buffer	8M urea, 50 mM Tris-HCl pH 7.4
Towbin buffer	48 mM Tris, 38.6 mM glycine, 0.0037% [v/v] SDS, 20% [v/v] methanol
Tris-buffered saline (TBS)	10 mM Tris pH 7.5, 150 mM NaCl
Tris-buffered saline-Tween (TBS-T)	0.1% [v/v] Tween 20 in 1X TBS
Western blot blocking solution	5% [v/v] milk in TBS-T

4.1.10 Softwares and algorithms

The softwares and algorithms used in this thesis are listed in

Table 15.

Table 15. List of softwares and algorithms

Softwares and algorithms	Source	Identifier
Adobe Illustrator CS5	Adobe	RRID:SCR_010279
Adobe Photoshop CS5	Adobe	RRID:SCR_014199
BioRender	BioRender.com	RRID:SCR_018361
ChemDraw 18.1.0.535	PerkinElmer	RRID:SCR_016768
Clustal Omega	EBI	RRID:SCR_001591
GraphPad Prism 9.5.1	GraphPad Software	RRID:SCR_002798
NCBI database	https://www.ncbi.nlm.nih.gov/	RRID:SCR_006472
Odyssey Clx	LI-COR	RRID:SCR_014579
ProtParam Tool	SIB	RRID:SCR_018087
Quantity One 1-D Analysis Software	BioRad	RRID:SCR_014280
UCSC Genome Browser	http://genome.ucsc.edu/	RRID:SCR_005780
Uniprot	http://www.uniprot.org/	RRID:SCR_002380

4.2 MOLECULAR CLONING

If not otherwise described below, general methods like DNA gel electrophoresis, PCR, purification and extraction of DNA were performed according to Sambrook *et al.,* 1989 or as described in the according manufacturer's manuals.

For DNA isolation from *E.coli,* the NucleoSpin® Plasmid Kit (Macherey-Nagel, Düren, Germany) or NucleoBond® XtraMidi Kit (Macherey-Nagel, Düren, Germany) was used. For the elution of DNA fragments from agarose gels, the NucleoSpin® Gel and PCR-cleanup Kit (Macherey-Nagel, Düren, Germany) was used.

4.3 RNA METHODS

If not otherwise described below, general methods like RNA gel electrophoresis, purification and extraction of RNA were performed according to Sambrook *et al.,* 1989 or as described in the according manufacturer's manuals.

4.3.1 Total RNA isolation

Total cellular RNA was collected from cultured cells with TRIzol™ Reagent (Invitrogen™) according to the manufacturer's protocol. RNA pellet was washed once with 100% ethanol, once with 70% ethanol. After air-drying the pellet, RNA was resuspended in nuclease-free water. RNA can be incubated at 65˚C for 5 min to help the dissolution of the pellet. RNA was stored at -80˚C until further use.

4.3.2 RNA synthesis and modification

4.3.2.1 *In vitro* transcription

Equal amount of 100 µM ssDNA template sense and antisense single-stranded DNA oligonucleotides containing the T7 promoter (Table 11) were heated up at 95°C for 30 seconds and annealed by cooling down to 25°C. The generate dsDNA template stock solution was diluted to 10 µM. RNA was transcribed in a 500 µl reaction containing 0.2 µM of dsDNA template, 30 mM Tris pH 8.0, 10 mM DTT, 0.01% Triton X-100, 25 mM $MgCl_2$, 2 mM spermidine, 30% DMSO, 5 mM ATP, 5 mM CTP, 5 mM UTP, 5 mM GTP, 0.4 U/ml thermostable inorganic pyrophosphatase (NEB) and 0.1 mg/ml of T7-polymerase (lab produced) overnight at 37°C.

NADylated RNAs were *in vitro* transcribed with the following modifications. The T7 ϕ2.5 promoter was used for the DNA templates. NAD was added in the reaction at a concentration of 4 mM, and concentration of ATP, CTP, UTP and GTP was adjusted to 1 mM each. If the transcript only contained a unique initiating adenosine (+1A), NAD can be used as initiating nucleotide at a concentration of 1 mM and ATP can be omitted from the mix. GTP can be substituted by [α-^{32}P]GTP for decapping assay. After 16h, the transcription reaction was treated with DNAse I for 30 min at 37°C. Reaction was mixed with 2x RNA denaturing sample buffer and purified on PAA gel (4.3.4).

4.3.2.2 Preparation of 5'-NADylated RNA by phosphorimidazolide coupling

First, NMN-phosphorimidazolide (Im-NMN) was synthesized by the reaction of NMN with Carbonyldiimidazole (CDI) as reported in Höfer *et al.*, 2016a. Then, 5'-NADylateds RNA were prepared by incubating monophosphorylated RNAs in the presence of a 1000-fold excess of Im-NMN, 50 mM $MgCl_2$ for 2h at 50°C (Höfer *et al.*, 2016a). RNA was analyzed by (HPLC 4.7.4) or by ethanol precipitation.

4.3.2.3 Preparation of m^{7}G-capped RNA and monophosphorylated RNA

To generate m^{7}G-capped RNA, 7-methylguanylate cap was added to 5′-end of *in vitro* transcribed RNA with the Vaccinia Capping System (NEB) according to the manufacturer instructions. The modified RNA reaction was purified on a 0.2%APB gel as described in 4.3.4 and 4.3.5 to separate m^{7}G-RNA and ppp-RNA.

To generate p-RNA, the γ and β phosphate of *in vitro* transcribed RNA were removed with RNA 5'-Polyphosphatase (Epicentre) according to manufacturer instructions. RNA was purified with the Oligo Clean & Concentrator Kit (Zymo) according to manufacturer instructions.

4.3.2.4 3'-end radiolabeling of RNA

30 pmol of RNA were labeled with [^{32}P]-pCp by T4 RNA ligase in 30 µl (Thermo Fisher) according to manufacturer instruction. After incubation for 16 hours at 4˚C, unincorporated nucleotides were separated by gel filtration on a Microspin G-25 Columns (Cytiva) according to the manufacturer instructions.

4.3.3 RNA purification from enzymatic reactions

RNA was purified from enzymatic reactions by phenol/chloroform extraction and ethanol precipitation. Reaction volume was adjusted to 200 µl by adding nuclease-free water. An equal volume of ROTI Aqua-Phenol/Chloroform/Isoamyl alcohol was added. The sample was vortexed at maximum setting for 15 sec and centrifugated at 12000 g for 15 min at 4˚C. The aqueous upper phase was transferred to a new tube. RNA was precipitated by the addition of 0.1 volume of 3 M NaOAc, 3 volume of ethanol 100% and 1 µl glycogen as a carrier. Precipitation was carried at -80 ˚C for 30 min, or -20˚C for a minimum of 2 hours or ideally overnight. RNA was pelleted at 12000 g for 30 min at 4˚C and washed and resuspended as in 4.3.1.

4.3.4 Denaturing polyacrylamide gel electrophoresis

The ROTIPHORESE Sequencing gel system (Roth) was used to prepare denaturing polyacrylamide-urea gel for RNA electrophoresis. Appropriate volume of concentrate, diluent, and 10xTBE (PAA gel) or 10xTAE (APB gel) was mixed according to manufacturer's instruction to the desired polyacrylamide percentage. After addition of TEMED and fresh APS the gel was casted and allowed to polymerized for a minimum of one hour at room temperature.

Gel was prerun for 30 min at 400 V in 1x TBE or TAE buffer to equilibrate and preheat the gel. Gel wells were rinsed with TBE buffer. Samples were heated for 2-5 min at 95˚C before loading. Gel was run at 350-400 V for PAA gels in 1xTBE, or at 200-250 V

for APB gels in 1xTAE. RNA was detected by ethidium bromide staining (5 µl in 250 ml for 10 min) or by UV shadowing (254 nm).

4.3.5 Northern blot

The nucleic acids were transferred onto a nylon membrane (Hybond-N, GE Healthcare) by semi-dry blotting. For PAA gels, blotting was carried out at 20 V for 30 min with water as transfer buffer at 25°C. For APB gels, blotting was carried out at 2 mA/cm^2 for 2h30 with 0.5 x TAE as transfer buffer at 4˚C (Nübel *et al.,* 2017). When interested in NAD-capped RNAs, RNA was crosslinked by UV exposure of 120 µJ/cm^2 twice (autocrosslink feature on UV Stratalinker).

5'-end of DNA oligonucleotide probe was labeled with γ-[^{32}P]-ATP by T4 polynucleotide kinase in the forward reaction (Thermo Fisher) according to manufacturer instruction. After an incubation at 37˚C for 1 h, reaction was stopped by the addition of 30 µl of 30 mM EDTA pH 8.0. Unincorporated nucleotides were separated by gel filtration on a Microspin G-25 Columns (Cytiva) according to the manufacturer's instructions.

After crosslinking, membrane was rinsed in water and transferred into a cylindrical bottle. 50 ml of hybridization buffer was added and the membrane was pre-hybridized for 1 h at 50˚C on a rotating wheel. ^{32}P-labeled probe was directly added in the hybridization buffer and the set up was incubated rotating overnight at 50˚C. The membrane was washed twice with Wash Solution I for 10 min, once with Wash Solution II for 10 min. The radioactive signals were analyzed using storage screens and a PMI system (Biorad). After exposure, the probes were stripped of the membranes using two washes of boiling 0.1% SDS solution. An overnight exposure was performed to ensure total loss of the hybridization signal.

4.3.6 RNA extraction from gel

Band of interest was visualized by ethidium bromide staining or UV shadowing, cut out from the gel with a clean razor blade, crushed between plastic film and transferred to a 15 ml conical tube. 2 volumes of 0.3 M sodium acetate were added. Tube was incubated for 30 min at -80˚C. Passive elution was carried out on a rotating wheel in a cold room overnight. Sample was centrifuged at 16000x g for 10 min to pellet the

gel debris. Supernatant was transferred to a Costar Spin-X centrifuge tube filter (Sigma-Aldrich) and spin down 1 min at 16000xg to remove any left debris. RNA was precipitated by the addition of 1 volume of isopropanol and 1 µl glycogen as a carrier. Precipitation was carried at -20˚C for a minimum of 2 hours until 16 hours. RNA was pelleted at 12000xg for 30 min at 4˚C and washed as usual.

4.3.7 RNA *in vitro* decapping assays

RNA *in vitro* decapping assays with were performed as in Sharma *et al.*, 2020. Briefly, ^{32}P-G-NAD-RNA-, ^{32}P-G-m^{7}G-capped RNAs, and ^{32}P-G-pppA-RNA generated by *in vitro* transcription were incubated with GST-Nudt12 or His-Nudt12 in Nudt12 decapping buffer in 20 µl total volume and incubated at 37 ˚C for 30 min. Reaction was heat-inactivated at 90 ˚C for 2 min. Afterwards 10 U of Nuclease T1 (Sigma-Aldrich) was added and reaction was incubated at 37 ˚C for 30 min. RNA was analysed on a 20% PAA as described in (Bergman *et al.*, 2004).

Decapping of 3'-end radiolabeled NADylated RNA and m^{7}G-capped RNA was performed as described above for 37˚C. RNA was purified by phenol/chloroform 4.3.3 and resuspend in water. The samples were divided in two aliquots and ran on a 8% PAA or 0.2% APB gels. (4.3.4).

4.3.8 5'-end enzymatic analysis

1 µg of *in vitro* transcribed RNAs was digested with 20 U of RNA 5′ Polyphosphatase (Epicentre) in 1x Polyphosphatase buffer (Epicentre) supplemented with 20 U of RiboLock (Thermo Scientific) for 1h at 37°C according to manufacturer's instructions (Epicentre). Reaction was purified with the Oligo Clean & Concentrator (Zymo) according to manufacturer's instruction. After resuspension in water, RNA was digested with 1 U of XNR-1 (NEB) in 1X NEB buffer 3 (NEB) supplemented with 20 U of RiboLock (Thermo Scientific) for 1h at 37°C The reaction was divided in two aliquots and stopped with 2X RNA loading dye. The digested RNAs were analyzed by PAA and APB gel electrophoresis (4.3.4)

4.3.9 Electrophoretic mobility assay (EMSA)

1 µl of 3'-end radiolabeled RNA (4.3.2.4) at 0.1 Bq/µl was incubated with various volume of hybridoma supernatants or purified antibodies in EMSA buffer in a 20 µl total reaction. The reaction was incubated at RT for 30 min rotating. Complexes were resolved on 8% native polyacrylamide gels (6 %-gel: 12 ml 30 % acrylamide, 3 ml glycerol, 6 ml 10 x EMSA buffer, 480 µl 10 % APS, 48 µl TEMED and 39 ml H2O). Electrophoresis was carried out at 260 V for 45 min at 4°C and in 0.5X native TB buffer. Gel was dried and signal was detected using the PMI System.

4.3.10 RNA immunoprecipitation

5 µg of 28C11 or 26D1 purified antibodies were coupled to 50 µl of Protein G Sepharose beads (GE Healthcare) overnight in 1X PBS, then washed three times in RNA IP buffer. *In vitro* transcribed NADylated RNA and triphosphorylated RNA was added to the beads and incubated in 500 µL NET buffer rotating at 4°C overnight. The setup was washed once with NET buffer, twice with NET wash buffer. RNA was eluted from the beads with 2x RNA loading dye. Supernatant and washes were collected and precipitated with ethanol as previously described. RNA was resolved on PAA gel (4.3.4)

4.3.11 Aptamer-based pulldown of NADylated RNAs

100 pmol amount of the *in vitro* transcribed aptamers were mixed with equimolar amount of 3′-biotinylated 2′-O-methyl-RNA adaptor were mixed together and heated at 95°C for 1 min in 50 µl of their respective aptamer buffer (NMN aptamer buffer or NAD-class II riboswitch buffer), slowly cooled down until reaching 65°C, then $MgCl_2$ was added at a final concentration of 20 mM, and the aptamer-adaptor were further cooled down to 4°C to promote folding of the aptamer and annealing between the aptamer and the adaptor. In the meantime, 50 µL of streptavidin magnetic beads (Dynabeads, Invitrogen) were washed three times with 1 mL of the appropriate aptamer buffer supplemented with 20 mM $MgCl_2$. The beads were resuspended in 150 µL aptamer buffer. The aptamer-adaptor setup was added to the beads and incubated at least for 1h at 4°C rotating. Afterwards, the beads were washed three times with the aptamer buffer to remove unbound aptamer-adaptor. 3'-end labeled of in vitro

transcribed NAD-RNA, m7G-RNA, or ppp-RNA were linearized at 85°C for 2 min and directly cooled down on ice. Then the RNAs was incubated with the aptamer-beads set up in aptamer buffer supplemented with 20 mM $MgCl_2$ for 1h-4h at 8°C gently shaking. Finally, the pull down set-up was washed three times with aptamer buffer supplemented with 20 mM $MgCl_2$.RNA was either eluted from beads with 2X RNA loading. Alternatively, elution was done by incubating with 100 µM of NMN or NAD. Nudt12-catalyzed elution was performed as described in 4.3.7. Supernatant and washes were collected when indicated and ethanol precipitated. RNA were resolved on PAA gel (4.3.4).

4.3.12 Capture of NADylated RNAs by ADPRC-catalyzed CuAAC-based biotinylation method

4.3.12.1 ADPRC-catalyzed CuAAC-based biotinylation of NADylated RNAs

In vitro transcribed RNAs or isolated U1 snRNA were subjected to the ADPRC-catalysed, CuAAC-based biotinylation as described by Winz *et al.*, 2017 and with the following modifications. RNA was treated with 10 µl 4-pentyn-1-ol and 3 U of ADP ribosylcyclase in a 100 µl reaction of 1X ADRPC reaction buffer (50 mM HEPES pH 7.0, 25 mM $MgCl_2$) and 40 U RiboLock at 37 °C for 1 h. In parallel, the same reaction was perfromed without the ADPRC enzyme for negative control. RNA was purified from the reaction by phenol/chloroform extraction followed by ethanol precipitation (4.3.3). RNA was resuspended in 1X ADPRC reaction buffer. Copper solution was freshly prepared by mixing 1 mM CuSO4, 0.5 mM THPTA, and 2 mM sodium ascorbate and kept on ince. The RNA was combined on ice to the copper mix, 250 µM of biotin-PEG3-azide, 40 U of RiboLock and incubated at 30°C for 30 min. RNA was purified from the reaction by phenol/chloroform extraction followed by ethanol precipitation (4.3.3).

4.3.12.2 Detection of biotinylated RNAs

5 µl of biotinylated RNAs were immobilized on a nylon membrane (dot blot assay), or RNA were resolved by PAA gel electrophoresis after mixing with 2X RNA loading dye (4.3.4) and transferred onto a membrane by semi-dry blotting (4.3.5), followed by UV crosslinking (120 µJ/cm^2 twice, autocrosslink feature on UV Stratalinker).

Afterwards, the membranes were incubated at RT with IR-dye conjugated Streptavidin diluted 1:10000 in biotinylation blocking solution for 20 min shaking in the dark. Membranes were then washed twice with the biotinylation blocking solution, twice with biotinylation wash solution I, twice with the biotinylation wash solution II, for 10 min each time. Finally, labeled RNAs were visualized using a LI-COR Odyssey imaging platform.

4.3.12.3 Capture of biotinylated RNAs

Streptavidin magnetic beads (Dynabeads™ M-270, Invitrogen™) were pre-washed according to manufacturer's instruction and blocked with 100 µg/mL acetylated BSA in immobilization buffer for 1 h at RT. Biotinylated RNAs were captured by streptavidin magnetic beads as in by incubation for 1 h at RT rotating in 100 µl of immobilization buffer supplemented with 40 U of RiboLock. Beads were washed three times with streptavidin wash buffer, and twice with water. RNA were eluted from the beads with 2X RNA loading dye and analyzed on a PAA gel (4.3.4).

4.3.13 Purification of U1 snRNA

The purification of U1 spliceosomal snRNA was performed by two consecutive pulldown rounds with biotinylated oligonucleotides complementary to the U1 snRNA sequence (Table 10) and magnetic streptavidin beads (Dynabeads™ M-270, Invitrogen™) as described in Hasler *et al.*, 2020. RNA was extracted from the last eluate by TRIzol™ reagent (4.3.1).

4.4 CELL BIOLOGICAL METHODS

4.4.1 Cell culture conditions

Adherent cells were cultivated in Dulbecco's modified Eagle's (DMEM) medium supplement with 10% fetal bovine serum and appropriate antibiotics (

Table 16) under 5% CO_2 at 37°C. DIS3 overexpression in Flp-In 293 T-REx cell lines was induced by 1 µg/ mL of doxycycline for 48 h.

Table 16. Cell lines and culture media

Cell Line	Source	Culture media
HEK293T	Our lab	DMEM, 10% FBS, 1% P/S
DIS3 KO	Gifted from Z. Warkocki, Polish Academy of Sciences, Poland	DMEM, 10% FBS, 1% P/S
Flp-In™ 293 T-REx ™	Invitrogen	DMEM, 10% FBS, 15 mg/ml blasticidin, 100 mg/ml zeocin
Flp-In™ T-Rex 293™, expressing Flag-HA taggedDIS3, endogenous DIS3 knocked-out	Generated by C. Latini, our lab	DMEM, 10% FBS, 15 mg/ml blasticidin, 150 mg/ml hygromycin B

4.4.2 Harvesting cells

Confluent adherent cells dishes were washed twice with ice-cold PBS. Cells were detached from the plate with a cell scrapper and transferred to a conical tube. Cells were wash one time in PBS by pipetting gently and centrifugated at 300 g for 5 min at 4˚C. Supernatant was discarded and the resulting cell pellet was flash-frozen and stored at -80˚C until further use.

4.5 PROTEIN BIOCHEMISTRY METHODS

4.5.1 Whole cell extract

Cell pellet was resuspended in an appropriate amount of NP-40 lysis buffer and incubated 20 min on ice. After a quick vortexing, cells suspension was centrifugated at maximum speed for 30 min at 4˚C. Supernatant constituted the total cell lysate and was transferred to a new tube and conserved at -80˚C for further use. Sample were diluted in 5x SDS Loading buffer before loading on gel.

4.5.2 SDS-PAGE gel electrophoresis

Proteins were resolved on a 10% SDS-PAGE gel (separation gel: 380 mM Tris/HCl pH 8.8, 6-15 % Acrylamide/Bis solution (37.5:1), 0.1 % SDS, 0.1 % TEMED, 0.05 % APS; stacking gel:125 mM Tris-HCl pH 6.8, 5 % Acrylamide/Bis solution (37.5:1), 0.1 % SDS, 0.15 % TEMED, 0.05 % APS). Samples in Laemli buffer were heated 2 to 5 min at 95˚C before loading. The gel was run at 180 V until the loading dye ran out. Afterwards, gel could be stained (4.5.3) or be transferred to a membrane for further analysis (4.5.3)

4.5.3 Coomassie staining

The SDS-gel was incubated in Coomassie staining solution for 1 h at RT, shaking. The gel was transferred in Coomassie destaining solution and incubating overnight at 4˚C. The Destaining solution was regularly changed until the bands of interest could be visualized on the destained gel with minimal background.

4.5.4 Western blot

Proteins were separated on SDS-PAGE gel (4.5.2) transferred onto a nitrocellulose membrane (GE healthcare) by semi-dry-blotting with Towbin blotting buffer at 2 mA/cm^2 for 1 min/kDa. The membrane was blocked in 1 x TBS-T containing 5% skimmed milk for 1 h at 4˚C. Then the membrane was incubated with the primary antibody at the appropriate dilution in 5% milk in 1X TBS-T (Table 4) overnight at 4˚C. After three washes with 1 x TBS-T for 10 min at room temperature, the membrane was incubated with the secondary antibody at the appropriate dilution in 1X TBS-T (Table 4) for 1 hour at room temperature. Membrane was washed three times with 1X TBS-T for 5 min at room temperature. Detection was performed with the Odyssey scanner system (LI-COR Biosciences).

4.5.5 Protein expression and purification

The NUDT12 sequence (UniProtKB: Q9BQG2-1) was amplified from HEK293T cells cDNA and cloned in expression vectors pGEX-4T-1 and pCold I, so that the protein would be expressed with a N-terminal GST-tag or His_6-tag respectively. *E. coli* Rosetta(DE3) transformed with the vectors were grown to an OD_{600} of 0.6 at 37°C and induced with 1 m M IPTG. The induced culture was grown overnight at 25°C.

For the GST-Nudt12 protein, the bacteria were lysed by sonification in GST-Trap Buffer 1. The lysate was cleared by centrifugation at 50000 g for 35 min at 4°C and the supernatant was filtered through a 0.45µm filter membrane (Roth). To capture the recombinant protein, the lysate was run over a 5 mL GSTrap column (Cytiva). After extensive washing with the GST-Trap Buffer 1, the protein was eluted with GST-Trap Buffer 2.

For the His_6-Nudt12 protein, the bacteria were lysed by sonification in His-Trap Solution A. The lysate was cleared by centrifugation at 50000 g for 35 min at 4°C and the supernatant was filtered through a 0.45µm filter membrane (Roth). To capture the recombinant protein, the lysate was run over a 1 mL HisTrap HP Column (Cytiva). After extensive washing with the His-Trap Solution A, the protein was eluted with His-Trap Solution B.

Afterwards, the pooled protein-containing fractions were concentrated to 2 mL of total volume by Vivaspin 20 ultrafiltration device (MWCO 10000, Sartorius). Sample was loaded on a Superdex 200 10/300 GL Columns (Cytiva) equilibrated with gel filtration buffer. The peak fractions containing the protein of interest were pooled, concentrated to 1 mg/ml, and adjusted to 5% (v/v) glycerol. Aliquots were flash-frozen in liquid nitrogen and stored at −80°C.

4.5.6 Protein analysis by mass spectrometry

Purified protein sample were run on a 10% SDS-PAGE gel according to 4.5.2.

Protein preparation and analysis by Mass Spectrometry were performed by the Mass Spectrometry Facility (University of Regensburg).

Protein bands were cut out from the gel, washed 7 with 50 mM NH_4HCO_3, 7 50 mM NH_4HCO_3/acetonitrile (3/1), 50 mM NH_4HCO_3/acetonitrile (1/1) and lyophilized. After a reduction/alkylation treatment and additional washing steps, proteins were *in gel* digested with trypsin (Trypsin Gold, mass spectrometry grade, Promega) overnight at 37°C. The resulting peptides were sequentially extracted with 50 mM NH_4HCO_3 and 50 mM NH_4HCO_3 in 50% acetonitrile.

After lyophilization, peptides were reconstituted in 20 µl 1% TFA and separated by reversed-phase chromatography. An UltiMate 3000 RSLCnano System (Thermo Fisher Scientific, Dreieich) equipped with a C18 Acclaim Pepmap100 preconcentration column (100µm i.D.x20mm, Thermo Fisher Scientific) and an Acclaim Pepmap100 C18 nano column (75 µm i.d.x250 mm, Thermo Fisher Scientific) was operated at flow rate of 300 nl/min and a 60 min linear gradient of 4 % to 40 % acetonitrile in 0.1 % formic acid. The LC was online-coupled to a maXis plus UHR-QTOF System (Bruker Daltonics) via a CaptiveSpray nanoflow electrospray source.

Acquisition of MS/MS spectra after CID fragmentation was performed in data-dependent mode at a resolution of 60000. The precursor scan rate was 2 Hz processing a mass range between m/z 175 and m/z 2000. A dynamic method with a fixed cycle time of 3 s was applied via the Compass 1.7 acquisition and processing software (Bruker Daltonics).

Prior to database searching with Protein Scape 3.1.3 (Bruker Daltonics) connected to Mascot 2.5.1 (Matrix Science), raw data were processed in Data Analysis 4.2 (Bruker Daltonics). A customized database comprising the SwissProt *Homo sapiens* database plus common contaminants, was used for database search with the following parameters: enzyme specificity trypsin with 2 missed cleavages allowed, precursor tolerance 10 ppm, MS/MS tolerance 0.04 Da. As general variable modifications, deamidation of asparagine and glutamine, oxidation of methionine, carbamidomethylation or propionamide modification of cysteine were set.

4.6 NAD DETECTION AND QUANTITATION

4.6.1.1 Fluorometric detection

Fluorometric detection was adapted from Putt and Hergenrother, 2004. 50 µl of sample was sequentially mixed with 20 µl of EtOH, 10 µl of Acetophenone and 40 µl of 2.5 M NaOH. The mixture was incubated on ice for 20 min. Then 80 µl of formic acid was added to each sample, followed by vortexing for 15 sec and incubation at 95°C for 4 min. The total sample (100 µl) was transferred to a 96-well opaque bottom plate and fluorescence (Excitation/Emission = 355/460 nm) was measured using a Mithras LB 940 plate reader. To be noted, NAD excitation and emission maxima are 382 and 445 nm, thus our setup does not allow to use this method for proper NAD quantification based on fluorescent signal intensity.

4.6.1.2 Luminescent detection

Total RNA was isolated from cells by TRIzol Reagent (4.3.1) and prepared as in Grudzien-Nogalska *et al.*, 2018 to remove free copurifying NAD. Briefly, RNA was dissolved in a solution of 2 M urea, 10 mM Tris-HCl pH 7.5 and incubated at 65°C for 2 min. RNA was then precipitated with isopropanol in presence of 2 M ammonium

acetate overnight . *In vitro* transcribed RNA or total RNA were digested with nuclease P1 (Sigma-Aldrich) in a 50 µL reaction containing 10 mM Tris (pH 7.0), 20 µM ZnCl2 at 37°C for 30-60 min min to release NAD. In parallel, reactions for each samples were carried out either without NP1, with equal amount of 50% glycerol as a mock treatment, or with heat-inactivated NP1 to assess the background. Similarly, NAD standard were prepared in the same buffer condition as that for the nuclease P1 reaction. Afterwards, the samples were used in bioluminescent assay (Promega NAD/NADH-Glo™ assay) by adding equal amount of NAD/NADH-Glo™ Detection Reagent and following manufacturer's instruction to measure liberated NAD. The luminescent signal was measured using the Mithras LB 940 plate reader.

4.7 ANTIBODY-RELATED METHOD

4.7.1 Coupling of NAD and NMN to ovalbumin and BSA

The coupling of NADH and NMN to cationized ovalbumin (OVA) and BSA was performed based on the method described by Erlanger and Beiser 1964 and with the amended modifications from Weichmann *et al.*, 2020. by R. Hett (our lab).

4.7.2 Generation of monoclonal antibodies against NAD cap

Immunization, work with hybridoma cells and ELISA screening were performed by Dr. R. Feederlee (Core Facility Monoclonal Antibodies, Helmholtz Munich). Rats and mice were immunized with a mixture of 40 µg OVA-coupled compounds, 6 nmol CpG (Tib Molbiol, Berlin) and incomplete Freund's adjuvant. A boost was given 4 months after the primary injection and spleens were fused with myeloma cell line P3X63-Ag8.653 (ATCC, American Type Culture Collection) by standard procedures. Hybridoma supernatants were screened 10 days later in a flow cytometry assay (iQue, Intellicyt; Sartorius, Gottingen, Germany). Supernatants were incubated for 90 min with BSA-conjugated NAD and NMN coupled to 3D-Caroboxy beads (PolyAN, Berlin, Germany) together with Atto-488-coupled isotype-specific monoclonal mouse-anti-rat IgG secondary antibodies (IgG1 TIB170, IgG2a TIB173, IgG2b TIB174 all from ATCC; IgG2c in house) or isotype-specific monoclonal rat-anti-mouse IgG secondary antibodies (IgG1, IgG2a, IgG2b all from in house, IgG3 HB128 from ATCC). Antibody

binding was analysed using ForeCyt software (Sartorius). Selected NMN hybridoma cells from immunized mice were subcloned twice by limiting dilution to obtain stable monoclonal cell lines NMN 28C11 and NMN 26D11 (both mouse IgG3 isotype).

Table 17. List of antibody clones against NAD generated in the course of this thesis.

Antigen	Source	Clone	Subtype
NMN	Rat	13D5	2b
NMN	Rat	8A11	g1
NMN	Rat	5C7	2b
NMN	Rat	13A12	2b
NMN	Rat	11G7	2b
NMN	Rat	14H6	2b
NMN	Rat	20C2	2b
NMN	Rat	13G3	2b
NMN	Rat	7C6	2b
NMN	Rat	4D10	2b
NMN	Rat	16C11	2b
NMN	Rat	15B7	2b
NMN	Rat	16D4	2b
NMN	Rat	11B8	2b
NMN	Rat	2D8	2b
NMN	Rat	16B12	2b
NMN	Rat	18F12	2b
NMN	Rat	12C4	2b
NMN	Rat	15F2	2b
NMN	Rat	13F6	2b
NMN	Rat	1E1	2b
NMN	Rat	10A1	2b
NMN	Rat	15G8	2b
NMN	Rat	10E6	2b
NMN	Rat	22G1	2b
NMN	Rat	14A2	2b
NMN	Rat	7D1	2b
NMN	Rat	3F2	2b
NMN	Rat	3E10	2b
NMN	Rat	7C9	2b
NMN	Rat	4A9	2b
NMN	Rat	1C6	2b
NMN	Rat	11B11	2b
NMN	Rat	4C2	2b
NMN	Rat	22B9	2b
NMN	Rat	22F4	2b
NMN	Rat	3C5	2b
NMN	Rat	4B8	2b
NMN	Rat	13D9	2b

NMN	Rat	22D2	2b
NMN	Rat	12A3	2b
NMN	Rat	22C9	2b
NMN	Rat	14A11	2b
NMN	Rat	3H5	2b
NMN	Rat	17C12	2b
NMN	Rat	2G4	2b
NMN	Rat	15H7	2b
NMN	Rat	9G1	2b
NMN	Rat	11B6	2b
NMN	Rat	14D3	2b
NMN	Rat	1R3	2b
NMN	Rat	12H6	2b
NMN	Rat	8G5	2b
NMN + NAD	Rat	19B2	2b
NMN + NAD	Rat	7B3	2c
NMN + NAD	Rat	9H1	2c
NMN + NAD	Rat	16E4	2c
NMN + NAD	Mouse	26D11	3
NMN + NAD	Mouse	28C11	3
NAD + BSA	Rat	7D6	2c
NAD + BSA	Rat	10H8	2c
NAD + BSA	Rat	24B12	2c
NAD + BSA	Rat	23A12	2c
NAD	Rat	18C10	
NAD	Rat	1C12	

4.7.3 Determination of the antibody-bound fraction of NAD

Experimental work, HPLC analysis and calculation were performed by R. Hett (our lab). For the determination of the antibody-bound fraction of NAD, an equimolar mixture of NAD with adenosine as an internal standard was prepared at a concentration of 0,1 mM. A volume of 10 µl of this mixture was pipetted to 50 µl solutions of PBS/TBS (Input sample) and to 50 µl solutions containing the different antibodies, leading to an initial nucleoside concentration of 16,7 µM. After the incubation of the mixtures for 2 h at 4° C the unbound NAD of the antibody containing samples was separated by centrifugation (14 000 g for 1 min) using a 10 kDa cut-off spin filter (Roti-Spin MINI). A volume of 10 µl of each input- and filtrate-sample was then applied to the HPLC (4.7.4). The two peaks of each chromatogram were integrate. The peak area of the NAD normalized to the peak area of the adenosine, which eventually gave the normalized peak areas of the NAD in the input sample (nucleoside

input, NI) and in the filtrate of the antibody samples (nucleoside-antibody, NA). The antibody-bound fraction (BF) of NAD can then be calculated by: BF = (NI − NA)/NI. It can be used to derive the concentrations of bound ([AbN]) and free nucleoside ([N]) from the initial nucleoside concentration ([N0]): [AbN] = BF × [N0] and [N] = (1 − BF) ×[N0]. To get a first estimation of the value for KD and the maximal concentration of binding sites of the antibody ([Bmax]), the ratio [AbN]/[N] was plotted against [AbN] to obtain a Scatchard plot. From this, the K_D (dissociation constant) was estimated using the negative reciprocal value of the slope of the resulting regression line for a single-point. Measurements as well as the calculations were done by Robert Hett.

4.7.4 HPLC analysis

HPLC analysis of RNA were performed by R. Hett (our lab) using the HPLC-system "WellChrom" from Knauer, equipped with Pump K-1001, Diode Array Detector K-2800, column oven and a Vacuum Degasser from Techlab GmbH (Germany). The experiments were done, detecting at wavelengths ranging from 260 to 280 nm. The resulting chromatograms were analysed with the software ChromGate Client/Server Vers. 3.1.7.

The 5-mer RNAs were resolved on a YMC-Pac ODS-AQ column (5 µm, 100 x 2.1). Gradients using the buffers A (0,1 M TEAA (Triethylammoniumacetat) pH 6.5) and buffer B (80% $NH_4CH_3CO_2$, 20% acetonitrile [v/v]) were applied with a flow rate of 0.25 mL/min (Table 18).

Table 18. HPLC gradient protocols (C18-Oligo)

Time (min)	Flow (ml/min)	Buffer A (%)	Buffer B (%)
0,00	0,25	80	20
2,00	0,25	80	20
32,00	0,25	0	100
37,00	0,25	0	100
37,10	0,25	80	20
55,00	0,25	80	20

Input- and filtrate-sample for the analysis of bound/unbound NAD by antibodies were resolved on a YMC-Pac ODS-AQ column (5 µm, 100 x 2.1). Gradients using the buffers A (H20) and buffer B (80% 20 mM TEAA pH .5/ 20% acetonitrile [v/v]) were applied with a flow rate of 0.2 mL/min (Table 19)

Table 19. HPLC gradient protocols (NAD+A-TBS)

Time (min)	Flow (ml/min)	Buffer A (%)	Buffer B (%)
0,00	0,200	95	5
5,00	0,200	95	5
35,00	0,200	0	100
35,10	0,200	95	5

5 REFERENCES

Abbas, YM, Laudenbach, BT, Martínez-Montero, S, Cencic, R, Habjan, M, Pichlmair, A, Damha, MJ, Pelletier, J, and Nagar, B (2017). Structure of human IFIT1 with capped RNA reveals adaptable mRNA binding and mechanisms for sensing N1 and N2 ribose 2′-O methylations. Proc Natl Acad Sci 114, E2106–E2115.

Abdelraheim, SR, Spiller, DG, and McLennan, AG (2003). Mammalian NADH diphosphatases of the Nudix family: cloning and characterization of the human peroxisomal NUDT12 protein. Biochem J 374, 329–335.

Abele, F, Höfer, K, Bernhard, P, Grawenhoff, J, Seidel, M, Krause, A, Kopf, S, Schröter, M, and Jäschke, A (2020). A Novel NAD-RNA Decapping Pathway Discovered by Synthetic Light-Up NAD-RNAs. Biomolecules 10, 513.

Adams, JM, and Cory, S (1975). Modified nucleosides and bizarre 5'-termini in mouse myeloma mRNA. Nature 255, 28–33.

Akichika, S, Hirano, S, Shichino, Y, Suzuki, T, Nishimasu, H, Ishitani, R, Sugita, A, Hirose, Y, Iwasaki, S, Nureki, O, *et al.* (2019). Cap-specific terminal N 6-methylation of RNA by an RNA polymerase II-associated methyltransferase. Science 363, eaav0080.

Akiyama, S, Ikezaki, K, Kuramochi, H, Takahashi, K, and Kuwano, M (1981). Bleomycin-resistant cells contain increased bleomycin-hydrolase activities. Biochem Biophys Res Commun 101, 55–60.

Ali, MH, Elsherbiny, ME, and Emara, M (2019). Updates on Aptamer Research. Int J Mol Sci 20, 2511.

Allmang, C, Kufel, J, Chanfreau, G, Mitchell, P, Petfalski, E, and Tollervey, D (1999). Functions of the exosome in rRNA, snoRNA and snRNA synthesis. EMBO J 18, 5399–5410.

Almeida, MV, de Jesus Domingues, AM, Lukas, H, Mendez-Lago, M, and Ketting, RF (2019). RppH can faithfully replace TAP to allow cloning of 5′-triphosphate carrying small RNAs. MethodsX 6, 265–272.

Anreiter, I, Tian, YW, and Soller, M (2023). The cap epitranscriptome: Early directions to a complex life as mRNA. BioEssays 45, 2200198.

Archibald, JM (2015). Endosymbiosis and Eukaryotic Cell Evolution. Curr Biol CB 25, R911-921.

Bail, S, and Kiledjian, M (2008). DcpS, a general modulator of cap-binding protein-dependent processes? RNA Biol 5, 216–219.

Barile, M, Giancaspero, TA, Leone, P, Galluccio, M, and Indiveri, C (2016). Riboflavin transport and metabolism in humans. J Inherit Metab Dis 39, 545–557.

Behm-Ansmant, I, Helm, M, and Motorin, Y (2011). Use of Specific Chemical Reagents for Detection of Modified Nucleotides in RNA. J Nucleic Acids 2011, 1–17.

Bélanger, F, Stepinski, J, Darzynkiewicz, E, and Pelletier, J (2010). Characterization of hMTr1, a human Cap1 2'-O-ribose methyltransferase. J Biol Chem 285, 33037–33044.

Bellamacina, CR (1996). The nicotinamide dinucleotide binding motif: a comparison of nucleotide binding proteins. FASEB J 10, 1257–1269.

Benoni, B, Benoni, R, Trylcova, J, Grab, K, Pačes, J, Weber, J, Stanek, D, Kowalska, J, Bednarova, L, Keckesova, Z, *et al.* (2022). HIV-1 infection reduces NAD capping of host cell snRNA and snoRNA, Biochemistry.

Bergman, N, Milone, J, Bates, EJ, Opyrchal, M, Bellofatto, V, and Wilusz, J (2004). Assessing Messenger RNA Decapping in Cellular Extracts. In: mRNA Processing and Metabolism, New Jersey: Humana Press, 181–192.

Bird, JG, Basu, U, Kuster, D, Ramachandran, A, Grudzien-Nogalska, E, Towheed, A, Wallace, DC, Kiledjian, M, Temiakov, D, Patel, SS, *et al.* (2018). Highly efficient 5' capping of mitochondrial RNA with NAD+ and NADH by yeast and human mitochondrial RNA polymerase. eLife 7, e42179.

Bird, JG, Zhang, Y, Tian, Y, Panova, N, Barvík, I, Greene, L, Liu, M, Buckley, B, Krásný, L, Lee, JK, *et al.* (2016). The mechanism of RNA 5′ capping with NAD+, NADH and desphospho-CoA. Nature 535, 444–447.

Bochnig, P, Reuter, R, Bringmann, P, and Lührmann, R (1987). A monoclonal antibody against 2,2,7-trimethylguanosine that reacts with intact, class U, small nuclear ribonucleoproteins as well as with 7-methylguanosine-capped RNAs. Eur J Biochem 168, 461–467.

Bojarska, E, Kraciuk, R, Wierzchowski, J, Wieczorek, Z, Stepiński, J, Jankowska, M, Starzyńska, E, Guranowski, A, and Darzynkiewicz, E (1999). Hydrolysis of some mRNA 5'-cap analogs catalyzed by the human Fhit protein--and lupin ApppA hydrolases. Nucleosides Nucleotides 18, 1125–1126.

Bollu, A, Peters, A, and Rentmeister, A (2022). Chemo-Enzymatic Modification of the 5′ Cap To Study mRNAs. Acc Chem Res 55, 1249–1261.

Brenner, C, Bieganowski, P, Pace, HC, and Huebner, K (1999). The histidine triad superfamily of nucleotide-binding proteins. J Cell Physiol 181, 179–187.

Burgstaller, P, and Famulok, M (1994). Isolation of RNA Aptamers for Biological Cofactors by In Vitro Selection. Angew Chem Int Ed Engl 33, 1084–1087.

Burke, DH, and Hoffman, DC (1998). A Novel Acidophilic RNA Motif That Recognizes Coenzyme A. Biochemistry 37, 4653–4663.

Busch, H, Reddy, R, Rothblum, L, and Choi, YC (1982). SnRNAs, SnRNPs, and RNA processing. Annu Rev Biochem 51, 617–654.

Buschmann, J, Moritz, B, Jeske, M, Lilie, H, Schierhorn, A, and Wahle, E (2013). Identification of Drosophila and human 7-methyl GMP-specific nucleotidases. J Biol Chem 288, 2441–2451.

Byszewska, M, Śmietański, M, Purta, E, and Bujnicki, JM (2014). RNA methyltransferases involved in 5′ cap biosynthesis. RNA Biol 11, 1597–1607.

Cahová, H, Winz, M-L, Höfer, K, Nübel, G, and Jäschke, A (2015). NAD captureSeq indicates NAD as a bacterial cap for a subset of regulatory RNAs. Nature 519, 374–377.

Carmo-Fonseca, M (2002). The Contribution of Nuclear Compartmentalization to Gene Regulation. Cell 108, 513–521.

Carreras-Puigvert, J, Zitnik, M, Jemth, A-S, Carter, M, Unterlass, JE, Hallström, B, Loseva, O, Karem, Z, Calderón-Montaño, JM, Lindskog, C, *et al.* (2017). A comprehensive structural, biochemical and biological profiling of the human NUDIX hydrolase family. Nat Commun 8, 1541.

Chang, C-T, Bercovich, N, Loh, B, Jonas, S, and Izaurralde, E (2014). The activation of the decapping enzyme DCP2 by DCP1 occurs on the EDC4 scaffold and involves a conserved loop in DCP1. Nucleic Acids Res 42, 5217–5233.

Chang, H-M, Triboulet, R, Thornton, JE, and Gregory, RI (2013). A role for the Perlman syndrome exonuclease Dis3l2 in the Lin28-let-7 pathway. Nature 497, 244–248.

Chang, JH, Jiao, X, Chiba, K, Oh, C, Martin, CE, Kiledjian, M, and Tong, L (2012). Dxo1 is a new type of eukaryotic enzyme with both decapping and 5′-3′ exoribonuclease activity. Nat Struct Mol Biol 19, 1011–1017.

Chen, H, Egger, M, Xu, X, Flemmich, L, Krasheninina, O, Sun, A, Micura, R, and Ren, A (2020). Structural distinctions between NAD+ riboswitch domains 1 and 2 determine differential folding and ligand binding. Nucleic Acids Res 48, 12394–12406.

Chen, YG, Kowtoniuk, WE, Agarwal, I, Shen, Y, and Liu, DR (2009). LC/MS analysis of cellular RNA reveals NAD-linked RNA. Nat Chem Biol 5, 879–881.

Cheng, H, Dufu, K, Lee, C-S, Hsu, JL, Dias, A, and Reed, R (2006). Human mRNA export machinery recruited to the 5' end of mRNA. Cell 127, 1389–1400.

Chini, CCS, Zeidler, JD, Kashyap, S, Warner, G, and Chini, EN (2021). Evolving concepts in NAD+ metabolism. Cell Metab 33, 1076–1087.

Chlebowski, A, Lubas, M, Jensen, TH, and Dziembowski, A (2013). RNA decay machines: The exosome. Biochim Biophys Acta BBA - Gene Regul Mech 1829, 552–560.

Chu, C, Das, K, Tyminski, JR, Bauman, JD, Guan, R, Qiu, W, Montelione, GT, Arnold, E, and Shatkin, AJ (2011). Structure of the guanylyltransferase domain of human mRNA capping enzyme. Proc Natl Acad Sci U S A 108, 10104–10108.

Covarrubias, AJ, Perrone, R, Grozio, A, and Verdin, E (2021). NAD+ metabolism and its roles in cellular processes during ageing. Nat Rev Mol Cell Biol 22, 119–141.

Cowling, VH (2009). Regulation of mRNA cap methylation. Biochem J 425, 295–302.

Cramer, P (2019). Organization and regulation of gene transcription. Nature 573, 45–54.

Crick, F (1970). Central dogma of molecular biology. Nature 227, 561–563.

Cui, X, Liang, Z, Shen, L, Zhang, Q, Bao, S, Geng, Y, Zhang, B, Leo, V, Vardy, LA, Lu, T, *et al.* (2017). 5-Methylcytosine RNA Methylation in *Arabidopsis Thaliana*. Mol Plant 10, 1387–1399.

Dallas, A, Vlassov, AV, and Kazakov, SA (2004). Principles of Nucleic Acid Cleavage by Metal Ions. In: Artificial Nucleases, ed. MA Zenkova, Berlin, Heidelberg: Springer Berlin Heidelberg, 61–88.

Dantsuji, S, Ohno, M, and Taniguchi, I (2023). The hnRNP C tetramer binds to CBC on mRNA and impedes PHAX recruitment for the classification of RNA polymerase II transcripts. Nucleic Acids Res, gkac1250.

Davidson, L, Francis, L, Cordiner, RA, Eaton, JD, Estell, C, Macias, S, Cáceres, JF, and West, S (2019). Rapid Depletion of DIS3, EXOSC10, or XRN2 Reveals the Immediate Impact of Exoribonucleolysis on Nuclear RNA Metabolism and Transcriptional Control. Cell Rep 26, 2779-2791.e5.

Deng, Q, Watson, CJ, and Kennedy, RT (2003). Aptamer affinity chromatography for rapid assay of adenosine in microdialysis samples collected in vivo. J Chromatogr A 1005, 123–130.

Depmeier, H, Hoffmann, E, Bornewasser, L, and Kath-Schorr, S (2021). Strategies for Covalent Labeling of Long RNAs. ChemBioChem 22, 2826–2847.

Despic, V, and Jaffrey, SR (2023). mRNA ageing shapes the Cap2 methylome in mammalian mRNA. Nature 614, 358–366.

Devarkar, SC, Wang, C, Miller, MT, Ramanathan, A, Jiang, F, Khan, AG, Patel, SS, and Marcotrigiano, J (2016). Structural basis for m7G recognition and 2′-O-methyl discrimination in capped RNAs by the innate immune receptor RIG-I. Proc Natl Acad Sci 113, 596–601.

Dever, TE, Dinman, JD, and Green, R (2018). Translation Elongation and Recoding in Eukaryotes. Cold Spring Harb Perspect Biol 10, a032649.

van Dijk, E, Cougot, N, Meyer, S, Babajko, S, Wahle, E, and Séraphin, B (2002). Human Dcp2: a catalytically active mRNA decapping enzyme located in specific cytoplasmic structures. EMBO J 21, 6915–6924.

Doamekpor, SK, Gozdek, A, Kwasnik, A, Kufel, J, and Tong, L (2020a). A novel 5'-hydroxyl dinucleotide hydrolase activity for the DXO/Rai1 family of enzymes. Nucleic Acids Res 48, 349–358.

Doamekpor, SK, Grudzien-Nogalska, E, Mlynarska-Cieslak, A, Kowalska, J, Kiledjian, M, and Tong, L (2020b). DXO/Rai1 enzymes remove 5′-end FAD and dephospho-CoA caps on RNAs. Nucleic Acids Res.

Doamekpor, SK, Sharma, S, Kiledjian, M, and Tong, L (2022). Recent insights into noncanonical 5′ capping and decapping of RNA. J Biol Chem 298, 102171.

Dominissini, D, Moshitch-Moshkovitz, S, Schwartz, S, Salmon-Divon, M, Ungar, L, Osenberg, S, Cesarkas, K, Jacob-Hirsch, J, Amariglio, N, Kupiec, M, *et al.* (2012). Topology of the human and mouse m^6A RNA methylomes revealed by m^6A-seq. Nature 485, 201.

Drazkowska, K, Tomecki, R, Warminski, M, Baran, N, Cysewski, D, Depaix, A, Kasprzyk, R, Kowalska, J, Jemielity, J, and Sikorski, PJ (2022). 2'-O-Methylation of the second transcribed nucleotide within the mRNA 5' cap impacts the protein production level in a cell-specific manner and contributes to RNA immune evasion. Nucleic Acids Res 50, 9051–9071.

Dunn, JJ, Studier, FW, and Gottesman, M (1983). Complete nucleotide sequence of bacteriophage T7 DNA and the locations of T7 genetic elements. J Mol Biol 166, 477–535.

Edelheit, S, Schwartz, S, Mumbach, MR, Wurtzel, O, and Sorek, R (2013). Transcriptome-Wide Mapping of 5-methylcytidine RNA Modifications in Bacteria, Archaea, and Yeast Reveals m5C within Archaeal mRNAs. PLOS Genet 9, e1003602.

Ellington, AD, and Szostak, JW (1990). In vitro selection of RNA molecules that bind specific ligands. Nature 346, 818–822.

Erlanger, BF, and Beiser, SM (1964). Antibodies specific for ribonucleosides and ribonucleotides and their reaction with DNA. Proc Natl Acad Sci 52, 68–74.

Fan, H, Sakuraba, K, Komuro, A, Kato, S, Harada, F, and Hirose, Y (2003). PCIF1, a novel human WW domain-containing protein, interacts with the phosphorylated RNA polymerase II. Biochem Biophys Res Commun 301, 378–385.

Feederle, R, and Schepers, A (2017). Antibodies specific for nucleic acid modifications. RNA Biol 14, 1089–1098.

Ferguson, F, McLennan, AG, Urbaniak, MD, Jones, NJ, and Copeland, NA (2020). Re-evaluation of Diadenosine Tetraphosphate (Ap4A) From a Stress Metabolite to Bona Fide Secondary Messenger. Front Mol Biosci 7, 606807.

Fischer, NM, Polêto, MD, Steuer, J, and van der Spoel, D (2018). Influence of Na+ and Mg2+ ions on RNA structures studied with molecular dynamics simulations. Nucleic Acids Res 46, 4872–4882.

Flaherty, SM, Fortes, P, Izaurralde, E, Mattaj, IW, and Gilmartin, GM (1997). Participation of the nuclear cap binding complex in pre-mRNA 3' processing. Proc Natl Acad Sci U S A 94, 11893–11898.

František Potužník, J, Nešuta, O, Škríba, A, Voleníková, B, Mititelu, M-B, Mancini, F, Serianni, V, Fernandez, H, Spustová, K, Trylčová, J, *et al.* (2023). Diadenosine Tetraphosphate (Ap4 A) Serves as a 5' RNA Cap in Mammalian Cells. Angew Chem Int Ed Engl, e202314951.

Frindert, J, Zhang, Y, Nübel, G, Kahloon, M, Kolmar, L, Hotz-Wagenblatt, A, Burhenne, J, Haefeli, WE, and Jäschke, A (2018). Identification, Biosynthesis, and Decapping of NAD-Capped RNAs in B. subtilis. Cell Rep 24, 1890-1901.e8.

Fuchs, A-L, Neu, A, and Sprangers, R (2016). A general method for rapid and cost-efficient large-scale production of 5′ capped RNA. RNA 22, 1454–1466.

Fuchs, A-L, Wurm, JP, Neu, A, and Sprangers, R (2020). Molecular basis of the selective processing of short mRNA substrates by the DcpS mRNA decapping enzyme. Proc Natl Acad Sci U S A 117, 19237–19244.

Furuichi, Y (2015). Discovery of m(7)G-cap in eukaryotic mRNAs. Proc Jpn Acad Ser B Phys Biol Sci 91, 394–409.

Gagliardi, D, and Dziembowski, A (2018). 5′ and 3′ modifications controlling RNA degradation: from safeguards to executioners. Philos Trans R Soc B Biol Sci 373, 20180160.

Gallie, DR (1991). The cap and poly(A) tail function synergistically to regulate mRNA translational efficiency. Genes Dev 5, 2108–2116.

Galloway, A, and Cowling, VH (2019). mRNA cap regulation in mammalian cell function and fate. Biochim Biophys Acta BBA - Gene Regul Mech 1862, 270–279.

Gao, A, Vasilyev, N, Kaushik, A, Duan, W, and Serganov, A (2020). Principles of RNA and nucleotide discrimination by the RNA processing enzyme RppH. Nucleic Acids Res 48, 3776–3788.

Ghosh, T, Peterson, B, Tomasevic, N, and Peculis, BA (2004). Xenopus U8 snoRNA binding protein is a conserved nuclear decapping enzyme. Mol Cell 13, 817–828.

Girard, C, Verheggen, C, Neel, H, Cammas, A, Vagner, S, Soret, J, Bertrand, E, and Bordonné, R (2008). Characterization of a short isoform of human Tgs1 hypermethylase associating with small nucleolar ribonucleoprotein core proteins and produced by limited proteolytic processing. J Biol Chem 283, 2060–2069.

Girbig, M, Misiaszek, AD, and Müller, CW (2022). Structural insights into nuclear transcription by eukaryotic DNA-dependent RNA polymerases. Nat Rev Mol Cell Biol 23, 603–622.

Gomes-Filho, JV, Breuer, R, Morales-Filloy, HG, Pozhydaieva, N, Borst, A, Paczia, N, Soppa, J, Höfer, K, Jäschke, A, and Randau, L (2023). Identification of NAD-RNA species and ADPR-RNA decapping in Archaea. Nat Commun 14, 7597.

Gonatopoulos-Pournatzis, T, and Cowling, VH (2014). Cap-binding complex (CBC). Biochem J 457, 231–242.

Gonatopoulos-Pournatzis, T, Dunn, S, Bounds, R, and Cowling, VH (2011). RAM/Fam103a1 Is Required for mRNA Cap Methylation. Mol Cell 44, 585–596.

Görnemann, J, Kotovic, KM, Hujer, K, and Neugebauer, KM (2005). Cotranscriptional Spliceosome Assembly Occurs in a Stepwise Fashion and Requires the Cap Binding Complex. Mol Cell 19, 53–63.

Götz, KH, Mex, M, Stuber, K, Offensperger, F, Scheffner, M, and Marx, A (2019). Formation of the Alarmones Diadenosine Triphosphate and Tetraphosphate by Ubiquitin- and Ubiquitin-like-Activating Enzymes. Cell Chem Biol 26, 1535-1543.e5.

Gout, I (2018). Coenzyme A, protein CoAlation and redox regulation in mammalian cells. Biochem Soc Trans 46, 721–728.

Graille, M, and Séraphin, B (2012). Surveillance pathways rescuing eukaryotic ribosomes lost in translation. Nat Rev Mol Cell Biol 13, 727–735.

Grozhik, AV, Olarerin-George, AO, Sindelar, M, Li, X, Gross, SS, and Jaffrey, SR (2019). Antibody cross-reactivity accounts for widespread appearance of m1A in 5'UTRs. Nat Commun 10, 5126.

Grudzien-Nogalska, E, Bird, JG, Nickels, BE, and Kiledjian, M (2018). "NAD-capQ" detection and quantitation of NAD caps. RNA 24, 1418–1425.

Grudzien-Nogalska, E, Jiao, X, Song, M-G, Hart, RP, and Kiledjian, M (2016). Nudt3 is an mRNA decapping enzyme that modulates cell migration. RNA 22, 773–781.

Grudzien-Nogalska, E, and Kiledjian, M (2017). New insights into decapping enzymes and selective mRNA decay. WIREs RNA 8, e1379.

Grudzien-Nogalska, E, Wu, Y, Jiao, X, Cui, H, Mateyak, MK, Hart, RP, Tong, L, and Kiledjian, M (2019). Structural and mechanistic basis of mammalian Nudt12 RNA deNADding. Nat Chem Biol 15, 575–582.

Gruss, OJ, Meduri, R, Schilling, M, and Fischer, U (2017). UsnRNP biogenesis: mechanisms and regulation. Chromosoma 126, 577–593.

Grüter, P, Tabernero, C, von Kobbe, C, Schmitt, C, Saavedra, C, Bachi, A, Wilm, M, Felber, BK, and Izaurralde, E (1998). TAP, the human homolog of Mex67p, mediates CTE-dependent RNA export from the nucleus. Mol Cell 1, 649–659.

Grzela, R, Nasilowska, K, Lukaszewicz, M, Tyras, M, Stepinski, J, Jankowska-Anyszka, M, Bojarska, E, and Darzynkiewicz, E (2018). Hydrolytic activity of human Nudt16

enzyme on dinucleotide cap analogs and short capped oligonucleotides. RNA 24, 633–642.

Gu, M, Fabrega, C, Liu, S-W, Liu, H, Kiledjian, M, and Lima, CD (2004). Insights into the structure, mechanism, and regulation of scavenger mRNA decapping activity. Mol Cell 14, 67–80.

Gupta, S, Busch, RK, Singh, R, and Reddy, R (1990). Characterization of U6 small nuclear RNA cap-specific antibodies. Identification of gamma-monomethyl-GTP cap structure in 7SK and several other human small RNAs. J Biol Chem 265, 19137–19142.

Guranowski, A (2000). Studies on Dinucleoside Polyphosphates. J Clin Biochem Nutr 28, 177–189.

Guth-Metzler, R, Mohamed, AM, Cowan, ET, Henning, A, Ito, C, Frenkel-Pinter, M, Wartell, RM, Glass, JB, and Williams, LD (2023). Goldilocks and RNA: where Mg2+ concentration is just right. Nucleic Acids Res 51, 3529–3539.

Hafner, M, Katsantoni, M, Köster, T, Marks, J, Mukherjee, J, Staiger, D, Ule, J, and Zavolan, M (2021). CLIP and complementary methods. Nat Rev Methods Primer 1, 1–23.

Haline-Vaz, T, Silva, TCL, and Zanchin, NIT (2008). The human interferon-regulated ISG95 protein interacts with RNA polymerase II and shows methyltransferase activity. Biochem Biophys Res Commun 372, 719–724.

Hamm, J, Darzynkiewicz, E, Tahara, SM, and Mattaj, IW (1990). The trimethylguanosine cap structure of U1 snRNA is a component of a bipartite nuclear targeting signal. Cell 62, 569–577.

Harlen, KM, and Churchman, LS (2017a). Subgenic Pol II interactomes identify region-specific transcription elongation regulators. Mol Syst Biol 13, 900.

Harlen, KM, and Churchman, LS (2017b). The code and beyond: transcription regulation by the RNA polymerase II carboxy-terminal domain. Nat Rev Mol Cell Biol 18, 263–273.

Hasler, D, Meduri, R, Bąk, M, Lehmann, G, Heizinger, L, Wang, X, Li, Z-T, Sement, FM, Bruckmann, A, Dock-Bregeon, A-C, *et al.* (2020). The Alazami Syndrome-Associated Protein LARP7 Guides U6 Small Nuclear RNA Modification and Contributes to Splicing Robustness. Mol Cell 77, 1014-1031.e13.

Hasler, D, Meister, G, and Fischer, U (2021). Stabilize and connect: the role of LARP7 in nuclear non-coding RNA metabolism. RNA Biol 18, 290–303.

Hausmann, S, and Shuman, S (2005). Specificity and mechanism of RNA cap guanine-N2 methyltransferase (Tgs1). J Biol Chem 280, 4021–4024.

Hausmann, S, Zheng, S, Costanzo, M, Brost, RL, Garcin, D, Boone, C, Shuman, S, and Schwer, B (2008). Genetic and biochemical analysis of yeast and human cap trimethylguanosine synthase: functional overlap of 2,2,7-trimethylguanosine caps,

small nuclear ribonucleoprotein components, pre-mRNA splicing factors, and RNA decay pathways. J Biol Chem 283, 31706–31718.

Helm, M, Lyko, F, and Motorin, Y (2019). Limited antibody specificity compromises epitranscriptomic analyses. Nat Commun 10, 5669.

Hirose, Y, Iwamoto, Y, Sakuraba, K, Yunokuchi, I, Harada, F, and Ohkuma, Y (2008). Human phosphorylated CTD-interacting protein, PCIF1, negatively modulates gene expression by RNA polymerase II. Biochem Biophys Res Commun 369, 449–455.

Ho, CK, and Shuman, S (1999). Distinct roles for CTD Ser-2 and Ser-5 phosphorylation in the recruitment and allosteric activation of mammalian mRNA capping enzyme. Mol Cell 3, 405–411.

Ho, CK, Sriskanda, V, McCracken, S, Bentley, D, Schwer, B, and Shuman, S (1998). The guanylyltransferase domain of mammalian mRNA capping enzyme binds to the phosphorylated carboxyl-terminal domain of RNA polymerase II. J Biol Chem 273, 9577–9585.

Höfer, K, Abele, F, Schlotthauer, J, and Jäschke, A (2016a). Synthesis of 5′-NAD-Capped RNA. Bioconjug Chem 27, 874–877.

Höfer, K, Li, S, Abele, F, Frindert, J, Schlotthauer, J, Grawenhoff, J, Du, J, Patel, DJ, and Jäschke, A (2016b). Structure and function of the bacterial decapping enzyme NudC. Nat Chem Biol 12, 730–734.

Hsieh, P, Richards, J, Liu, Q, and Belasco, JG (2013). Specificity of RppH-dependent RNA degradation in Bacillus subtilis. Proc Natl Acad Sci U S A 110, 8864–8869.

Hsu, CL, and Stevens, A (1993). Yeast Cells Lacking 5’→3’ Exoribonuclease 1 Contain mRNA Species That are Poly(A) Deficient and Partially Lack the 5’ Cap Structure. Mol Cell Biol 13, 4826–4835.

Hu, H, Flynn, N, Zhang, H, You, C, Hang, R, Wang, X, Zhong, H, Chan, Z, Xia, Y, and Chen, X (2021). SPAAC-NAD-seq, a sensitive and accurate method to profile NAD+-capped transcripts. Proc Natl Acad Sci 118.

Huang, F (2003). Efficient incorporation of CoA, NAD and FAD into RNA by in vitro transcription. Nucleic Acids Res 31, e8–e8.

Huang, L, Wang, J, and Lilley, DMJ (2020). Structure and ligand binding of the ADP-binding domain of the NAD+ riboswitch. RNA 26, 878–887.

Huber, J, Cronshagen, U, Kadokura, M, Marshallsay, C, Wada, T, Sekine, M, and Lührmann, R (1998). Snurportin1, an m3G-cap-specific nuclear import receptor with a novel domain structure. EMBO J 17, 4114–4126.

Hudeček, O, Benoni, R, Reyes-Gutierrez, PE, Culka, M, Šanderová, H, Hubálek, M, Rulíšek, L, Cvačka, J, Krásný, L, and Cahová, H (2020). Dinucleoside polyphosphates act as 5′-RNA caps in bacteria. Nat Commun 11, 1052.

Hussain, S, Sajini, AA, Blanco, S, Dietmann, S, Lombard, P, Sugimoto, Y, Paramor, M, Gleeson, JG, Odom, DT, Ule, J, *et al.* (2013). NSun2-mediated cytosine-5 methylation of vault noncoding RNA determines its processing into regulatory small RNAs. Cell Rep 4, 255–261.

Igloi, GL, and Kössel, H (1987). [27] Use of boronate-containing gels for electrophoretic analysis of both ends of RNA molecules. In: Methods in Enzymology, Elsevier, 433–448.

Inesta-Vaquera, F, Chaugule, VK, Galloway, A, Chandler, L, Rojas-Fernandez, A, Weidlich, S, Peggie, M, and Cowling, VH (2018). DHX15 regulates CMTR1-dependent gene expression and cell proliferation. Life Sci Alliance 1.

Ishigaki, Y, Li, X, Serin, G, and Maquat, LE (2001). Evidence for a pioneer round of mRNA translation: mRNAs subject to nonsense-mediated decay in mammalian cells are bound by CBP80 and CBP20. Cell 106, 607–617.

Izaurralde, E, Lewis, J, McGuigan, C, Jankowska, M, Darzynkiewicz, E, and Mattaj, IW (1994). A nuclear cap binding protein complex involved in pre-mRNA splicing. Cell 78, 657–668.

Jády, BE, Bertrand, E, and Kiss, T (2004). Human telomerase RNA and box H/ACA scaRNAs share a common Cajal body–specific localization signal. J Cell Biol 164, 647–652.

Jeronimo, C, Forget, D, Bouchard, A, Li, Q, Chua, G, Poitras, C, Thérien, C, Bergeron, D, Bourassa, S, Greenblatt, J, *et al.* (2007). Systematic Analysis of the Protein Interaction Network for the Human Transcription Machinery Reveals the Identity of the 7SK Capping Enzyme. Mol Cell 27, 262–274.

Jia, D, Cai, L, He, H, Skogerbø, G, Li, T, Aftab, MN, and Chen, R (2007). Systematic identification of non-coding RNA 2,2,7-trimethylguanosine cap structures in Caenorhabditis elegans. BMC Mol Biol 8, 86.

Jiao, X, Chang, JH, Kilic, T, Tong, L, and Kiledjian, M (2013). A mammalian pre-mRNA 5' end capping quality control mechanism and an unexpected link of capping to pre-mRNA processing. Mol Cell 50, 104–115.

Jiao, X, Doamekpor, SK, Bird, JG, Nickels, BE, Tong, L, Hart, RP, and Kiledjian, M (2017). 5′ End Nicotinamide Adenine Dinucleotide Cap in Human Cells Promotes RNA Decay through DXO-Mediated deNADding. Cell 168, 1015-1027.e10.

Jiao, X, Xiang, S, Oh, C, Martin, CE, Tong, L, and Kiledjian, M (2010). Identification of a quality-control mechanism for mRNA 5′-end capping. Nature 467, 608–611.

Julius, C, and Yuzenkova, Y (2017). Bacterial RNA polymerase caps RNA with various cofactors and cell wall precursors. Nucleic Acids Res 45, 8282–8290.

Kahvejian, A, Svitkin, YV, Sukarieh, R, M'Boutchou, M-N, and Sonenberg, N (2005). Mammalian poly(A)-binding protein is a eukaryotic translation initiation factor, which acts via multiple mechanisms. Genes Dev 19, 104–113.

Kastern, WH, and Berry, SJ (1976). Non-methylated guanosine as the 5′ terminus of capped mRNA from insect oocytes. Biochem Biophys Res Commun 71, 37–44.

Kataoka, N (2023). The Nuclear Cap-Binding Complex, a multitasking binding partner of RNA polymerase II transcripts. J Biochem (Tokyo), mvad081.

Khatter, H, Vorländer, MK, and Müller, CW (2017). RNA polymerase I and III: similar yet unique. Curr Opin Struct Biol 47, 88–94.

Kirschning, A (2022). On the evolution of coenzyme biosynthesis. Nat Prod Rep 39, 2175–2199.

Klinge, S, and Woolford, JL (2019). Ribosome assembly coming into focus. Nat Rev Mol Cell Biol 20, 116–131.

Knutson, SD, Arthur, RA, Johnston, HR, and Heemstra, JM (2020). Selective Enrichment of A-to-I Edited Transcripts from Cellular RNA Using Endonuclease V. J Am Chem Soc 142, 5241–5251.

Kowtoniuk, WE, Shen, Y, Heemstra, JM, Agarwal, I, and Liu, DR (2009). A chemical screen for biological small molecule–RNA conjugates reveals CoA-linked RNA. Proc Natl Acad Sci 106, 7768–7773.

Kramer, S, and McLennan, AG (2019). The complex enzymology of mRNA decapping: Enzymes of four classes cleave pyrophosphate bonds. WIREs RNA 10, e1511.

Krempl, C, Lazzaretti, D, and Sprangers, R (2023). A structural biology view on the enzymes involved in eukaryotic mRNA turnover. Biol Chem.

Kufel, J, and Grzechnik, P (2019). Small Nucleolar RNAs Tell a Different Tale. Trends Genet 35, 104–117.

Kummer, E, and Ban, N (2021). Mechanisms and regulation of protein synthesis in mitochondria. Nat Rev Mol Cell Biol 22, 307–325.

Łabno, A, Tomecki, R, and Dziembowski, A (2016a). Cytoplasmic RNA decay pathways - Enzymes and mechanisms. Biochim Biophys Acta 1863, 3125–3147.

Łabno, A, Warkocki, Z, Kuliński, T, Krawczyk, PS, Bijata, K, Tomecki, R, and Dziembowski, A (2016b). Perlman syndrome nuclease DIS3L2 controls cytoplasmic non-coding RNAs and provides surveillance pathway for maturing snRNAs. Nucleic Acids Res 44, 10437–10453.

Langberg, SR, and Moss, B (1981). Post-transcriptional modifications of mRNA. Purification and characterization of cap I and cap II RNA (nucleoside-2'-)-methyltransferases from HeLa cells. J Biol Chem 256, 10054–10060.

Lauhon, CT, and Szostak, JW (1995). RNA aptamers that bind flavin and nicotinamide redox cofactors. J Am Chem Soc 117, 1246–1257.

Lesk, AM (1995). NAD-binding domains of dehydrogenases. Curr Opin Struct Biol 5, 775–783.

Lewis, JD, Izaurralde, E, Jarmolowski, A, McGuigan, C, and Mattaj, IW (1996). A nuclear cap-binding complex facilitates association of U1 snRNP with the cap-proximal 5' splice site. Genes Dev 10, 1683–1698.

Li, J, Bonkowski, MS, Moniot, S, Zhang, D, Hubbard, BP, Ling, AJY, Rajman, LA, Qin, B, Lou, Z, Gorbunova, V, *et al.* (2017). A conserved NAD+ binding pocket that regulates protein-protein interactions during aging. Science 355, 1312–1317.

Li, Y, Ho, ES, Gunderson, SI, and Kiledjian, M (2009). Mutational analysis of a Dcp2-binding element reveals general enhancement of decapping by 5′-end stem-loop structures. Nucleic Acids Res 37, 2227–2237.

Li, Y, Song, M, and Kiledjian, M (2011). Differential utilization of decapping enzymes in mammalian mRNA decay pathways. RNA 17, 419–428.

Li, Y, Song, M-G, and Kiledjian, M (2008). Transcript-specific decapping and regulated stability by the human Dcp2 decapping protein. Mol Cell Biol 28, 939–948.

Liere, K, Weihe, A, and Börner, T (2011). The transcription machineries of plant mitochondria and chloroplasts: Composition, function, and regulation. J Plant Physiol 168, 1345–1360.

Lim, J, Ha, M, Chang, H, Kwon, SC, Simanshu, DK, Patel, DJ, and Kim, VN (2014). Uridylation by TUT4 and TUT7 marks mRNA for degradation. Cell 159, 1365–1376.

Liu, H, Rodgers, ND, Jiao, X, and Kiledjian, M (2002). The scavenger mRNA decapping enzyme DcpS is a member of the HIT family of pyrophosphatases. EMBO J 21, 4699–4708.

Liudkovska, V, and Dziembowski, A (2021). Functions and mechanisms of RNA tailing by metazoan terminal nucleotidyltransferases. Wiley Interdiscip Rev RNA 12, e1622.

Luciano, DJ, and Belasco, JG (2020). Np4A alarmones function in bacteria as precursors to RNA caps. Proc Natl Acad Sci U S A 117, 3560–3567.

Luciano, DJ, Levenson-Palmer, R, and Belasco, JG (2019). Stresses that Raise Np4A Levels Induce Protective Nucleoside Tetraphosphate Capping of Bacterial RNA. Mol Cell 75, 957-966.e8.

Lukaszewicz, M, Ferenc-Mrozek, A, Bojarska, E, Stelmach, J, Stepinski, J, and Darzynkiewicz, E (2023). Contribution of Nudt12 enzyme to differentially methylated dinucleotides of 5'RNA cap structure. Biochim Biophys Acta BBA - Gen Subj 1867, 130400.

Luo, M, and Reed, R (1999). Splicing is required for rapid and efficient mRNA export in metazoans. Proc Natl Acad Sci 96, 14937–14942.

Lykke-Andersen, J (2002). Identification of a human decapping complex associated with hUpf proteins in nonsense-mediated decay. Mol Cell Biol 22, 8114–8121.

Malkowski, SN, Spencer, TCJ, and Breaker, RR (2019). Evidence that the nadA motif is a bacterial riboswitch for the ubiquitous enzyme cofactor NAD+. RNA 25, 1616–1627.

Malygin, AG, and Shemyakin, MF (1979). Adenosine, NAD and FAD can initiate template-dependent RNA a synthesis catalyzed by Escherichia Coli RNA polymerase. FEBS Lett 102, 51–54.

Mandal, SS, Chu, C, Wada, T, Handa, H, Shatkin, AJ, and Reinberg, D (2004). Functional interactions of RNA-capping enzyme with factors that positively and negatively regulate promoter escape by RNA polymerase II. Proc Natl Acad Sci U S A 101, 7572–7577.

Marcotrigiano, J, Gingras, AC, Sonenberg, N, and Burley, SK (1997). Cocrystal structure of the messenger RNA 5' cap-binding protein (eIF4E) bound to 7-methyl-GDP. Cell 89, 951–961.

Marshallsay, C, and Lührmann, R (1994). In vitro nuclear import of snRNPs: cytosolic factors mediate m3G-cap dependence of U1 and U2 snRNP transport. EMBO J 13, 222–231.

Martinez, A, Yamashita, S, Nagaike, T, Sakaguchi, Y, Suzuki, T, and Tomita, K (2017a). Human BCDIN3D monomethylates cytoplasmic histidine transfer RNA. Nucleic Acids Res 45, 5423–5436.

Martinez, I, Hayes, KE, Barr, JA, Harold, AD, Xie, M, Bukhari, SIA, Vasudevan, S, Steitz, JA, and DiMaio, D (2017b). An Exportin-1–dependent microRNA biogenesis pathway during human cell quiescence. Proc Natl Acad Sci 114, E4961–E4970.

Matsuzawa, S, Wakata, Y, Ebi, F, Isobe, M, and Kurosawa, N (2019). Development and validation of monoclonal antibodies against N6-methyladenosine for the detection of RNA modifications. PLOS ONE 14, e0223197.

Mattaj, IW (1986). Cap trimethylation of U snRNA is cytoplasmic and dependent on U snRNP protein binding. Cell 46, 905–911.

Mattay, J (2022). Noncanonical metabolite RNA caps: Classification, quantification, (de)capping, and function. WIREs RNA n/a, e1730.

McCloskey, A, Taniguchi, I, Shinmyozu, K, and Ohno, M (2012). hnRNP C tetramer measures RNA length to classify RNA polymerase II transcripts for export. Science 335, 1643–1646.

McCracken, S, Fong, N, Rosonina, E, Yankulov, K, Brothers, G, Siderovski, D, Hessel, A, Foster, S, Shuman, S, and Bentley, DL (1997). 5'-Capping enzymes are targeted to pre-mRNA by binding to the phosphorylated carboxy-terminal domain of RNA polymerase II. Genes Dev 11, 3306–3318.

Merkle, T, Holder, IT, and Hartig, JS (2016). The dual aptamer approach: rational design of a high-affinity FAD aptamer. Org Biomol Chem 14, 447–450.

Meyer, KD, Saletore, Y, Zumbo, P, Elemento, O, Mason, CE, and Jaffrey, SR (2012). Comprehensive Analysis of mRNA Methylation Reveals Enrichment in 3′ UTRs and near Stop Codons. Cell 149, 1635–1646.

Micura, R, and Höbartner, C (2020). Fundamental studies of functional nucleic acids: aptamers, riboswitches, ribozymes and DNAzymes. Chem Soc Rev 49, 7331–7353.

Mikkola, S (2020). Nucleotide Sugars in Chemistry and Biology. Mol Basel Switz 25, 5755.

Mishima, E, Jinno, D, Akiyama, Y, Itoh, K, Nankumo, S, Shima, H, Kikuchi, K, Takeuchi, Y, Elkordy, A, Suzuki, T, *et al.* (2015). Immuno-Northern Blotting: Detection of RNA Modifications by Using Antibodies against Modified Nucleosides. PLOS ONE 10, e0143756.

Misra, VK, and Draper, DE (1998). On the role of magnesium ions in RNA stability. Biopolymers 48, 113–135.

Möhler, M, and Jäschke, A (2023). Future Perspectives for the Identification and Sequencing of Nicotinamide Adenine Dinucleotide-Capped RNAs. Acc Chem Res, acs.accounts.3c00446.

Monaghan, L, Longman, D, and Cáceres, JF (2023). Translation-coupled mRNA quality control mechanisms. EMBO J 42, e114378.

Monecke, T, Dickmanns, A, and Ficner, R (2009). Structural basis for m7G-cap hypermethylation of small nuclear, small nucleolar and telomerase RNA by the dimethyltransferase TGS1. Nucleic Acids Res 37, 3865–3877.

Motorin, Y, and Helm, M (2024). General Principles and Limitations for Detection of RNA Modifications by Sequencing. Acc Chem Res 57, 275–288.

Mouaikel, J, Narayanan, U, Verheggen, C, Matera, AG, Bertrand, E, Tazi, J, and Bordonné, R (2003). Interaction between the small-nuclear-RNA cap hypermethylase and the spinal muscular atrophy protein, survival of motor neuron. EMBO Rep 4, 616–622.

Mouaikel, J, Verheggen, C, Bertrand, E, Tazi, J, and Bordonné, R (2002). Hypermethylation of the Cap Structure of Both Yeast snRNAs and snoRNAs Requires a Conserved Methyltransferase that Is Localized to the Nucleolus. Mol Cell 9, 891–901.

Mugridge, JS, Coller, J, and Gross, JD (2018). Structural and molecular mechanisms for the control of eukaryotic 5′–3′ mRNA decay. Nat Struct Mol Biol 25, 1077–1085.

Muthukrishnan, S, Both, GW, Furuichi, Y, and Shatkin, AJ (1975). 5'-Terminal 7-methylguanosine in eukaryotic mRNA is required for translation. Nature 255, 33–37.

Niu, K, Zhang, J, Ge, S, Li, D, Sun, K, You, Y, Qiu, J, Wang, K, Wang, X, Liu, R, *et al.* (2023). ONE-seq: epitranscriptome and gene-specific profiling of NAD-capped RNA. Nucleic Acids Res 51, e12.

Nübel, G, Sorgenfrei, FA, and Jäschke, A (2017). Boronate affinity electrophoresis for the purification and analysis of cofactor-modified RNAs. Methods 117, 14–20.

O'Farrell, PA, Gonzalez, F, Zheng, W, Johnston, SA, and Joshua-Tor, L (1999). Crystal structure of human bleomycin hydrolase, a self-compartmentalizing cysteine protease. Struct Lond Engl 1993 7, 619–627.

Ohira, T, and Suzuki, T (2016). Precursors of tRNAs are stabilized by methylguanosine cap structures. Nat Chem Biol 12, 648–655.

Ohno, M, Segref, A, Bachi, A, Wilm, M, and Mattaj, IW (2000). PHAX, a Mediator of U snRNA Nuclear Export Whose Activity Is Regulated by Phosphorylation. Cell 101, 187–198.

Osman, S, and Cramer, P (2020). Structural Biology of RNA Polymerase II Transcription: 20 Years On. Annu Rev Cell Dev Biol 36, 1–34.

Ou, L, Zhao, X, Wu, I (Jing), Yu, Z, Xiong, Z, Xia, LC, Wang, Y, Zhou, G, and Chen, W (2024). Molecular mechanism of NAD+ and NMN binding to the Nudix homology domains of DBC1. Int J Biol Macromol 262, 130131.

Pabis, M, Neufeld, N, Steiner, MC, Bojic, T, Shav-Tal, Y, and Neugebauer, KM (2013). The nuclear cap-binding complex interacts with the U4/U6·U5 tri-snRNP and promotes spliceosome assembly in mammalian cells. RNA N Y N 19, 1054–1063.

Palazzo, L, Mikoč, A, and Ahel, I (2017). ADP-ribosylation: new facets of an ancient modification. FEBS J 284, 2932–2946.

Pan, S, Li, K-E, Huang, W, Zhong, H, Wu, H, Wang, Y, Zhang, H, Cai, Z, Guo, H, Chen, X, *et al.* (2020). Arabidopsis DXO1 possesses deNADding and exonuclease activities and its mutation affects defense-related and photosynthetic gene expression. J Integr Plant Biol 62, 967–983.

Panchapakesan, SSS, Corey, L, Malkowski, SN, Higgs, G, and Breaker, RR (2021). A second riboswitch class for the enzyme cofactor NAD+. RNA 27, 99–105.

Passmore, LA, and Coller, J (2022). Roles of mRNA poly(A) tails in regulation of eukaryotic gene expression. Nat Rev Mol Cell Biol 23, 93–106.

Pelletier, J, Schmeing, TM, and Sonenberg, N (2021). The multifaceted eukaryotic cap structure. WIREs RNA 12, e1636.

Perry, KL, Watkins, KP, and Agabian, N (1987). Trypanosome mRNAs have unusual "cap 4" structures acquired by addition of a spliced leader. Proc Natl Acad Sci 84, 8190–8194.

Peyrin, E (2009). Nucleic acid aptamer molecular recognition principles and application in liquid chromatography and capillary electrophoresis. J Sep Sci 32, 1531–1536.

Piccirillo, C, Khanna, R, and Kiledjian, M (2003). Functional characterization of the mammalian mRNA decapping enzyme hDcp2. RNA 9, 1138–1147.

Pietrocola, F, Galluzzi, L, Bravo-San Pedro, JM, Madeo, F, and Kroemer, G (2015). Acetyl Coenzyme A: A Central Metabolite and Second Messenger. Cell Metab 21, 805–821.

Pillutla, RC, Yue, Z, Maldonado, E, and Shatkin, AJ (1998). Recombinant human mRNA cap methyltransferase binds capping enzyme/RNA polymerase IIo complexes. J Biol Chem 273, 21443–21446.

Pirouz, M, Du, P, Munafò, M, and Gregory, RI (2016). Dis3l2-Mediated Decay Is a Quality Control Pathway for Noncoding RNAs. Cell Rep 16, 1861–1873.

Piton, J, Larue, V, Thillier, Y, Dorléans, A, Pellegrini, O, Li de la Sierra-Gallay, I, Vasseur, J-J, Debart, F, Tisné, C, and Condon, C (2013). Bacillus subtilis RNA deprotection enzyme RppH recognizes guanosine in the second position of its substrates. Proc Natl Acad Sci U S A 110, 8858–8863.

Plescia, OJ, and Braun, W (1967). Nucleic acids as antigens. Adv Immunol 6, 231–252.

Plessel, G, Fischer, U, and Lührmann, R (1994). m3G cap hypermethylation of U1 small nuclear ribonucleoprotein (snRNP) in vitro: evidence that the U1 small nuclear RNA-(guanosine-N2)-methyltransferase is a non-snRNP cytoplasmic protein that requires a binding site on the Sm core domain. Mol Cell Biol 14, 4160–4172.

Putt, KS, and Hergenrother, PJ (2004). An enzymatic assay for poly(ADP-ribose) polymerase-1 (PARP-1) via the chemical quantitation of NAD+: application to the high-throughput screening of small molecules as potential inhibitors. Anal Biochem 326, 78–86.

Rambout, X, and Maquat, LE (2020). The nuclear cap-binding complex as choreographer of gene transcription and pre-mRNA processing. Genes Dev 34, 1113–1127.

Ray, A, and Frick, DN (2020). Fluorescent probe displacement assays reveal unique nucleic acid binding properties of human nudix enzymes. Anal Biochem 595, 113622.

Reddy, R, Henning, D, and Busch, H (1979). Nucleotide sequence of nucleolar U3B RNA. J Biol Chem 254, 11097–11105.

Rissland, O (2016). The organization and regulation of mRNA-protein complexes. Wiley Interdiscip Rev RNA 8.

Roithová, A, Feketová, Z, Vaňáčová, Š, and Staněk, D (2020). DIS3L2 and LSm proteins are involved in the surveillance of Sm ring-deficient snRNAs. Nucleic Acids Res 48, 6184–6197.

Romig, TS, Bell, C, and Drolet, DW (1999). Aptamer affinity chromatography: combinatorial chemistry applied to protein purification. J Chromatogr B Biomed Sci App 731, 275–284.

Sahu, S, Wang, Z, Jiao, X, Gu, C, Jork, N, Wittwer, C, Li, X, Hostachy, S, Fiedler, D, Wang, H, *et al.* (2020). InsP7 is a small-molecule regulator of NUDT3-mediated mRNA decapping and processing-body dynamics. Proc Natl Acad Sci 117, 19245–19253.

Schoenberg, DR (2011). Mechanisms of endonuclease-mediated mRNA decay. WIREs RNA 2, 582–600.

Schwartz, S, and Motorin, Y (2017). Next-generation sequencing technologies for detection of modified nucleotides in RNAs. RNA Biol 14, 1124–1137.

Segref, A, Mattaj, IW, and Ohno, M (2001). The evolutionarily conserved region of the U snRNA export mediator PHAX is a novel RNA-binding domain that is essential for U snRNA export. RNA N Y N 7, 351–360.

Sengupta, A, Gavvala, K, Koninti, RK, and Hazra, P (2014). Role of Mg^{2+} ions in flavin recognition by RNA aptamer. J Photochem Photobiol B 140, 240–248.

Shanmugasundaram, M, Senthilvelan, A, and Kore, AR (2022). Recent Advances in Modified Cap Analogs: Synthesis, Biochemical Properties, and mRNA Based Vaccines. Chem Rec N Y N 22, e202200005.

Shao, X, Zhang, H, Zhu, Z, Ji, F, He, Z, Yang, Z, Xia, Y, and Cai, Z (2023). DpCoA tagSeq: Barcoding dpCoA-Capped RNA for Direct Nanopore Sequencing via Maleimide-Thiol Reaction. Anal Chem 95, 11124–11131.

Sharma, S, Grudzien-Nogalska, E, Hamilton, K, Jiao, X, Yang, J, Tong, L, and Kiledjian, M (2020). Mammalian Nudix proteins cleave nucleotide metabolite caps on RNAs. Nucleic Acids Res, gkaa402.

Sharma, S, Yang, J, Doamekpor, SK, Grudizen-Nogalska, E, Tong, L, and Kiledjian, M (2022a). Identification of a novel deFADding activity in human, yeast and bacterial 5' to 3' exoribonucleases. Nucleic Acids Res 50, 8807–8817.

Sharma, S, Yang, J, Favate, J, Shah, P, and Kiledjian, M (2023). NADcapPro and circNC: methods for accurate profiling of NAD and non-canonical RNA caps in eukaryotes. Commun Biol 6, 1–14.

Sharma, S, Yang, J, Grudzien-Nogalska, E, Shivas, J, Kwan, KY, and Kiledjian, M (2022b). Xrn1 is a deNADding enzyme modulating mitochondrial NAD-capped RNA. Nat Commun 13, 889.

Shatsky, IN, Terenin, IM, Smirnova, VV, and Andreev, DE (2018). Cap-Independent Translation: What's in a Name? Trends Biochem Sci 43, 882–895.

She, M, Decker, CJ, Svergun, DI, Round, A, Chen, N, Muhlrad, D, Parker, R, and Song, H (2008). Structural Basis of Dcp2 Recognition and Activation by Dcp1. Mol Cell 29, 337–349.

Shestakova, ED, Smirnova, VV, Shatsky, IN, and Terenin, IM (2023). Specific mechanisms of translation initiation in higher eukaryotes: the eIF4G2 story. RNA 29, 282–299.

Shimba, S, Buckley, B, Reddy, R, Kiss, T, and Filipowicz, W (1992). Cap structure of U3 small nucleolar RNA in animal and plant cells is different. gamma-Monomethyl phosphate cap structure in plant RNA. J Biol Chem 267, 13772–13777.

Shokolenko, IN, and Alexeyev, MF (2017). Mitochondrial transcription in mammalian cells. Front Biosci Landmark Ed 22, 835–853.

Shukla, S, and Parker, R (2014). Quality control of assembly-defective U1 snRNAs by decapping and 5′-to-3′ exonucleolytic digestion. Proc Natl Acad Sci 111, E3277–E3286.

Shumyatsky, GP, Tillib, SV, and Kramerov, DA (1990). B2 RNA and 7SK RNA, RNA polymerase III transcripts, have a cap-like structure at their 5′ end. Nucleic Acids Res 18, 6347–6351.

Singh, R, Gupta, S, and Reddy, R (1990). Capping of mammalian U6 small nuclear RNA in vitro is directed by a conserved stem-loop and AUAUAC sequence: conversion of a noncapped RNA into a capped RNA. Mol Cell Biol 10, 939–946.

Singh, R, and Reddy, R (1989). Gamma-monomethyl phosphate: a cap structure in spliceosomal U6 small nuclear RNA. Proc Natl Acad Sci U S A 86, 8280–8283.

Song, M-G, Bail, S, and y, M (2013). Multiple Nudix family proteins possess mRNA decapping activity. RNA 19, 390–399.

Song, M-G, Li, Y, and Kiledjian, M (2010). Multiple mRNA Decapping Enzymes in Mammalian Cells. Mol Cell 40, 423–432.

Srouji, JR, Xu, A, Park, A, Kirsch, JF, and Brenner, SE (2017). The evolution of function within the Nudix homology clan. Proteins Struct Funct Bioinforma 85, 775–811.

Strasser, A, Dickmanns, A, Lührmann, R, and Ficner, R (2005). Structural basis for m3G-cap-mediated nuclear import of spliceosomal UsnRNPs by snurportin1. EMBO J 24, 2235–2243.

Syal, K, Rs, N, and Reddy, MVNJ (2021). The extended (p)ppGpp family: New dimensions in Stress response. Curr Res Microb Sci 2, 100052.

Tatosyan, KA, Ustyantsev, IG, and Kramerov, DA (2020). RNA Degradation in Eukaryotic Cells. Mol Biol 54, 485–502.

Taverniti, V, and Séraphin, B (2015). Elimination of cap structures generated by mRNA decay involves the new scavenger mRNA decapping enzyme Aph1/FHIT together with DcpS. Nucleic Acids Res 43, 482–492.

Thompson, MG, Sacco, MT, and Horner, SM (2021). How RNA modifications regulate the antiviral response. Immunol Rev 304, 169–180.

Tomasevic, N, and Peculis, B (1999). Identification of a U8 snoRNA-specific binding protein. J Biol Chem 274, 35914–35920.

Treiber, T, Treiber, N, and Meister, G (2018). Identification of microRNA Precursor-Associated Proteins. In: miRNA Biogenesis: Methods and Protocols, ed. UAV Ørom, New York, NY: Springer, 103–114.

Treiber, T, Treiber, N, Plessmann, U, Harlander, S, Daiß, J-L, Eichner, N, Lehmann, G, Schall, K, Urlaub, H, and Meister, G (2017). A Compendium of RNA-Binding Proteins that Regulate MicroRNA Biogenesis. Mol Cell 66, 270-284.e13.

Tsukamoto, T, Shibagaki, Y, Murakoshi, T, Suzuki, M, Nakamura, A, Gotoh, H, and Mizumoto, K (1998a). Cloning and characterization of two human cDNAs encoding the mRNA capping enzyme. Biochem Biophys Res Commun 243, 101–108.

Tsukamoto, T, Shibagaki, Y, Niikura, Y, and Mizumoto, K (1998b). Cloning and characterization of three human cDNAs encoding mRNA (guanine-7-)-methyltransferase, an mRNA cap methylase. Biochem Biophys Res Commun 251, 27–34.

Tuerk, C, and Gold, L (1990). Systematic evolution of ligands by exponential enrichment: RNA ligands to bacteriophage T4 DNA polymerase. Science 249, 505–510.

Tyc, K, and Steitz, JA (1989). U3, U8 and U13 comprise a new class of mammalian snRNPs localized in the cell nucleolus. EMBO J 8, 3113–3119.

Ustianenko, D, Hrossova, D, Potesil, D, Chalupnikova, K, Hrazdilova, K, Pachernik, J, Cetkovska, K, Uldrijan, S, Zdrahal, Z, and Vanacova, S (2013). Mammalian DIS3L2 exoribonuclease targets the uridylated precursors of let-7 miRNAs. RNA 19, 1632–1638.

Ustianenko, D, Pasulka, J, Feketova, Z, Bednarik, L, Zigackova, D, Fortova, A, Zavolan, M, and Vanacova, S (2016). TUT-DIS3L2 is a mammalian surveillance pathway for aberrant structured non-coding RNAs. EMBO J 35, 2179–2191.

Vidya, E, and Duchaine, TF (2022). Eukaryotic mRNA Decapping Activation. Front Genet 13.

Visa, N, Izaurralde, E, Ferreira, J, Daneholt, B, and Mattaj, IW (1996). A nuclear cap-binding complex binds Balbiani ring pre-mRNA cotranscriptionally and accompanies the ribonucleoprotein particle during nuclear export. J Cell Biol 133, 5–14.

Vvedenskaya, IO, Bird, JG, Zhang, Y, Zhang, Y, Jiao, X, Barvík, I, Krásný, L, Kiledjian, M, Taylor, DM, Ebright, RH, *et al.* (2018). CapZyme-Seq Comprehensively Defines Promoter-Sequence Determinants for RNA 5′ Capping with NAD+. Mol Cell 70, 553-564.e9.

Walsh, CT, and Wencewicz, TA (2012). Flavoenzymes: Versatile catalysts in biosynthetic pathways. Nat Prod Rep 30, 175–200.

Walter, J-G, Stahl, F, and Scheper, T (2012). Aptamers as affinity ligands for downstream processing. Eng Life Sci 12, 496–506.

Walters, RW, Matheny, T, Mizoue, LS, Rao, BS, Muhlrad, D, and Parker, R (2017). Identification of NAD+ capped mRNAs in Saccharomyces cerevisiae. Proc Natl Acad Sci 114, 480–485.

Wang, J, Alvin Chew, BL, Lai, Y, Dong, H, Xu, L, Balamkundu, S, Cai, WM, Cui, L, Liu, CF, Fu, X-Y, *et al.* (2019a). Quantifying the RNA cap epitranscriptome reveals novel caps in cellular and viral RNA. Nucleic Acids Res.

Wang, J, Chew, BLA, Lai, Y, Dong, H, Xu, L, Liu, Y, Fu, X-Y, Lin, Z, Shi, P-Y, Lu, TK, *et al.* (2023). A systems-level mass spectrometry-based technique for accurate and sensitive quantification of the RNA cap epitranscriptome. Nat Protoc, 1–28.

Wang, Y, Li, S, Zhao, Y, You, C, Le, B, Gong, Z, Mo, B, Xia, Y, and Chen, X (2019b). NAD+-capped RNAs are widespread in the Arabidopsis transcriptome and can probably be translated. Proc Natl Acad Sci U S A 116, 12094–12102.

Wang, Y, Ludwig, J, Schuberth, C, Goldeck, M, Schlee, M, Li, H, Juranek, S, Sheng, G, Micura, R, Tuschl, T, *et al.* (2010). Structural and functional insights into 5′-ppp RNA pattern recognition by the innate immune receptor RIG-I. Nat Struct Mol Biol 17, 781–787.

Wang, Z, Jiao, X, Carr-Schmid, A, and Kiledjian, M (2002). The hDcp2 protein is a mammalian mRNA decapping enzyme. Proc Natl Acad Sci U S A 99, 12663–12668.

Wang, Z, and Kiledjian, M (2001). Functional link between the mammalian exosome and mRNA decapping. Cell 107, 751–762.

Warminski, M, Mamot, A, Depaix, A, Kowalska, J, and Jemielity, J (2023). Chemical Modifications of mRNA Ends for Therapeutic Applications. Acc Chem Res 56, 2814–2826.

Warminski, M, Sikorski, PJ, Kowalska, J, and Jemielity, J (2017). Applications of Phosphate Modification and Labeling to Study (m)RNA Caps. Top Curr Chem 375, 16.

Wei, C, Gershowitz, A, and Moss, B (1975a). N6, O2'-dimethyladenosine a novel methylated ribonucleoside next to the 5' terminal of animal cell and virus mRNAs. Nature 257, 251–253.

Wei, CM, Gershowitz, A, and Moss, B (1975b). Methylated nucleotides block 5' terminus of HeLa cell messenger RNA. Cell 4, 379–386.

Weichmann, F (2019). Detection and biochemical investigation of RNA base modifications. University of Regensburg. Thesis, University of Regensburg.

Weichmann, F, Hett, R, Schepers, A, Ito-Kureha, T, Flatley, A, Slama, K, Hastert, FD, Angstman, NB, Cardoso, MC, König, J, *et al.* (2020). Validation strategies for antibodies targeting modified ribonucleotides. RNA 26, 1489–1506.

Weinberg, Z, Lünse, CE, Corbino, KA, Ames, TD, Nelson, JW, Roth, A, Perkins, KR, Sherlock, ME, and Breaker, RR (2017). Detection of 224 candidate structured RNAs by comparative analysis of specific subsets of intergenic regions. Nucleic Acids Res 45, 10811–10823.

Weixler, L, Feijs, KLH, and Zaja, R (2022). ADP-ribosylation of RNA in mammalian cells is mediated by TRPT1 and multiple PARPs. Nucleic Acids Res 50, 9426–9441.

Wen, Y, and Shatkin, AJ (1999). Transcription elongation factor hSPT5 stimulates mRNA capping. Genes Dev 13, 1774–1779.

Werner, M, Purta, E, Kaminska, KH, Cymerman, IA, Campbell, DA, Mittra, B, Zamudio, JR, Sturm, NR, Jaworski, J, and Bujnicki, JM (2011). 2′-O-ribose methylation of cap2 in human: function and evolution in a horizontally mobile family. Nucleic Acids Res 39, 4756–4768.

White, HB (1976). Coenzymes as fossils of an earlier metabolic state. J Mol Evol 7, 101–104.

Wiedermannova, J, Babu, R, and Yuzenkova, Y (2023). 5'-NADylation of RNA is well-tolerated by bacterial cell. 2023.03.31.535138.

Will, CL, and Lührmann, R (2011). Spliceosome Structure and Function. Cold Spring Harb Perspect Biol 3, a003707–a003707.

Winz, M-L, Cahová, H, Nübel, G, Frindert, J, Höfer, K, and Jäschke, A (2017). Capture and sequencing of NAD-capped RNA sequences with NAD captureSeq. Nat Protoc 12, 122–149.

Wolfram-Schauerte, M, and Höfer, K (2023). NAD-capped RNAs – a redox cofactor meets RNA. Trends Biochem Sci 48, 142–155.

Wu, H, Li, L, Chen, K-M, Homolka, D, Gos, P, Fleury-Olela, F, McCarthy, AA, and Pillai, RS (2019). Decapping Enzyme NUDT12 Partners with BLMH for Cytoplasmic Surveillance of NAD-Capped RNAs. Cell Rep 29, 4422-4434.e13.

Wurth, L, Gribling-Burrer, A-S, Verheggen, C, Leichter, M, Takeuchi, A, Baudrey, S, Martin, F, Krol, A, Bertrand, E, and Allmang, C (2014). Hypermethylated-capped selenoprotein mRNAs in mammals. Nucleic Acids Res 42, 8663–8677.

Xhemalce, B, Robson, SC, and Kouzarides, T (2012). Human RNA Methyltransferase BCDIN3D Regulates MicroRNA Processing. Cell 151, 278–288.

Xiang, S, Cooper-Morgan, A, Jiao, X, Kiledjian, M, Manley, JL, and Tong, L (2009). Structure and function of the 5′→3′ exoribonuclease Rat1 and its activating partner Rai1. Nature 458, 784–788.

Xu, X, Egger, M, Li, C, Chen, H, Micura, R, and Ren, A (2023). Structure-based investigations of the NAD+-II riboswitch. Nucleic Acids Res 51, 54–67.

Xue, Y, Yang, Z, Chen, R, and Zhou, Q (2010). A capping-independent function of MePCE in stabilizing 7SK snRNA and facilitating the assembly of 7SK snRNP. Nucleic Acids Res 38, 360–369.

Yang, Y, Eichhorn, CD, Wang, Y, Cascio, D, and Feigon, J (2019). Structural basis of 7SK RNA 5′-γ-phosphate methylation and retention by MePCE. Nat Chem Biol 15, 132–140.

Yoluç, Y, Ammann, G, Barraud, P, Jora, M, Limbach, PA, Motorin, Y, Marchand, V, Tisné, C, Borland, K, and Kellner, S (2021). Instrumental analysis of RNA modifications. Crit Rev Biochem Mol Biol 56, 178–204.

Yu, S, and Kim, VN (2020). A tale of non-canonical tails: gene regulation by post-transcriptional RNA tailing. Nat Rev Mol Cell Biol 21, 542–556.

Yu, X, Willmann, MR, Vandivier, LE, Trefely, S, Kramer, MC, Shapiro, J, Guo, R, Lyons, E, Snyder, NW, and Gregory, BD (2020). Messenger RNA 5′ NAD+ Capping Is a Dynamic Regulatory Epitranscriptome Mark That Is Required for Proper Response to Abscisic Acid in Arabidopsis. Dev Cell 0.

Zhang, D, Liu, Y, Wang, Q, Guan, Z, Wang, J, Liu, J, Zou, T, and Yin, P (2016). Structural basis of prokaryotic NAD-RNA decapping by NudC. Cell Res 26, 1062–1066.

Zhang, H, Zhong, H, Wang, X, Zhang, S, Shao, X, Hu, H, Yu, Z, Cai, Z, Chen, X, and Xia, Y (2021). Use of NAD tagSeq II to identify growth phase-dependent alterations in E. coli RNA NAD+ capping. PNAS, 11.

Zhang, H, Zhong, H, Zhang, S, Shao, X, Ni, M, Cai, Z, Chen, X, and Xia, Y (2019a). NAD tagSeq reveals that NAD+-capped RNAs are mostly produced from a large number of protein-coding genes in Arabidopsis. Proc Natl Acad Sci 116, 12072–12077.

Zhang, L-S, Liu, C, Ma, H, Dai, Q, Sun, H-L, Luo, G, Zhang, Z, Zhang, L, Hu, L, Dong, X, *et al.* (2019b). Transcriptome-wide Mapping of Internal *N*7-Methylguanosine Methylome in Mammalian mRNA. Mol Cell 74, 1304-1316.e8.

Zhang, Y, Kuster, D, Schmidt, T, Kirrmaier, D, Nübel, G, Ibberson, D, Benes, V, Hombauer, H, Knop, M, and Jäschke, A (2020). Extensive 5′-surveillance guards against non-canonical NAD-caps of nuclear mRNAs in yeast. Nat Commun 11, 5508.

Zhang, Y, Lu, L, and Li, X (2022). Detection technologies for RNA modifications. Exp Mol Med 54, 1601–1616.

Zhou, S, and Van Bortle, K (2023). The Pol III transcriptome: Basic features, recurrent patterns, and emerging roles in cancer. WIREs RNA 14, e1782.

Zhou, W, Guan, Z, Zhao, F, Ye, Y, Yang, F, Yin, P, and Zhang, D (2021). Structural insights into dpCoA-RNA decapping by NudC. RNA Biol, 15476286.2021.1936837.

Zhu, Y, Qi, C, Cao, W-Q, Yeldandi, AV, Rao, MS, and Reddy, JK (2001). Cloning and characterization of PIMT, a protein with a methyltransferase domain, which interacts

with and enhances nuclear receptor coactivator PRIP function. Proc Natl Acad Sci 98, 10380–10385.

Ziemniak, M, Szabelski, M, Lukaszewicz, M, Nowicka, A, Darzynkiewicz, E, Rhoads, RE, Wieczorek, Z, and Jemielity, J (2013). Synthesis and evaluation of fluorescent cap analogues for mRNA labelling. RSC Adv 3, 20943–20958.

Züst, R, Cervantes-Barragan, L, Habjan, M, Maier, R, Neuman, BW, Ziebuhr, J, Szretter, KJ, Baker, SC, Barchet, W, Diamond, MS, *et al.* (2011). Ribose 2′-O-methylation provides a molecular signature for the distinction of self and non-self mRNA dependent on the RNA sensor Mda5. Nat Immunol 12, 137–143.

ACKNOWLEDGEMENTS

First, I would like to thank my supervisor, Prof. Dr. Gunter Meister, for the opportunity to carry out my PhD in his lab and fully immerse myself into the RNA biochemistry field, for the interesting and challenging projects over the years, for his feedback and ideas during our meetings, and, more globally, for contributing to develop my critical thinking and guiding me along the path to become a better scientist.

I would like to thank the members of my examination committee for their time and availability to review my thesis: Prof. Dr. Remco Sprangers as second referee, Prof. Dr. Klaus Grasser as third referee, Prof. Dr. Joachim Griesenbeck as substitute examiner, and Prof. Dr. Thomas Dresselhaus as chairperson.

I would like to thank Robert Hett for the HPLC measurements, the antibody-related work and the discussions on NADylated RNAs synthesis, as well as Dr. Astrid Bruckmann, Dr. Rasha Elbashir, and Eduard Hochmuth for performing the mass spectrometry analysis.

I would like to thank for the scientific inputs and discussions: Michaela “Michi” Bauer and Kevin Heizler during our “MIN” meeting, Eva Schöller and Franziska “Franzi” Weichmann during our METTL meetings, and Daniele Hasler during our spliceosome meetings, as well as Tiana Hanelt and Simone Larivera for the additional troubleshooting, brainstorming, and thesis corrections. I would like to also thank PD Dr. Jan Medenbach, and PD Dr. Markus Kretz for the insightful comments during and after my progress reports.

I would like to thank for the technical and administrative support our engineers Norbert Eichner and Gerhard Lehmann, our technical assistants Sigrun “Sigi” Ammon and Corinna Friederich, and our secretary Birgit Clemens.

Many thanks to the rest of the AG Meister for the fun time in and out of the lab: Brent Cuveele, Julian Eichlinger, Julia Neumeier, Elisabetta Scarfiello, Carla Till, as well as the Alumni that welcomed me at the beginning of my PhD: Johannes Danner, Hung Ho-Xuan, Claudia Latini, Balagopal Pai, Thomas Treiber, Nora Treiber and Daniela Zeitler. Of course, the labs next door contributed strongly to a motivating working

atmosphere: especially Andreas “Hannes” Horn, Andreas “Nanni” Meindl, Rebecca “Becki” Moschall, and Markus Romberger from AG Medenbach, Johannes “Johnny G” Graf, Carolin “Caro” Molthof, Fabian “Fabi” Schabenberger, and Christian “Chris” Ziegler from AG Kretz, Philipp Becker, Florian “Flo” Heiss, and Julia Daiss from AG Engl, Michael “MJ” Jüttner and Nicolas Alexandre from AG Ferreira-Cerca.

Enfin, merci à ma famille, mes proches, et mes amis pour leur soutien tout au long de ces six années de doctorat.